arXiv:2002.11309v2 [math.NA] 15 Jun 2020

Neural Parametric Fokker-Planck Equations

Shu Liu*[1], Wuchen Li†[2], Hongyuan Zha‡[1], and Haomin Zhou§[1]

[1]Georgia Institute of Technology
[2]University of California, Los Angeles

Feburary 2020

Abstract

In this paper, we develop and analyze numerical methods for high dimensional Fokker-Planck equations by leveraging generative models from deep learning. Our starting point is a formulation of the Fokker-Planck equation as a system of ordinary differential equations (ODEs) on finite-dimensional parameter space with the parameters inherited from generative models such as normalizing flows. We call such ODEs *neural parametric Fokker-Planck equation*. The fact that the Fokker-Planck equation can be viewed as the L^2-Wasserstein gradient flow of Kullback–Leibler (KL) divergence allows us to derive the ODEs as the constrained L^2-Wasserstein gradient flow of KL divergence on the set of probability densities generated by neural networks. For numerical computation, we design a variational semi-implicit scheme for the time discretization of the proposed ODE. Such an algorithm is sampling-based, which can readily handle Fokker-Planck equations in higher dimensional spaces. Moreover, we also establish bounds for the asymptotic convergence analysis of the neural parametric Fokker-Planck equation as well as the error analysis for both the continuous and discrete versions. Several numerical examples are provided to illustrate the performance of the proposed algorithms and analysis.

Keywords Optimal transport; Transport information geometry; Deep learning; Neural parametric Fokker-Planck equation; Implicit Euler scheme; Numerical analysis.

1 Introduction

Fokker-Planck equation is a parabolic partial differential equation (PDE) that plays a crucial role in stochastic calculus, statistical physics, biology and many other disciplines [35, 41, 44]. Recently, it has seen many applications in machine learning as well [31, 38, 49]. Fokker-Planck equation describes the evolution of probability density of a stochastic differential equation (SDE). In this paper, we mainly focus on the following linear Fokker-Planck equation

$$\frac{\partial \rho(t,x)}{\partial t} = \nabla \cdot (\rho(t,x)\nabla V(x)) + \beta \Delta \rho(t,x), \quad \rho(0,x) = p(x), \tag{1}$$

where $x \in \mathbb{R}^d$, $V\colon \mathbb{R}^d \to \mathbb{R}$ is a given potential function, $\beta > 0$ is a diffusion coefficient, and $p(x)$ is the initial (or reference) density function. In numerical algorithms, there exist several classical methods [40] such as finite difference [10] or finite element [23] for solving the Fokker Planck equation. Most of the existing methods are grid based, which may be able to approximate the solution accurately if the grid sizes become small. However, they find limited usage in high dimensional problems, especially for $d > 3$, because the number of unknowns grows exponentially fast as the dimension increases. This is known as the curse of dimensionality. The main goal of this paper is providing an alternative strategy, with provable error estimates, to solve high dimensional Fokker-Planck equations.

*sliu459@gatech.edu
†wcli@math.ucla.edu
‡zha@cc.gatech.edu
§hmzhou@math.gatech.edu

1.1 Neural parametric Fokker-Planck equation

To overcome the challenges imposed by high dimensionality, we leverage the generative models in machine learning [43] and a new interpretation of the Fokker-Planck equation in the theory of optimal transport [52]. We first introduce the KL divergence, also known as relative entropy, defined by

$$\mathrm{D}_{\mathrm{KL}}(\rho||\rho_*) = \int \rho(x) \log\left(\frac{\rho(x)}{\rho_*(x)}\right) dx \quad \rho_*(x) = \frac{1}{Z_\beta} e^{-\frac{V}{\beta}}, \text{ with } Z_\beta = \int e^{-\frac{V(x)}{\beta}}\ dx.$$

Here $\rho_*(x)$ is the Gibbs distribution. A well-known fact is that the Fokker-Planck equation (1) can be viewed as the gradient flow of the functional $\beta\ \mathrm{D}_{\mathrm{KL}}(\rho||\rho_*)$ on the probability space $\mathcal{P}$ equipped with Wasserstein metric [17, 36]. Recently, this line of research has been extended to parameter space in the field of information geometry [1, 2, 5], leading to an emergent area called transport information geometry [25, 30, 28, 29].

Inspired by aforementioned work, we study the Fokker-Planck equation defined on parametric space Θ equipped with metric tensor G that is compatible with the Wasserstein metric. In this paper, we focus on the parameter space from generative models using neural networks. Our line of thoughts can be summarized as following. We start with a given reference distribution p, and consider a suitable family of parametric pushforward map $\{T_\theta\}_{\theta\in\Theta}$. The so-called pushforward operator $T_\# : \Theta \to \mathcal{P}(\theta \mapsto T_{\theta\#}p)$ can be treated as an immersion from parametric manifold Θ to probability manifold $\mathcal{P}$. We derive the metric tensor $G(\theta)$ by pulling back the Wasserstein metric via immersion $T_\#$. Once we have established (Θ, G), we compute the G-gradient flow of function $H(\theta) = \beta\ D_{\mathrm{KL}}(T_{\theta\#}p||\rho_*)$ defined on the parameter manifold. This leads to an ODE system that can be viewed as a parametric version of Fokker Planck equation:

$$\dot{\theta}_t = -G(\theta_t)^{-1}\nabla_\theta H(\theta_t). \tag{2}$$

Here (and for the rest of the paper) dot symbol $\dot{\theta}$ stands for time derivative $\frac{d\theta_t}{dt}$. Using the pushforward $\rho_\theta = T_{\theta\#}p$, in which θ is the solution of (2), we can approximate the solution ρ_t in (1).

1.2 Computational method

For the computation of (2), we want to point out that metric tensor $G(\theta)$ doesn't have an explicit form and thus the direct computation of $G(\theta)^{-1}\nabla_\theta H(\theta)$ is not tractable. To deal with this issue, we design a numerical algorithm based on the semi-implicit Euler scheme of (2) with time step size h. To be more precise, at each time step, the algorithm seeks to solve the following saddle point problem:

$$\theta_{k+1} = \operatorname*{argmin}_{\theta\in\Theta} \max_{\phi} \left\{ \int 2\nabla\phi(x)\cdot((T_\theta - T_{\theta_k})\circ T_{\theta_k}^{-1}(x))\rho_{\theta_k}(x)\ dx - \int |\nabla\phi(x)|^2\rho_{\theta_k}(x)\ dx + 2hH(\theta) \right\}. \tag{3}$$

Here $\phi\colon \mathbb{R}^d \to \mathbb{R}$ is the Kantorovich dual potential variable for constrained probability models in optimal transport theory. Hence (3) is derived following the semi-implicit Euler scheme in the dual variable. The advantage of using this formulation is that it allows us to design an efficient implementation, purely based on sampling techniques which are computational friendly in high dimensional problems, to compute the solution of the parameteric Fokker-Planck equation (2).

In our implementation, we endow the pushforward map T_θ with certain kinds of deep neural network known as Normalizing Flow [43], because it is friendly to our scheme evaluations. The dual variable ϕ in the inner maximization is parametrized by the deep Rectified Linear Unit (ReLU) networks [39] . Once the network structures for T_θ and ϕ are chosen, the optimizations are carried out by stochastic gradient descent method [47], in which all terms involved can by computed using samples from the reference distribution p. We stress that this is critical in scaling up the computations in high dimensions. It is worth mentioning that we use neural network as a computational tool without any actual data. Such "data-poor" computation is in significant contrast to the mainstream of deep learning research.

1.3 Major innovations of the proposed method

There are two main innovative points regarding our proposed method:

- (Dimension reduction) Reducing the high dimensional evolution PDE to a finite dimensional ODE system on parameter space. Equivalently, we use the dynamics in a finite dimensional parametric space to approximate the density evolution of particles that follow the Vlasov-type SDE

$$\dot{\boldsymbol{X}}_t = -\nabla V(\boldsymbol{X}_t) - \beta \nabla \log \rho_t(\boldsymbol{X}_t),$$

whose density function ρ_t corresponds to the Fokker-Planck equation (1).

- (Sampling-friendly) We distill the information of ρ_t into parameters $\{\theta_t\}$ by solving the parametric Fokker-Planck equation (2). By doing so, we are able to obtain an efficient sampling technique to generate samples from ρ_t for any time step t. To be more precise, we solve (2) for time-dependent parameters $\{\theta_t\}$, and we can then generate samples from ρ_t by pushing forward the samples drawn from a reference distribution p using the pushforward map T_{θ_t}. It worth mentioning that our method is very different from Langevin Monte Carlo (LMC, MALA) methods [14, 45], which aims at targeting the stationary distribution of the SDE associated to (1); or momentum methods [41] , which focuses on keeping track of certain statistical information of the density ρ_t.

1.4 Sketch of numerical analysis

In addition to the method proposed for solving (1), we also conducted a mathematical analysis on (2) and our algorithm. We established asymptotic convergence and error estimates for the parametric Fokker-Planck equation (2), which are summarized in the following two theorems:

Theorem 1 (Asymptotic convergence)**.** *Consider Fokker-Planck equation* (1) *with potential* V*. Suppose* V *can be decomposed as* $V = U + \phi$ *with* $U \in \mathcal{C}^2(\mathbb{R}^d)$*,* $\nabla^2 U \succeq KI$[1] *with* $K > 0$ *and* $\phi \in L^\infty(\mathbb{R}^d)$*, and* $\{\theta_t\}$ *solves* (2)*. Then we have the inequality:*

$$D_{KL}(\rho_{\theta_t} \| \rho_*) \leq \frac{\delta_0}{\tilde{\lambda}_\beta \beta^2}(1 - e^{-\beta \tilde{\lambda}_\beta t}) + D_{KL}(\rho_{\theta_0} \| \rho_*) e^{-\beta \tilde{\lambda}_\beta t},$$

where ρ_* *is the Gibbs distribution,* $\tilde{\lambda}_\beta > 0$ *is a constant related to potential function* V *and* β*.* δ_0 *is a constant depending on the approximation power of pushforward map* T_θ*.*

Theorem 2 (Approximation error)**.** *Suppose all assumptions in Theorem 1 hold, then for any time* $t > 0$*, the* L^2*-Wasserstein error* $W_2(\rho_{\theta_t}, \rho_t)$ *can be bounded above by* $K(E_0 + \sqrt{\delta_0})^\alpha$ *with some* $0 < \alpha \leq 1$*. Here* $E_0 = W_2(\rho_{\theta_0}, \rho_0)$*,* K *is a positive constant independent of time* t*.*

This result reveals that the difference between the solutions of parametric Fokker-Planck equation (2) and the orginal equation (1), measured by their Wasserstein distance $W_2(\rho_{\theta_t}, \rho_t)$, has a *uniformly* small upper bound if both the initial error E_0 and δ_0 are small enough. Most of the techniques used in our analysis for establishing such a result rely on the theory of optimal transport and Wasserstein manifold, which are still not commonly used for numerical analysis in relevant literature. Besides error analysis for the continuous version of (2), we are able to provide the order of W_2-error for the numerical scheme when (2) is computed at discrete time by numerical schemes. To be more precise, if we apply forward-Euler scheme to (2) and compute $\{\theta_k\}$ at different time nodes $\{t_k\}$, we can show that error at t_k: $W_2(\rho_{\theta_k}, \rho_{t_k})$ is of order $O(\sqrt{\delta_0}) + O(C_N h) + O(E_0)$ for finite time t. This is summarized in the following theorem:

Theorem 3. *Assume that* $\{\rho_t\}_{t \geq 0}$ *is the solution of* (1) *with potential satisfying* $\lambda I \preceq \nabla^2 V \preceq \Lambda I$*,* $\{\theta_k\}_{k=0}^N$ *is the numerical solution of* (2) *at time nodes* $t_k = kh$ *for* $k = 0, 1, ..., N$ *computed by forward Euler scheme with time step* h*. Then*

$$W_2(\rho_{\theta_k}, \rho_{t_k}) \leq (\sqrt{\delta_0} h + C_N h^2) \frac{(1 - e^{-\lambda t_k})}{1 - e^{-\lambda h}} + e^{-\lambda t_k} E_0 \sim O(\sqrt{\delta_0}) + O(C_N h) + O(E_0), \quad 0 \leq k \leq N,$$

where C_N *is a constant depending on* N *and* h*.*

[1] The matrix $\nabla^2 U(x) - KI_{d \times d}$ is non-negative definite for any $x \in \mathbb{R}^d$.

This indicates that the W_2-error is dominated by three different terms: $O(\sqrt{\delta_0})$ is the intrinsic error originated from the approximation mechanism of parametric Fokker-Planck equation; $O(C_N h)$ term is induced by the time discretization; and $O(E_0)$ term is the initial error. We further prove that the difference between the forward Euler scheme and our semi-implicit Euler scheme is of order $O(h^2)$, which implies that the proposed semi-implicit Euler scheme can achieve a similar error bounds as the one presented in Theorem 3.

It worth mentioning that we establish Theorem 3 based on totally different techniques than those used for Theorem 2. Since the ODE (2) contains the term $G(\theta)^{-1}$, which is hard to handle by the traditional strategies, we interpret it as a particle system governed by a stochastic differential equations (SDEs) of Vlasov type, and obtain the analysis results shown in Theorem 3.

1.5 Literature review

There are many existing work on applying neural networks to solve PDE of various types in recent years [53, 42, 19, 20, 55]. Among them, [53] and [20] focus on high dimensional parabolic PDEs, to which the Fokker-Planck equation belongs. Our approach differ from these existing works in many aspects, including motivations, strategies, and the associated numerical analysis.

For example, in [53], the authors propose to use the non-linear Feynmann-Kac formula to re-write certain parabolic PDEs as the Backward Stochastic Differential Equation (BSDE), which is then reformulated as an optimal control problem (also known as reinforcement learning in machine learning community). By applying deep neural network as the control function and optimizing over network parameters, the solution at any given space-time location can be evaluated. Another example is [20], which mainly focuses on computing the committor function that solves a steady-state (time-independent) Fokker-Planck equation with specific boundary conditions. This committor function can be treated as the solution to a variational problem associated with an energy functional. A neural network is used to replace the solution in the variational problem. When optimizing over network parameters, the neural network can be used to approximate the committor function.

In this paper, we focus on designing a sampling-friendly method for the time dependent Fokker-Planck equation. There are two main reasons that motivate us for this investigation. One, as mentioned before, is to design sample based algorithm to solve PDEs in high dimensions. The other is to provide an alternative sampling strategy that can be potentially faster than LMC. Our approaches are different in terms of how deep networks are leveraged to approximate the solution of the PDE. We use pushforward of a given reference measure by neural networks to create a generative model. This is to approximate the stream of probability distributions, which can be used to generate samples not only at the terminal time, but also any time in between. More importantly, we prove results, obtained by using newly developed techniques based on Wasserstein metric on probability manifold, on the asymptotic convergence and error control of our numerical schemes. To the best of our knowledge, similar results are still lacking in existing studies.

1.6 Organization of this paper

We organize the paper as follows. In section 2, we briefly introduce some background knowledge of Fokker-Planck equation, including its relation with SDE and its Wasserstein gradient flow structure. In section 3, we introduce the Wasserstein statistical manifold (Θ, G) and derive our parametric Fokker-Planck equation as the manifold gradient flow of relative entropy on Θ. We study the geometric property of this equation, including an insightful particle motion based interpretation of the parametric Fokker-Planck equation. In section 4, we design a numerical scheme that is tractable for computing our parametric Fokker-Planck equation using deep learning framework. Some important details of implementation will be discussed. We present asymptotic convergence and error estimates for the parametric Fokker-Planck equation in section 5, and provide some numerical examples in section 6.

2 Background on Fokker-Planck equation

In this section, we review some basic knowledge about Fokker-Planck equations.

2.1 As the density evolution of stochastic differential equation

The general form of Fokker-Planck equation is:

$$\frac{\partial \rho(x,t)}{\partial t} = -\nabla \cdot (\rho(x,t)\boldsymbol{\mu}(x,t)) + \frac{1}{2}\nabla \cdot (\boldsymbol{D}(x,t)\nabla\rho(x,t)), \quad \rho(x,0) = \rho_0(x),$$

where $\nabla\cdot$ and ∇ are the divergence and gradient operators in $\mathbb{R}^d$ respectively, $\boldsymbol{\mu}$ is the drift function and $\boldsymbol{D} = \boldsymbol{\sigma}\boldsymbol{\sigma}^T$ is the diffusion tensor. Here $\boldsymbol{\sigma}(x,t)$ is a $d \times \tilde{d}$ matrix. The derivation of Fokker-Planck Equation originates from the following stochastic differential equation(SDE) [44],

$$d\boldsymbol{X}_t = \boldsymbol{\mu}(\boldsymbol{X}_t, t)\ dt + \boldsymbol{\sigma}(\boldsymbol{X}_t, t)\ d\boldsymbol{B}_t, \quad \boldsymbol{X}_0 \sim \rho_0,$$

where $\{\boldsymbol{B}_t\}_{t\geq 0}$ is the standard Brownian motion in $\mathbb{R}^{\tilde{d}}$. It is well known that the evolution of the density $\rho(x,t)$ of the stochastic process $\{\boldsymbol{X}_t\}_{t\geq 0}$ is described by the Fokker-Planck equation.

In this paper, we consider a more specific type of (2.1) by setting $\boldsymbol{\mu}(x,t) = -\nabla V(x)$, $\boldsymbol{\sigma}(x,t) = \sqrt{2\beta}\ I_{d\times d}$ ($\beta > 0$), where $I_{d\times d}$ is the d by d identity matrix, and so $\boldsymbol{D} = 2\beta\ I_{d\times d}$. Then (2.1) is,

$$d\boldsymbol{X}_t = -\nabla V(\boldsymbol{X}_t)\ dt + \sqrt{2\beta}\ d\boldsymbol{B}_t \quad \boldsymbol{X}_0 \sim \rho_0. \tag{4}$$

This equation is also called over-damped Langevin dynamics which has broad applications in computational physics, computational biology, Bayesian statistics etc. [14, 48, 54]. The corresponding Fokker-Planck equation is simplified to

$$\frac{\partial \rho(x,t)}{\partial t} = \nabla \cdot (\rho(x,t)\nabla V(x)) + \beta\Delta\rho(x,t), \quad \rho(x,0) = \rho_0(x). \tag{5}$$

In addition, we would like to mention that there is a Vlasov-type SDE corresponding to the Fokker-Planck equation (5):

$$\frac{d\boldsymbol{X}_t}{dt} = -\nabla V(\boldsymbol{X}_t) - \beta\ \nabla \log \rho(\boldsymbol{X}_t, t), \quad \boldsymbol{X}_0 \sim \rho_0, \tag{6}$$

in which $\rho(\cdot, t)$ is the density of $\boldsymbol{X}_t$. This Vlasov-type SDE (6) will be very useful in our proofs for the error estimates.

2.2 As the Wasserstein gradient flow of relative entropy

Another useful viewpoint states that (5) is the Wasserstein gradient flow of relative entropy. We briefly present some of the notations and basic results in this regard.

2.2.1 Wasserstein manifold

Denote the probability space supported on $\mathbb{R}^d$ with densities having finite second order moments as

$$\mathcal{P} = \left\{\rho\colon \int \rho(x)dx = 1,\ \rho(x) \geq 0,\ \int |x|^2\rho(x)\ dx < \infty\right\}.$$

The so-called Wasserstein distance (also known as L^2-Wasserstein distance) on $\mathcal{P}$ is defined as [52]

$$W_2(\rho_1, \rho_2) = \left(\inf_{\pi\in\Pi(\rho_1,\rho_2)} \iint |x-y|^2\ d\pi(x,y)\right)^{1/2}, \tag{7}$$

where $\Pi(\rho_1, \rho_2)$ is the set of joint distributions defined on $\mathbb{R}^d \times \mathbb{R}^d$ with fixed marginal distributions whose densities are ρ_1, ρ_2. If we treat $\mathcal{P}$ as an infinite dimensional manifold, the Wasserstein distance W_2 can induce a metric g^W on the tangent bundle $T\mathcal{P}$, with which $\mathcal{P}$ becomes a Riemannian manifold. For simplicity, here we directly give the definition of g^W. One can identify the tangent space at ρ as:

$$T_\rho\mathcal{P} = \left\{\dot{\rho}\colon \int \dot{\rho}(x)dx = 0\right\}.$$

For a specific $\rho \in \mathcal{P}$ and $\dot{\rho}_i \in T_\rho \mathcal{P}$, $i = 1, 2$, we define the Wasserstein metric tensor g^W as [24, 36]

$$g^W(\rho)(\dot{\rho}_1, \dot{\rho}_2) = \int \nabla \psi_1(x) \cdot \nabla \psi_2(x) \rho(x) \, dx, \tag{8}$$

where ψ_1, ψ_2 satisfies

$$\dot{\rho}_i = -\nabla \cdot (\rho_i \nabla \psi_i) \quad i = 1, 2, \tag{9}$$

with boundary conditions

$$\lim_{x \to \infty} \rho(x) \nabla \psi_i(x) = 0 \quad i = 1, 2.$$

Use the above definition, we can also write

$$g^W(\rho)(\dot{\rho}_1, \dot{\rho}_2) = \int \psi_1(-\nabla \cdot (\rho \nabla \psi_2)) \, dx = \int (-\nabla \cdot (\rho \nabla))^{-1}(\dot{\rho}_1) \cdot \dot{\rho}_2 \, dx.$$

Thus, we can identify $g^W(\rho)$ as $(-\nabla \cdot (\rho \nabla))^{-1}$. When $\mathrm{supp}(\rho) = \mathbb{R}^d$, $g^W(\rho)$ is a positive definite bilinear form defined on tangent bundle $T\mathcal{P} = \{(\rho, \dot{\rho}) \colon \rho \in \mathcal{P}, \ \dot{\rho} \in T_\rho \mathcal{P}\}$. Hence we can treat $\mathcal{P}$ as a Riemannian manifold, which we call Wasserstein manifold and denoted as $(\mathcal{P}, g^W)$ [36].

2.2.2 Wasserstein gradient

We denote the Wasserstein gradient grad_W as the manifold gradient on $(\mathcal{P}, g^W)$. In Riemannian geometry, the manifold gradient must be compatible with the metric, implying that for any smooth $\mathcal{F}$ defined on $\mathcal{P}$ and any $\rho \in \mathcal{P}$, considering arbitrary differentiable curve $\{\rho_t\}_{t \in (-\delta, \delta)}$ with $\rho_0 = \rho$, we have

$$\frac{d}{dt} \mathcal{F}(\rho_t)\Big|_{t=0} = g^W(\rho)(\mathrm{grad}_W \mathcal{F}(\rho), \ \dot{\rho}_0).$$

Since we can write

$$\frac{d}{dt} \mathcal{F}(\rho_t)\Big|_{t=0} = \int \frac{\delta \mathcal{F}(\rho)}{\delta \rho(x)}(x) \cdot \dot{\rho}_0(x) \, dx = \left\langle \frac{\delta \mathcal{F}(\rho)}{\delta \rho}, \dot{\rho}_0 \right\rangle_{L^2},$$

here $\frac{\delta \mathcal{F}(\rho)}{\delta \rho(x)}(x)$ is the L^2 variation of $\mathcal{F}$ at point $x \in \mathbb{R}^d$, we then have

$$\left\langle \frac{\delta \mathcal{F}(\rho)}{\delta \rho}, \dot{\rho}_0 \right\rangle_{L^2} = g^W(\rho)(\mathrm{grad}_W \mathcal{F}(\rho), \ \dot{\rho}_0) \quad \forall \ \dot{\rho}_0 \in T_\rho \mathcal{P}.$$

This leads to the following useful formula for computing Wasserstein gradient of functional $\mathcal{F}$

$$\mathrm{grad}_W \mathcal{F}(\rho) = g^W(\rho)^{-1} \left(\frac{\delta \mathcal{F}}{\delta \rho} \right)(x) = -\nabla \cdot \left(\rho(x) \nabla \ \frac{\delta \mathcal{F}(\rho)}{\delta \rho(x)}(x) \right). \tag{10}$$

In particular, if $\mathcal{F}$ is taken as the relative entropy functional given by

$$\mathcal{H}(\rho) = \beta \ D_{\mathrm{KL}} \left(\rho \middle\| \rho_* \right) = \int V(x) \rho(x) + \beta \rho(x) \log \rho(x) \, dx + \beta \ \log Z_\beta, \tag{11}$$

we have $\nabla \frac{\delta \mathcal{H}(\rho)}{\delta \rho} = \nabla V + \beta \nabla \log \rho$. Using (10), and noticing $\nabla \log \rho = \frac{\nabla \rho}{\rho}$, then $\nabla \cdot (\rho \nabla \log \rho) = \nabla \cdot (\nabla \rho) = \Delta \rho$, the Wasserstein gradient flow of $\mathcal{H}$ can be written as

$$\frac{\partial \rho}{\partial t} = -\mathrm{grad}_W \mathcal{H}(\rho) = \nabla \cdot (\rho \nabla V) + \beta \nabla \cdot (\rho \nabla \log \rho)),$$

which is exactly the Fokker-Planck equation (5).

3 Parametric Fokker-Planck equation

In this section, we provide detailed derivation for our parametric Fokker-Planck equation.

3.1 Wasserstein statistical manifold

Consider a parameter space Θ as an open set in $\mathbb{R}^m$, and assume the sample space is $\mathbb{R}^d$. Let T_θ be a map from $\mathbb{R}^d$ to $\mathbb{R}^d$ parametrized by θ. In our discussion, we will always assume that T_θ is invertible and smooth with respect to parameter θ and variable x.

Remark 1. *There are many different choices for T_θ:*

- *We can set $T_\theta(x) = Ux + b$, with $\theta = (U, b), U \in GL_d(\mathbb{R}),\ b \in \mathbb{R}^d$;*
- *We may also choose T_θ as the linear combination of basis functions $T_\theta(x) = \sum_{k=1}^m \theta_k \vec{\Phi}_k(x)$, where $\{\vec{\Phi}_k\}_{k=1}^m$ are the basis functions and the parameter θ will be the coefficients: $\theta = (\theta_1, ..., \theta_m)$;*
- *We can also treat T_θ as neural network. Its general structure can be written as the composition of l affine and non-linear activation functions: $T_\theta(x) = \sigma_l(W_l(\sigma_{l-1}(...\sigma_1(W_1 x + b_1)...)) + b_l)$. In this case, the parameter θ will be the weight matrices and bias vectors of the neural network, i.e. $\theta = (W_1, b_1, ..., W_l, b_l)$.*

Definition 1. *Suppose X, Y are two measurable spaces, λ is a probability measure defined on X; let $T : X \to Y$ be a measurable map. We define $T_\# \lambda$ as: $T_\#\lambda(E) = \lambda(T^{-1}(E))$ for all measurable $E \subset Y$. We call $T_\# p$ the pushforward of measure p by map T.*

Let $p \in \mathcal{P}$ as a reference probability measure with positive density defined on $\mathbb{R}^d$, such as the standard Gaussian. We denote ρ_θ as the density of $T_{\theta\#}p$. Such kind of mechanism of producing parametric probability distributions is also known as **generative model**, which has broad applications in deep learning research [13, 4, 7]. We further require:

$$\int |z|^2 \rho_\theta(z)\ dz = \int |T_\theta(x)|^2\ dp(x) < \infty \quad \forall\ \theta \in \Theta. \tag{12}$$

This ensures that $\rho_\theta \in \mathcal{P}$ for each $\theta \in \Theta$. In order to introduce Wasserstein metric to the parameter space Θ, we assume that the Frobenius norm of the operator $\partial_\theta T_\theta : \mathbb{R}^d \to \mathbb{R}^{d\times m}$ is bounded, i.e.

$$\exists\ L(x),\ s.t.\ \|\partial_\theta T_\theta(x)\|_F \le L(x)\ \forall x \in \mathbb{R}^d, \theta \in \Theta \quad \text{and} \int L(x)\ dp(x) < \infty. \tag{13}$$

We define the parametric submanifold $\mathcal{P}_\Theta \subset \mathcal{P}$ as:

$$\mathcal{P}_\Theta = \{\rho_\theta \text{ is density function of } \ T_{\theta\#}p \mid \theta \in \Theta\}.$$

Clearly, the connection between $\mathcal{P}$ and Θ is the pushforward operation $T_\# : \Theta \to \mathcal{P}_\Theta \subset \mathcal{P}, \theta \mapsto \rho_\theta$, which is an isometric immersion from Θ to $\mathcal{P}$. The pullback $(T_\#)^* g^W$ of the Wasserstein metric g^W by $T_\#$ defines the metric tensor on Θ that we will use in this study. Let us denote $G = (T_\#)^* g^W$. Then for each θ, $G(\theta)$ is a bilinear form on $T_\theta\Theta \simeq \mathbb{R}^m$, thus $G(\theta)$ can be identified as an $m \times m$ matrix, whose formula is given in the following theorem:

Theorem 4. *Assume Θ satisfies (12),(13). T_θ is invertible and smooth with respect to θ and x. Then Θ can be equipped with the metric tensor $G = (T_\#)^* g^W$, which is a $m \times m$ non-negative definite symmetric matrix of the form:*

$$G(\theta) = \int \nabla \mathbf{\Psi}(T_\theta(x)) \nabla \mathbf{\Psi}(T_\theta(x))^T\ dp(x) \tag{14}$$

at every $\theta \in \Theta$. More precisely, in entry-wise form,

$$G_{ij}(\theta) = \int \nabla \psi_i(T_\theta(x)) \cdot \nabla \psi_j(T_\theta(x))\ dp(x), \quad 1 \le i, j \le m,$$

in which $\mathbf{\Psi} = (\psi_1, \cdots, \psi_m)^T$ and $\nabla \mathbf{\Psi}$ is $m \times d$ Jacobian matrix of $\mathbf{\Psi}$. For each $j = 1, 2, \cdots, m$, ψ_j solves the following equation:

$$\nabla \cdot (\rho_\theta \nabla \psi_j(x)) = \nabla \cdot (\rho_\theta\ \frac{\partial T_\theta}{\partial \theta_j}(T_\theta^{-1}(x))). \tag{15}$$

with boundary conditions

$$\lim_{x\to\infty} \rho_\theta(x) \nabla \psi_j(x) = 0.$$

Proof. Suppose $\xi \in T\Theta$ is a vector field on Θ, for a fixed $\theta \in \Theta$, we first compute the pushforward $(T_\#|_\theta)_*\xi(\theta)$ of ξ at point θ: We choose any smooth curve $\{\theta_t\}_{t\geq 0}$ on Θ with $\theta_0 = \theta$ and $\dot{\theta}_0 = \xi(\theta)$. If we denote $\rho_{\theta_t} = T_{\theta_t \#}p$, we have $(T_\#)_*\xi(\theta) = \frac{\partial \rho_{\theta_t}}{\partial t}\Big|_{t=0}$.

To compute $\frac{\partial \rho_{\theta_t}}{\partial t}\Big|_{t=0}$, we consider an arbitrary $\phi \in C_0^\infty(M)$. On one hand, $\frac{\rho_{\theta_{\Delta t}}(y) - \rho_{\theta_0}(y)}{\Delta t} = \frac{\partial}{\partial t}\rho(\theta_{\tilde{t}_1}, y)$, where $\tilde{t}_1$ is some point between $0, \Delta t$, since $\phi \in C_0^\infty$ and $\rho(\theta_t, y)$ is smooth with respect to t, y, we can show that the function $\varphi(x) = \sup_{s\in[0,\Delta t]} |\phi(x)\frac{\partial}{\partial t}\rho(\theta_s, y)|$ is continuous on a compact set and thus integrable on $\mathbb{R}^d$. Using dominant convergence theorem, we have:

$$\frac{\partial}{\partial t}\left(\int \phi(y)\rho_{\theta_t}(y)\ dy\right)\Big|_{t=0} = \int \phi(y)\frac{\partial \rho_{\theta_t}(y)}{\partial t}\Big|_{t=0}\ dy. \tag{16}$$

On the other hand, we have:

$$\frac{\phi(T_{\theta_{\Delta t}}(y)) - \phi(T_{\theta_0}(y))}{\Delta t} = \dot{\theta}_{\tilde{t}_2}^T\ \partial_\theta T_{\theta_{\tilde{t}_2}}(x)^T\ \nabla\phi(T_{\theta_{\tilde{t}_2}}(y)),$$

in which $\tilde{t}_2$ is also between $0, \Delta t$. For any Δt small enough and $\tilde{t} \in [0, \Delta t]$, we can easily find upper bounds for $\|\dot{\theta}_{\tilde{t}}\| \leq A$ and $\|\nabla\phi(\cdot)\|_\infty \leq B$. Using (13) we have

$$|\dot{\theta}_{\tilde{t}}^T\ \partial_\theta T_{\theta_{\tilde{t}}}(x)^T\ \nabla\phi(T_{\theta_{\tilde{t}}}(y))| \leq AB\|\partial_\theta T_{\theta_{\tilde{t}}}(x)\|_F \leq ABL(x).$$

Applying dominated convergence theorem, we obtain:

$$\frac{\partial}{\partial t}\left(\int \phi(T_{\theta_t}(x))dp\right)\Big|_{t=0} = \int \dot{\theta_t}^T \partial_\theta T_{\theta_t}(x)^T \nabla\phi(T_{\theta_t}(x))|_{t=0} dp. \tag{17}$$

Since $\frac{\partial}{\partial t}\int \phi(y)\rho_{\theta_t}(y)\ dy = \frac{\partial}{\partial t}\int \phi(T_{\theta_t}(x))\ dp(x)$, we use (16) and (17) to get:

$$\begin{aligned}
\int \phi(y)\frac{\partial \rho_{\theta_t}}{\partial t}(y)\Big|_{t=0}\ dy &= \int \dot{\theta_t}^T \partial_\theta T_{\theta_t}(x)^T \nabla\phi(T_{\theta_t}(x))|_{t=0}\ dp(x) \\
&= \int \dot{\theta}_t^T \left(\frac{\partial T_{\theta_t}}{\partial \theta}(T_{\theta_t}^{-1}(x))\right)^T \nabla\phi(x)\ \rho_{\theta_t}(x)|_{t=0}\ dx \\
&= \int \phi(x)\left(-\nabla\cdot\left(\rho_{\theta_t}(x)\frac{\partial T_{\theta_t}}{\partial \theta}(T_{\theta_t}^{-1}(x))\ \dot{\theta}_t\right)\right)|_{t=0}\ dx.
\end{aligned}$$

Because $\phi(x)$ is arbitrary, this weak formulation reveals that

$$(T_\#|_\theta)_*\xi(\theta) = \frac{\partial \rho_{\theta_t}}{\partial t}\Big|_{t=0} = -\nabla\cdot\left(\rho_\theta(x)\ \frac{\partial T_\theta}{\partial \theta}(T_\theta^{-1}(x))\xi(\theta)\right). \tag{18}$$

Now let us compute the metric tensor G. Since $T_\#$ is isometric immersion from Θ to $\mathcal{P}$, the pullback of g^W by $T_\#$ gives G, i.e. $(T_\#)^* g^W = G$. By definition of pullback map, for any $\xi \in T\Theta$ and for any $\theta \in \Theta$, we have:

$$G(\theta)(\xi(\theta), \xi(\theta)) = g^W(\rho_\theta)((T_\#|_\theta)_*\xi(\theta), (T_\#|_\theta)_*\xi(\theta)) \tag{19}$$

To compute the right hand side of (19), recall (8), we need to solve for φ from:

$$\frac{\partial \rho_{\theta_t}}{\partial t}\Big|_{t=0} = -\nabla\cdot(\rho_\theta(x)\nabla\varphi(x)) \tag{20}$$

By (18), (20) is:

$$\nabla\cdot(\rho_\theta(x)\nabla\varphi(x)) = \nabla\cdot\left(\rho_\theta(x)\frac{\partial_\theta T_\theta}{\partial\theta}(T_\theta^{-1}(\cdot))\xi(\theta)\right). \tag{21}$$

We can straightforwardly check that $\varphi(x) = \mathbf{\Psi}^T(x)\xi(\theta)$ is the solution of (21). Then $G(\theta)$ is given by

$$\begin{aligned}
G(\theta)(\xi,\xi) &= \int |\nabla\varphi(y)|^2\ \rho_\theta(y)\ dy = \int |\nabla\varphi(T_\theta(x))|^2\ dp(x) \\
&= \int |\nabla\mathbf{\Psi}(T_\theta(x))^T\xi|^2 dp(x) = \xi^T\left(\int \nabla\mathbf{\Psi}(T_\theta(x))\nabla\mathbf{\Psi}(T_\theta(x))^T dp(x)\right)\xi.
\end{aligned}$$

Thus we verify that

$$G(\theta) = \int \nabla \mathbf{\Psi}(T_\theta(x)) \nabla \mathbf{\Psi}(T_\theta(x))^T \, dp(x),$$

which completes the proof. □

Generally speaking, the metric tensor G does not have an explicit form when $d \geq 2$. When $d = 1$, G has an explicit form and can be computed directly.

Corollary 4.1. *When dimension $d = 1$, the metric tensor $G(\theta)$ has the following explicit form:*

$$G(\theta) = \int \partial_\theta T_\theta(x)^T \partial_\theta T_\theta(x) \, dp(x). \tag{22}$$

Proof. When $d = 1$, (15) is

$$\frac{d}{dx}\left(\rho_\theta(x) \frac{d}{dx}\psi_k(x)\right) = \frac{d}{dx}\left(\rho_\theta(x) \frac{\partial T_\theta}{\partial \theta_k}(T_\theta^{-1}(x))\right), \tag{23}$$

with boundary conditions $\lim_{x \to \pm\infty} \rho_\theta(x)\psi_k'(x) = 0$. Using (13), we know that $\partial_\theta T_\theta$ is $L^1(p)$ integrable and $\rho_\theta(\cdot)\frac{\partial T_\theta}{\partial \theta}(T_\theta^{-1}(\cdot))$ is Lebesgue integrable. Then we can find a sequence $\{x_m\} \to -\infty$, such that $\rho_\theta(x_m)\frac{\partial T_\theta}{\partial \theta_{\theta_k}}(T_\theta^{-1}(x_m)) \to 0$ as $m \to \infty$. Now for any $x \in \mathbb{R}$, integrate (23) from x_m to x and send $m \to \infty$ we get:

$$\rho_\theta(x)\psi_k'(x) = \rho_\theta(x) \frac{\partial T_\theta}{\partial \theta_k}(T_\theta^{-1}(x)).$$

On the support of ρ_θ, we have $\psi_k'(x) = \frac{\partial T_\theta}{\partial \theta_k}(T_\theta^{-1}(x))$, thus we have:

$$G_{ij}(\theta) = \int \psi_i'(x)\psi_j'(x)\rho_\theta(x) \, dx = \int \partial_{\theta_i} T_\theta(x) \partial_{\theta_j} T_\theta(x) \, dp(x).$$

This finishes the proof. □

Following theorem given in [27], we can verify the positive definiteness of the metric tensor G:

Theorem 5. *G is a Riemannian metric if and only if for each $\theta \in \Theta$, any $\xi \in T_\theta\Theta$ ($\xi \neq 0$), there exists $z \in M$ such that $\nabla \cdot (\rho_\theta(z)\frac{\partial T_\theta}{\partial \theta}(T_\theta^{-1}(z))\xi) \neq 0$.*

Proof. We first establish the following identity according to Theorem 4. For any θ, ξ, x, we have

$$\nabla \cdot (\rho_\theta(x) \nabla(\xi^T \mathbf{\Psi}(x))) = \nabla \cdot (\rho_\theta(x) \frac{\partial T_\theta}{\partial \theta}(T_\theta^{-1}(x))\xi). \tag{24}$$

($\Leftarrow$): suppose for any $\theta \in \Theta$ and $\xi \in T_\theta\Theta$, at certain $z \in \mathbb{R}^d$, $\nabla \cdot (\rho_\theta(z)\frac{\partial T_\theta}{\partial \theta}(T_\theta^{-1}(z)\xi) \neq 0$, then $\nabla \cdot (\rho_\theta(z)\nabla(\xi^T \mathbf{\Psi}(z))) \neq 0$, thus $\rho_\theta \nabla(\xi^T \mathbf{\Psi})$ is not identically $\mathbf{0}$. Using continuity of $\rho_\theta \nabla(\xi^T \mathbf{\Psi})$, we know that: $|\nabla(\xi^T \mathbf{\Psi}(x))|^2 \rho_\theta(x) > 0$ in some small neighbourhood of z. Thus we have:

$$\xi^T G(\theta) \xi = \int |\nabla \mathbf{\Psi}(x)^T \xi|^2 \rho_\theta(x) \, dx > 0, \tag{25}$$

holds for any θ and ξ, this leads to the positive definiteness of G.
($\Rightarrow$): Now, (25) holds for all θ, ξ. We have

$$\int -\nabla \cdot (\rho_\theta(x) \nabla(\xi^T \mathbf{\Psi}(x))) \cdot \xi^T \mathbf{\Psi}(x) \, dx > 0.$$

This leads to the existence of a $z \in \mathbb{R}^d$ such that $-\nabla \cdot (\rho_\theta(z)\nabla(\xi^T \mathbf{\Psi}(z))) \neq 0$. Combining (24), we complete the proof. □

A more intuitive way to understand the positive definiteness of $G(\theta)$ is illustrated in the following theorem:

Theorem 6. *For $\theta \in \Theta$, $\{\psi_k\}_{k=1}^m$ satisfies (15), then $G(\theta)$ is positive definite if and only if $\{\nabla\psi_k\}_{k=1}^m$, when considered as m vectors in the space $L^2(\mathbb{R}^d; \mathbb{R}^d, \rho_{\theta_k})$, are linearly independent.*

To keep our discussion concise in the following sections, we will always assume $G(\theta)$ is positive definite for every $\theta \in \Theta$.

3.2 Parametric Fokker-Planck equation

We consider the pushforward $T_\#$ induced relative entropy functional $H = \mathcal{H} \circ T_\# : \Theta \to \mathbb{R}$,

$$H(\theta) = \mathcal{H}(\rho_\theta) = \int V(x)\rho_\theta(x)\ dx + \beta \int \rho_\theta(x) \log \rho_\theta(x)\ dx = \int V(T_\theta(x)) + \beta \log \rho_\theta(T_\theta(x))\ dp(x). \quad (26)$$

Following the theory in [1], the gradient flow of H on Wasserstein parameter manifold (Θ, G) satisfies

$$\dot{\theta} = -G(\theta)^{-1}\nabla_\theta H(\theta). \quad (27)$$

We call (27) *parametric Fokker-Planck equation*. The ODE (27) as the Wasserstein gradient flow on parameter space (Θ, G) is closely related to Fokker-Planck equation on probability submanifold $\mathcal{P}_\Theta$. We have the following theorem, which is a natural result derived from submanifold geometry.

Theorem 7. *Suppose $\{\theta_t\}_{t\geq 0}$ solves (27). Then $\{\rho_{\theta_t}\}$ is the gradient flow of $\mathcal{H}$ on probability submanifold $\mathcal{P}_\Theta$. Furthermore, at any time t, $\dot{\rho}_{\theta_t} = \frac{d}{dt}\rho_{\theta_t} \in T_{\rho_{\theta_t}}\mathcal{P}_\Theta$ is the orthogonal projection of $-grad_W \mathcal{H}(\rho_{\theta_t}) \in T_{\rho_{\theta_t}}\mathcal{P}$ onto the subspace $T_{\rho_{\theta_t}}\mathcal{P}_\Theta$ with respect to the Wasserstein metric g^W.*

Theorem 7 easily follows from the following two general results about manifold gradient.

Theorem 8. *Suppose $(N, g^N), (M, g^M)$ are Riemannian Manifolds. Suppose $\varphi : N \to M$ is isometry. Consider $\mathcal{F} \in \mathcal{C}^\infty(M)$, define $F = \mathcal{F} \circ \varphi \in \mathcal{C}^\infty(N)$. Suppose $\{x_t\}_{t\geq 0}$ is the gradient flow of F on N:*

$$\dot{x} = -grad_N F(x).$$

Then $\{y_t = \varphi(x_t)\}_{t\geq 0}$ is the gradient flow of $\mathcal{F}$ on M. That is, $\{y_t\}$ satisfies $\dot{y} = -grad_M \mathcal{F}(y)$.

Proof. Since we always have $\dot{y}_t = \varphi_* \dot{x}_t = -\varphi_* \mathrm{grad}_N F(x_t)$, we only need to show that $\varphi_* \mathrm{grad}_N F(x_t) = \mathrm{grad}_M \mathcal{F}(\varphi(x_t))$. Fix the time t, consider any curve $\{\xi_\tau\}$ on N passing through x_t at $\tau = 0$, since φ is isometry, we have $g^N = \varphi^* g^M$, thus:

$$\frac{d}{d\tau} F(\xi_\tau)\Big|_{\tau=0} = g^N(\mathrm{grad}_N F(x_t), \dot{\xi}_0) = \varphi^* g^M(\mathrm{grad}_N F(x_t), \dot{\xi}_0) = g^M(\varphi_* \mathrm{grad}_N F(x_t), \varphi_* \dot{\xi}_0).$$

On the other hand, denote $\eta_\tau = \varphi(\xi_\tau)$, we have:

$$\frac{d}{d\tau} F(\xi_\tau)\Big|_{\tau=0} = \frac{d}{d\tau} \mathcal{F}(\eta_\tau)\Big|_{\tau=0} = g^M(\mathrm{grad}_M \mathcal{F}(y_t), \dot{\eta}_0) = g^M(\mathrm{grad}_M \mathcal{F}(y_t), \varphi_* \dot{\xi}_0).$$

As a result, $g^M(\varphi_* \mathrm{grad}_N F(x_t) - \mathrm{grad}_M \mathcal{F}(y_t), \varphi_* \dot{\xi}_0) = 0$ for all $\dot{\xi}_0 \in T_{x_t} N$. Since φ_* is surjective, we have $\varphi_* \mathrm{grad}_N F(x_t) = \mathrm{grad}_M \mathcal{F}(\varphi(x_t))$.

□

Theorem 9. *Suppose (M, g^M) is Riemannian manifold, $M_{sub} \subset M$ is the submanifold of M. Assume M_{sub} inherits metric g^M, i.e. define $\iota : M_{sub} \to M$ as the inclusion map, then ι is isometry: $g^{M_{sub}} = \iota^* g^M$. For any $\mathcal{F} \in \mathcal{C}^\infty(M)$, we denote the restriction of $\mathcal{F}$ on M_{sub} as $\mathcal{F}^{sub}$. Then the gradient $grad_{M_{sub}} \mathcal{F}^{sub}(x) \in T_x M_{sub}$ is the orthogonal projection of $grad_M \mathcal{F}(x) \in T_x M$ onto subspace $T_x M_{sub}$ with respect to the metric g^M for any $x \in M_{sub}$.*

Proof. For any $x \in M_{\mathrm{sub}}$, consider any curve $\{\gamma_\tau\}$ on M_{sub} passing through x at $\tau = 0$. We have

$$\frac{d}{d\tau} \mathcal{F}^{\mathrm{sub}}(\gamma_\tau)\Big|_{\tau=0} = g^{M_{\mathrm{sub}}}(\mathrm{grad}_{M_{\mathrm{sub}}} \mathcal{F}^{\mathrm{sub}}(x), \dot{\gamma}_0) = g^M(\iota_* \mathrm{grad}_{M_{\mathrm{sub}}} \mathcal{F}^{\mathrm{sub}}(x), \iota_* \dot{\gamma}_0) = g^M(\mathrm{grad}_{M_{\mathrm{sub}}} \mathcal{F}^{\mathrm{sub}}(x), \dot{\gamma}_0).$$

The last equality is because ι_* restricted on TM_{sub} is identity. On the other hand, $\mathcal{F}^{\mathrm{sub}}(\gamma_\tau) = \mathcal{F}(\gamma_\tau)$ for all τ. We also have:

$$\frac{d}{d\tau} \mathcal{F}^{\mathrm{sub}}(\gamma_\tau)\Big|_{\tau=0} = g^M(\mathrm{grad}_M \mathcal{F}(x) \dot{\gamma}_0).$$

Combining them we know

$$g^M(\mathrm{grad}_{M_{\mathrm{sub}}} \mathcal{F}^{\mathrm{sub}}(x) - \mathrm{grad}_M \mathcal{F}(x), v) \quad \forall\ v \in T_x M_{\mathrm{sub}} \Rightarrow \mathrm{grad}_{M_{\mathrm{sub}}} \mathcal{F}^{\mathrm{sub}}(x) - \mathrm{grad}_M \mathcal{F}(x) \perp_{g^M} T_x M_{\mathrm{sub}},$$

which proves this result. □

Proof. (Theorem 7) To prove the first part of Theorem 7, we apply Theorem 8 with $(N, g^N) = (\Theta, G)$, $M = \mathcal{P}_\Theta$ with its metric inherited from $(\mathcal{P}, g^W)$ and $\varphi = T_\#$. To prove the second part, we apply Theorem 9 with $(M, g^M) = (\mathcal{P}, g^W)$, $M_{\text{sub}} = \mathcal{P}_\Theta$. □

The following theorem is closely related to Theorem 7 and useful for our future discussions.

Theorem 10 (Wasserstein gradient as solution to a least squares problem)**.** *For a fixed $\theta \in \Theta$, $\boldsymbol{\Psi} \subset \mathbb{R}^m$ as defined in Theorem 4, then*

$$G(\theta)^{-1}\nabla_\theta H(\theta) = \underset{\eta \in T_\theta\Theta \cong \mathbb{R}^m}{\arg\min} \left\{ \int |(\nabla \boldsymbol{\Psi}(T_\theta(x)))^T \eta - \nabla \left(V + \beta \log \rho_\theta\right) \circ T_\theta(x)|^2 dp(x) \right\}. \tag{28}$$

Proof. Direct computation shows that minimizing the function in (28) is equivalent to minimizing:

$$\eta^T \left(\int \nabla \boldsymbol{\Psi}(T_\theta(x)) \nabla \boldsymbol{\Psi}(T_\theta(x))^T \, dp(x) \right) \eta - 2 \, \eta^T \left(\int \nabla \boldsymbol{\Psi}(y) \nabla (V(y) + \beta \log \rho(y)) \rho_\theta(y) \, dy \right).$$

For each entry in the second term, we have:

$$\begin{aligned}
&\int \nabla \psi_k(y) \cdot \nabla (V(y) + \beta \log \rho_\theta(y)) \rho_\theta(y) \, dy = \int -\nabla \cdot (\rho_\theta(y) \nabla \psi_k(y)) \cdot (V(y) + \beta \log \rho_\theta(y)) \, dy \\
&= \int -\nabla \cdot (\rho_\theta(y) \partial_{\theta_k} T_\theta(T_\theta^{-1}(y))) \cdot (V(y) + \beta \log \rho_\theta(y)) \, dy \\
&= \partial_{\theta_k} \left(\int (V(T_\theta(x)) + \beta \log \rho_\theta(T_\theta(x))) \, dp(x) \right) = \partial_{\theta_k} H(\theta).
\end{aligned}$$

Recall the definition (14) of $G(\theta)$, the target function to be minimized is $\eta^T G(\theta) \eta - 2\eta^T \nabla_\theta H(\theta)$. And the minimizer is clearly $G(\theta)^{-1}\nabla_\theta H(\theta)$. □

In addition to the direct proof, the result in Theorem 10 can also be understood in a different way. Let us denote $\xi = G(\theta)^{-1}\nabla_\theta H(\theta)$, $\{\theta_t\}$ solves (27) with initial value $\theta_0 = \theta$. By Theorem 7, $\frac{d}{dt}\rho_{\theta_t}\Big|_{t=0} = (T_\#|_\theta)_* \xi \in T_{\rho_\theta}\mathcal{P}_\Theta$ is the orthogonal projection of $\text{grad}_W \mathcal{H}(\rho_\theta)$ onto $T_{\rho_\theta}\mathcal{P}_\Theta$ with respect to the metric g^W. This is equivalent to say that η solves the following least square problem:

$$\min_\eta g^W(\text{grad}_W \mathcal{H}(\rho_\theta) - (T_\#|_\theta)_* \eta, \ \text{grad}_W \mathcal{H}(\rho_\theta) - (T_\#|_\theta)_* \eta). \tag{29}$$

Recall the definition of g^W in section 2.2.1 and by (10), we have $\text{grad}_W \mathcal{H}(\rho_\theta) = -\nabla \cdot (\rho_\theta \nabla (V + \beta \log \rho_\theta))$. Because of (18), $(T_\#|_\theta)_* \eta = -\nabla \cdot (\rho_\theta \partial_\theta T_\theta(T_\theta^{-1}(\cdot))\eta)$, solving $-\nabla \cdot (\rho_\theta \nabla \varphi) = \text{grad}_W \mathcal{H}(\rho_\theta) - (T_\#|_\theta)_* \eta$ gives

$$\varphi = (V + \beta \log \rho_\theta) - \boldsymbol{\Psi}^T \eta,$$

and thus least squares problem (29) can be written as

$$\min_\eta \left\{ \int |\nabla \boldsymbol{\Psi}(x)^T \eta - \nabla (V(x) + \beta \log \rho_\theta(x))|^2 \rho_\theta(x) \, dx \right\},$$

which is exactly (28).

3.3 A particle viewpoint of the parametric Fokker Planck Equation

The motion of parameter θ_t solving (27) naturally induce a stochastic dynamics on $\mathbb{R}^d$ whose density evolution is exactly $\{\rho_{\theta_t}\}$. To see this, notice that $\{\theta_t\}$ directly leads to a time dependent map $\{T_{\theta_t}\}$. Let us denote a random variable $\boldsymbol{Z} \sim p$, i.e. $\boldsymbol{Z}$ is distributed according to the reference distribution p. We set $\boldsymbol{Y}_0 = T_{\theta_0}(\boldsymbol{Z}) \sim \rho_{\theta_0}$. At any time t, the map T_{θ_t} sends $\boldsymbol{Y}_0$ to $\boldsymbol{Y}_t = T_{\theta_t}(T_{\theta_0}^{-1}(\boldsymbol{Y}_0)) \sim \rho_{\theta_t}$. Thus, we construct a sequence of random variables $\{\boldsymbol{Y}_t\}$ whose density evolution is exactly $\{\rho_{\theta_t}\}$. We can characterize the

dynamical system satisfied by $\{\boldsymbol{Y}_t\}$ by taking time derivative: $\dot{\boldsymbol{Y}}_t = \partial_\theta T_{\theta_t}(\boldsymbol{Z})\dot{\theta}_t = \partial_\theta T_{\theta_t}(T_{\theta_t}^{-1}(\boldsymbol{Y}_t))\dot{\theta}_t$. It is actually more insightful to consider the following dynamic:

$$\dot{\boldsymbol{X}}_t = \nabla \boldsymbol{\Psi}_t(\boldsymbol{X}_t)^T \ \dot{\theta}_t, \quad \boldsymbol{X}_0 = T_{\theta_0}(\boldsymbol{Z}) \sim \rho_{\theta_0}. \tag{30}$$

Here $\boldsymbol{\Psi}_t$ is obtained from (15) with parameter θ_t. It is not hard to show that for any time t, $\boldsymbol{X}_t$ and $\boldsymbol{Y}_t$ has the same distribution. Thus $\boldsymbol{X}_t \sim \rho_{\theta_t}$ for all $t \geq 0$. Recall $\dot{\theta}_t = -G(\theta_t)^{-1}\nabla_\theta H(\theta_t)$, we are able to rewrite (30) as:

$$\dot{\boldsymbol{X}}_t = \nabla \boldsymbol{\Psi}_t(\boldsymbol{X}_t)^T \underbrace{\left(\int \nabla \boldsymbol{\Psi}_t(x)\nabla \boldsymbol{\Psi}_t(x)^T \ \rho_{\theta_t}(x) \ dx\right)}_{G(\theta_t)}{}^{-1} \underbrace{\left(\int \nabla \boldsymbol{\Psi}_t(\eta)(-\nabla V(\eta) - \beta \nabla \log \rho_{\theta_t}(\eta)) \ \rho_{\theta_t}(\eta) \ d\eta\right)}_{-\nabla_\theta H(\theta_t)}. \tag{31}$$

If we define the kernel function $K_\theta : \mathbb{R}^d \times \mathbb{R}^d \to \mathbb{R}^{d\times d}$ as

$$K_\theta(x,\eta) = \nabla \boldsymbol{\Psi}^T(x) \left(\int \nabla \boldsymbol{\Psi}(x)\nabla \boldsymbol{\Psi}(x)^T \ \rho_\theta(x) \ dx\right)^{-1} \nabla \boldsymbol{\Psi}(\eta).$$

This K_θ induces a linear operator $\mathcal{K}_\theta : L^2(\mathbb{R}^d;\mathbb{R}^d,\rho_\theta) \to L^2(\mathbb{R}^d;\mathbb{R}^d,\rho_\theta)$ by:

$$\mathcal{K}_\theta[\vec{v}] = (\mathcal{K}_\theta * \vec{v})(\cdot) = \int K_\theta(\cdot,\eta) \ \vec{v}(\eta) \ \rho_\theta(\eta) \ d\eta.$$

It can be verified that $\mathcal{K}_\theta$ is an orthogonal projection defined on the Hilbert space $L^2(\mathbb{R}^d;\mathbb{R}^d,\rho_\theta)$. The range of such projection is the subspace span $\{\nabla\psi_1, ..., \nabla\psi_m\} \subset L^2(\mathbb{R}^d;\mathbb{R}^d,\rho_\theta)$. Here $\psi_1, ..., \psi_m$ are the m components of $\boldsymbol{\Psi}$ solved from (15). Using the linear operator, we can rewrite (31) as:

$$\dot{\boldsymbol{X}}_t = -\mathcal{K}_{\theta_t}[\nabla V + \beta \nabla \log \rho_{\theta_t}](\boldsymbol{X}_t), \quad \text{where } \rho_{\theta_t} \text{ is the probability density of } \boldsymbol{X}_t \quad \boldsymbol{X}_0 \sim \rho_{\theta_0}. \tag{32}$$

We can compare (32) with the following dynamic without projection:

$$\dot{\tilde{\boldsymbol{X}}}_t = -(\nabla V + \beta \nabla \log \rho_t)(\tilde{\boldsymbol{X}}_t), \quad \text{where } \rho_t \text{ is the probability density of } \tilde{\boldsymbol{X}}_t \quad \boldsymbol{X}_0 \sim \rho_0. \tag{33}$$

As discussed in section 2.1, (33) is the Vlasov-type SDE that involves the density of random particle. If assuming (33) admits a regular solution, we have $\rho(x,t) = \rho_t(x)$, which solves the original Fokker Planck equation (5). From orthogonal projection viewpoint, we can treat that the approximate solution ρ_{θ_t} of (5) is actually originated from the projection of vector field that drives the SDE (33).

We would like to mention that the expectation of ℓ^2 discrepancy between $\nabla V + \beta \nabla \log \rho$ and its $\mathcal{K}_\theta$ projection is:

$$\mathbb{E}_{\boldsymbol{X}\sim\rho_\theta}|\mathcal{K}_\theta[\nabla V + \beta \nabla \log \rho_\theta](\boldsymbol{X}) - (\nabla V + \beta \nabla \log \rho_\theta)(\boldsymbol{X})|^2 = \int |\nabla \boldsymbol{\Psi}(x)^T \xi - (-\nabla V - \beta \nabla \log \rho_\theta)(x)|^2 \rho_\theta(x) \ dx, \tag{34}$$

in which $\xi = -G(\theta)^{-1}\nabla_\theta H(\theta)$. This is an essential term appeared in our error analysis part.

Remark 2. *We should mention the relationship between our kernel K_{θ_t} and the Neural Tangent Kernel (NTK) introduced in [16]. Using our notation, Neural Tangent Kernel can be written as $K_\theta^{NTK} = \partial_\theta T_\theta(x)\partial_\theta T_\theta(\xi)^T$. If we consider the flat gradient flow $\dot{\theta} = -\nabla_\theta H(\theta)$ of relative entropy on Θ, its corresponding particle dynamic is*

$$\dot{\boldsymbol{X}}_t = \int K_{\theta_t}^{NTK}(T_{\theta_t}^{-1}(\boldsymbol{X}_t), T_{\theta_t}^{-1}(\eta))(-\nabla V(\eta) - \beta \nabla \log \rho_{\theta_t}(\eta))\rho_{\theta_t}(\eta) \ d\eta$$

Different from our K_θ, which introduces an orthogonal projection, Neural Tangent Kernel introduces an non-negative definite transform to the vector field $-\nabla V - \beta \nabla \log \rho_{\theta_t}$.

Remark 3. *Figure 1 illustrates the relation between* (5)*,* (27)*,* (33) *and* (32)*. It is worth mentioning that the probability manifold point of view discussed in Theorem 7 is useful for our analysis of the continuous dynamics* (27)*, while particle point of view helps us on establishing the numerical analysis for the time discrete scheme (i.e. forward-Euler) of* (27)*.*

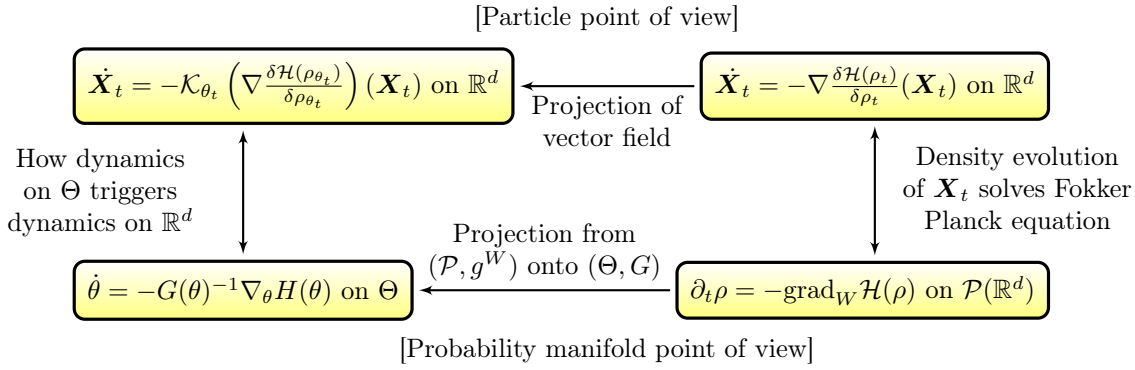

Figure 1: Illustrative diagram

3.4 An example of parametric Fokker-Planck equation with quadratic potential

The solution of parametric Fokker-Planck equation (27) can serve as an approximation to the solution of the original equation (5). In some special cases, ρ_{θ_t} exactly solves (5). In this section, we provide such examples.

Let us consider Fokker-Planck equations with quadratic potentials whose initial conditions are Gaussian:

$$V(x) = \frac{1}{2}(x-\mu)^T\Sigma^{-1}(x-\mu) \quad \text{and} \quad \rho_0 \sim \mathcal{N}(\mu_0, \Sigma_0). \tag{35}$$

Here $\mathcal{N}(\mu, \Sigma)$ denotes Gaussian distribution with mean μ and covariance Σ. We consider parameter space $\Theta = (\Gamma, b) \subset \mathbb{R}^m$ $(m = d(d+1))$, where Γ is a $d \times d$ invertible matrix with $\det(\Gamma) > 0$ and $b \in \mathbb{R}^d$. We define the parametric map as $T_\theta(x) = \Gamma x + b$, and choose the reference measure $p = \mathcal{N}(0, I)$.

Lemma 11. *Let $\mathcal{H}$ be the relative entropy defined in (11) and H defined in (26). For $\theta \in \Theta$, if the vector function $\nabla\left(\frac{\delta \mathcal{H}}{\delta \rho}\right) \circ T_\theta$ can be written as the linear combination of $\{\frac{\partial T_\theta}{\partial \theta_1}, ..., \frac{\partial T_\theta}{\partial \theta_m}\}$, i.e. there exists $\zeta \in \mathbb{R}^m$, such that $\nabla\left(\frac{\delta \mathcal{H}}{\delta \rho}\right) \circ T_\theta(x) = \partial_\theta T_\theta(x)\zeta$. Then:*
1) $\zeta = G(\theta)^{-1}\nabla_\theta H(\theta)$, which is the Wasserstein gradient of F at θ.
2) $\mathrm{grad}_W \mathcal{H}(\rho_\theta)|_{\mathcal{P}_\Theta} = \mathrm{grad}_W \mathcal{H}(\rho_\theta)$, where $\mathrm{grad}_W \mathcal{H}(\rho_\theta)|_{\mathcal{P}_\Theta}$ is the gradient of $\mathcal{H}$ on the submanifold $\mathcal{P}_\Theta$.

Proof. Suppose that $\zeta \in \mathbb{R}^m$ satisfies $\nabla\left(\frac{\delta \mathcal{H}}{\delta \rho}\right) \circ T_\theta(x) = \partial_\theta T_\theta(x)\zeta$, then we have

$$\int |\partial_\theta T_\theta(x)\zeta - \nabla(\frac{\delta \mathcal{H}}{\delta \rho}) \circ T_\theta(x)|^2 \, dp(x) = 0.$$

We apply Lemma 14, (14) and

$$(\nabla \boldsymbol{\Psi})^T\zeta - \nabla\left(\frac{\delta \mathcal{H}}{\delta \rho}\right) = \mathrm{Proj}_{\rho_\theta}[\partial_\theta T_\theta \circ T_\theta^{-1}\zeta - \nabla\left(\frac{\delta \mathcal{H}}{\delta \rho}\right)]$$

to obtain:

$$\int |(\nabla \boldsymbol{\Psi}(T_\theta(x)))^T\zeta - \nabla\left(\frac{\delta \mathcal{H}}{\delta \rho}\right) \circ T_\theta(x)|^2 \, dp(x) \le 0.$$

This implies,

$$\inf_\eta \int |(\nabla \boldsymbol{\Psi}(T_\theta(x)))^T\eta - \nabla\left(\frac{\delta \mathcal{H}}{\delta \rho}\right) \circ T_\theta(x)|^2 \, dp(x) = \int |(\nabla \boldsymbol{\Psi}(T_\theta(x)))^T\zeta - \nabla\left(\frac{\delta \mathcal{H}}{\delta \rho}\right) \circ T_\theta(x)|^2 \, dp(x) = 0.$$

By Theorem 10, we get $\zeta = G(\theta)^{-1}\nabla_\theta H(\theta)$ and $\|(T_\#|_\theta)_*\zeta - \mathrm{grad}_W \mathcal{H}(\rho_\theta)\|_{g^W(\rho_\theta)} = 0$. According to Theorem 7, $\mathrm{grad}_W \mathcal{H}(\rho_\theta)|_{\mathcal{P}_\Theta} = (T_\#|_\theta)_*\zeta$, we get $\mathrm{grad}_W \mathcal{H}(\rho_\theta)|_{\mathcal{P}_\Theta} = \mathrm{grad}_W \mathcal{H}(\rho_\theta)$. □

Back to our example with quadratic potential (35) and $T_\theta(x) = \Gamma x + b$, we can compute

$$\rho_\theta(x) = T_{\theta\#}p(x) = \frac{f(T_\theta^{-1}(x))}{|\det(\Gamma)|} = \frac{f(\Gamma^{-1}(x-b))}{|\det(\Gamma)|},\ f(x) = \frac{\exp(-\frac{1}{2}|x|^2)}{(2\pi)^{\frac{d}{2}}}.$$

Then we have,

$$\nabla\left(\frac{\delta\mathcal{H}(\rho_\theta)}{\delta\rho}\right)\circ T_\theta(x) = \nabla(V+\beta\log\rho_\theta)\circ T_\theta(x) = \Sigma^{-1}(\Gamma x + b - \mu) - \beta\Gamma^{-T}x,$$

which is affine with respect to x.

Notice that $\partial_{\Gamma_{ij}}T_\theta(x) = (\dots,0,\dots,\underset{i-\text{th}}{x_j},\dots,0,\dots)^T$ and $\partial_{b_i}T_\theta = (\dots,0,\dots,\underset{i-\text{th}}{1},\dots,0,\dots)^T$, we can verify that $\zeta = (\Sigma^{-1}\Gamma - \beta\Gamma^{-T}, \Sigma^{-1}(b-\mu))$ solves $\nabla\left(\frac{\delta\mathcal{F}(\rho_\theta)}{\delta\rho}\right)\circ T_\theta(x) = \partial_\theta T_\theta(x)\zeta$. By 1) of Lemma 11, $\zeta = G(\theta)^{-1}\nabla_\theta F(\theta)$. Thus ODE (27) for our example is:

$$\dot{\Gamma} = -\Sigma^{-1}\Gamma + \beta\Gamma^{-T} \quad \Gamma_0 = \sqrt{\Sigma_0}, \tag{36}$$

$$\dot{b} = \Sigma^{-1}(\mu - b) \quad b_0 = \mu_0. \tag{37}$$

By 2) of Lemma 11, we know $\text{grad}_{\text{W}}\mathcal{H}(\rho_\theta)|_{\mathcal{P}_\Theta} = \text{grad}_{\text{W}}\mathcal{H}(\rho_\theta)$ for all $\theta\in\Theta$, which indicates that there is no error between our parametric Fokker-Planck and the original equations.

Following the equations (36) and (37), we have the following corollary,

Corollary 11.1. *The solution of Fokker-Planck equation (5) with condition(35) is a Gaussian distribution for all $t > 0$.*

Proof. If we denote $\{\Gamma_t, b_t\}$ as the solutions to (36),(37), set $\theta_t = (\Gamma_t, b_t)$, then $\rho_t = T_{\theta_t\#}p$ solves the Fokker Planck Equation (5) with conditions (35). Since the pushforward of Gaussian distribution p by an affine transform T_θ is still a Gaussian, we conclude that for any $t > 0$, the solution $\rho_t = T_{\theta_t\#}p$ is always Gaussian distribution. □

Remark 4. *This is already a well known property for Ornstein–Uhlenbeck process [11]. We provide an alternative proof using our framework.*

4 Numerical methods

In this section, we introduce our sampling efficient numerical method to compute the proposed parametric Fokker-Planck equations.

Before we start, we want to mention that when dimension $d = 1$, $G(\theta)$ has explicit solution according to Corollary 4.1. Thus the push-forward approximation of 1D Fokker-Planck equation can be directly computed by solving the ODE system (27) with numerical methods, such as forward-Euler scheme [27]. In this section, our focus is on numerical methods for (27) with dimension $d \geq 2$. It turns out to be very challenging to compute (27) by the forward-Euler scheme directly. There are two reasons. One is that there is no known explicit formula for $G(\theta)$, and direct computation based on (14) can be expansive because it requires to solve multiple differential equations. The other is incurred by the high dimensionality, which is the main goal of this paper. To overcome the challenge of dimensionality, we choose to use deep neural networks to construct our $T(\theta)$. However, directly evaluating $G(\theta)^{-1}\nabla_\theta H(\theta)$ is difficult, alternative strategies must be sought.

There are a few papers investigating numerical methods for gradient flows on Riemannian manifolds, such as Fisher natural gradient [33] and Wasserstein gradient [9]. The well known JKO scheme [18] calculates the time discrete approximation of the Wasserstein gradient flow using an optimization formulation,

$$\partial_t\rho_t = -\text{grad}_W\mathcal{F}(\rho_t) \quad \Longleftrightarrow \quad \rho_{k+1} = \underset{\rho\in\mathcal{P}}{\text{argmin}}\left\{\frac{W_2^2(\rho,\rho_k)}{2h} + \mathcal{F}(\rho)\right\}, \tag{38}$$

where h is the time step size, $\mathcal{F}$ could be a suitable functional defined on $\mathcal{P}$. Along the line of JKO scheme, there are further developments in machine learning recently [26].

In our approach, we design schemes that computes the exact Wasserstein gradient flow directly with provable accuracy guarantee. Our algorithms are completely sample based so that they can be run efficiently under deep learning framework, and can scale up to high dimensional cases.

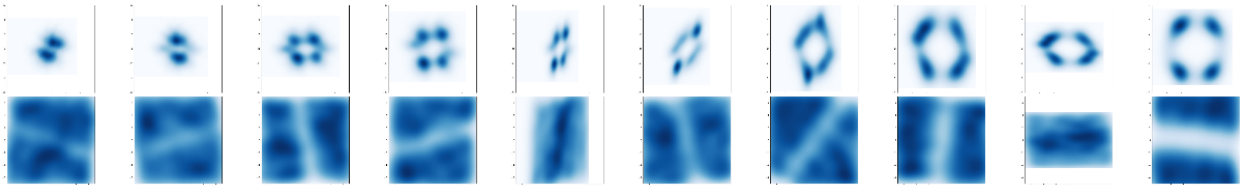

Figure 2: Top row from left to right are the probability densities of distributions $f_{1\#}p, (f_2 \circ f_1)_{\#}p, ..., (f_{10} \circ f_9 \circ ... \circ f_1)_{\#}p$. The last image displays our target distribution. Bottom row displays the push-forward effect of each single-layer transformation f_k $(1 \leq k \leq 10)$.

4.1 Normalizing Flow as push forward maps

We choose T_θ as the so-called normalizing flow [43]. Here is a brief sketch of its structure: T_θ is written as the composition of K invertible nonlinear transforms:

$$T_\theta = f_K \circ f_{K-1} \circ ... \circ f_2 \circ f_1,$$

where each f_k $(1 \leq k \leq K)$ takes the form

$$f_k(x) = x + h(w_k^T x + b_k)u_k.$$

Here $w_k, u_k \in \mathbb{R}^d$, $b_k \in \mathbb{R}$, and h is a nonlinear function, which can be chosen as tanh for example. In [43], it has been shown that f_k is invertible iff $w_k^T u_k \geq -1$. Figure 2 shows several snapshots of how a normalizing flow T_θ with length equal to 10 pushes forward standard Gaussian distribution to a target distribution.

In a normalizing flow, the parameters are: $\theta = (w_1, u_1, b_1, ..., w_K, u_K, b_K)$. The determinant of the Jacobi matrix of T_θ, an important quantity for our schemes, can be explicitly computed by

$$\mathbf{det}\left(\frac{\partial T_\theta(x)}{\partial x}\right) = \prod_{k=1}^{K}(1 + h'(w_k^T x_k + b_k)w_k^T u_k),$$

where $x_k = f_k \circ f_{k-1} \circ ... \circ f_1(x)$. Using the structure of normalizing flow, the logarithm of the density $\rho_\theta = T_{\theta\#}p$ can be written as

$$\log \rho_\theta(x) = \log p \circ t_\theta^{-1}(x) + \sum_{k=1}^{K} \log(1 + h'(w_k^T \tilde{x}_k)w_k^T u_k), \quad \tilde{x}_k = f_k \circ ... \circ f_1(T_\theta^{-1}(x)) = f_{k+1}^{-1} \circ ... \circ f_K^{-1}(x). \tag{39}$$

Then we can explicitly write the relative entropy functional $H(\theta)$ defined in (26) as,

$$H(\theta) = \mathbb{E}_{\mathbf{X}\sim p}[V(T_\theta(\mathbf{X})) + \mathcal{L}_\theta(\mathbf{X})], \tag{40}$$

where $\mathcal{L}_\theta$ is defined by,

$$\mathcal{L}_\theta(\cdot) = \log p(\cdot) + \sum_{k=1}^{K} \log(1 + h'(w_k^T F_k(\cdot))w_k^T u_k) \quad F_k(\cdot) = f_k \circ f_{k-1} \circ ... \circ f_1(\cdot).$$

Once $H(\theta)$ is computed explicitly, so does the gradient $\nabla_\theta H(\theta)$.

In summary, we choose the normalizing flow because it has sufficient expression power to approximate complicated distributions on $\mathbb{R}^d$ [43], and the relative entropy $H(\theta)$ has a very concise form (40), and its gradient can be conveniently computed.

Remark 5. *We want to emphasize here that the normalizing flow is not the only choice for T_θ. One may choose other network structures as long as they have sufficient approximation power and can compute the gradient of relative entropy efficiently.*

4.2 Numerical scheme

Our scheme is inspired by the following semi-implicit scheme of (27),

$$\frac{\theta_{k+1}-\theta_k}{h} = -G^{-1}(\theta_k)\nabla_\theta H(\theta_{k+1}).$$

Equivalently, we can write it as a proximal algorithm,

$$\theta_{k+1} = \operatorname*{argmin}_{\theta} \left\{ \langle \theta-\theta_k, G(\theta_k)(\theta-\theta_k)\rangle + 2hH(\theta) \right\}. \tag{41}$$

The main difficulty is to find an efficient way to compute $\langle \theta-\theta_k, G(\theta_k)(\theta-\theta_k)\rangle$. This is what we focus in the following derivation. Let us recall the definition (14) of $G(\theta_k)$. If setting $\psi(x) = (\theta-\theta_k)^T\mathbf{\Psi}(x)$, we have the expression $\int |\nabla\psi(x)|^2\rho_{\theta_k}(x)\ dx = \langle \theta-\theta_k, G(\theta_k)(\theta-\theta_k)\rangle$. We know that ψ satisfies

$$-\nabla\cdot(\rho_{\theta_k}(x)\nabla\psi(x)) = -\nabla\cdot(\rho_{\theta_k}(x)\partial_\theta T_{\theta_k}(T_{\theta_k}^{-1}(x))(\theta-\theta_k)). \tag{42}$$

We replace $\partial_\theta T_{\theta_k}(T_{\theta_k}^{-1}(x))(\theta-\theta_k)$ by a finite difference approximation $(T_\theta - T_{\theta_k})\circ T_{\theta_k}^{-1}(x)$ and denote $\hat{\psi}$ as the solution of (42) after this replacement. Furthermore, let us define

$$\mathcal{E}(\phi) = \int (2\nabla\phi(x)\cdot((T_\theta - T_{\theta_k})\circ T_{\theta_k}^{-1}(x)) - |\nabla\phi(x)|^2)\rho_{\theta_k}(x)\ dx. \tag{43}$$

It is easy to verify that $\hat{\psi}$ solves the variational problem: $\hat{\psi} = \operatorname*{argmax}_{\phi} \mathcal{E}(\phi)$ with maximum value

$$\max_{\phi}\mathcal{E}(\phi) = \int |\nabla\hat{\psi}(x)|^2\rho_{\theta_k}(x)\ dx. \tag{44}$$

If $\hat{\psi}$ is a accurate approximation of ψ, $\max_\phi \mathcal{E}(\phi)$ provides a good approximation of $\langle \theta-\theta_k, G(\theta_k)(\theta-\theta_k)\rangle$. Therefore replacing $\langle \theta-\theta_k, G(\theta_k)(\theta-\theta_k)\rangle$ in (41) by $\max_\phi \mathcal{E}(\phi)$, we obtain our numerical scheme for solving (27):

$$\theta_{k+1} = \operatorname*{argmin}_{\theta}\max_{\phi}\left\{ \int 2\nabla\phi(x)\cdot((T_\theta - T_{\theta_k})\circ T_{\theta_k}^{-1}(x))\rho_{\theta_k}(x)\ dx - \int |\nabla\phi(x)|^2\rho_{\theta_k}(x)\ dx + 2hH(\theta)\right\}. \tag{45}$$

Remark 6. *Our proposed scheme can be viewed as an approximation to the JKO scheme* (38) *with* $\mathbb{F}$ *being the relative entropy* $H(\theta)$*. To see this, let us denote* $\vec{v}_h(x) = \frac{1}{h}T_\theta\circ T_{\theta_k}^{-1}(x) - x$*. Under some mild conditions, one can show that*

$$W_2^2(\rho_\theta,\rho_{\theta_k}) = W_2^2((Id+h\vec{v}_h)_{\#}\rho_{\theta_k},\rho_{\theta_k}) = \int |\nabla\hat{\psi}|^2\rho_{\theta_k}\ dx + o(h^2) = \max_\phi \mathcal{E}(\phi) + o(h^2). \tag{46}$$

If replacing $W_2^2(\rho_\theta,\rho_{\theta_k})$ *in* (38) *by its approximation* $\max_\phi\mathcal{E}(\phi)$*, we have the proposed scheme* (45)*.*

Remark 7. *The variational problem* $\max_\phi\mathcal{E}(\phi)$ *is equivalent to:*

$$\min_\phi\left\{ \int_M |\nabla\phi(x) - ((T_\theta - T_{\theta_k})\circ T_{\theta_k}^{-1}(x))|^2\rho_{\theta_k}(x)\ dx \right\}. \tag{47}$$

The vector field $\nabla\hat{\psi}$ *can be treated as the* $L^2(\rho_{\theta_k})$ *orthogonal projection of the vector field* $(T_\theta - T_{\theta_k})\circ T_{\theta_k}^{-1}(\cdot)$ *onto the subspace of gradient fields.*

4.2.1 Local error of the proposed scheme

We now analyze the local error of scheme (45) compared with the semi-implicit scheme (41). Let us denote $\max_\phi\mathcal{E}(\phi)$ as $\widehat{W}_2^2(\theta,\theta_k)$ (Here $\widehat{W}_2$ is treated as an approximation of L^2-Wasserstein distance (remark 6)). It is straightforward to verify $\widehat{W}_2(\theta,\theta')\geq 0$ and $\widehat{W}_2(\theta,\theta) = 0$. Consider the following assumption,

$$\widehat{W}_2^2(\theta,\theta') \geq l(|\theta-\theta'|) \qquad \text{for any} \quad \theta,\theta'\in\Theta. \tag{48}$$

Here $l : \mathbb{R}_{\geq 0} \to \mathbb{R}_{\geq 0}$ satisfies $l(0) = 0$. $l(r)$ is continuous, strictly increasing when $r \leq r_0$ for a positive r_0 and is bounded below by $\lambda_0 > 0$ when $r > r_0$. Notice that this assumption generally guarantees positive definiteness of $\widehat{W}_2$. Clearly, (48) only depends on the structure of T_θ, and we expect that (48) holds for the neural networks used as pushforward maps, including the ones we used in this paper.

Theorem 12. *Suppose assumption* (48) *holds true for the class of pushforward maps* $\{T_\theta\}$. *Then the local error of scheme* (45) *is of order* h^2, *i.e., assume that* θ_{k+1} *is the optimal solution to* (45), *then*

$$|\theta_{k+1} - \theta_k + hG(\theta_k)^{-1}\nabla_\theta H(\theta_{k+1})| \sim O(h^2). \tag{49}$$

or equivalently: $\limsup_{h\to 0^+} \frac{|\theta_{k+1}-\theta_k+hG(\theta_k)^{-1}\nabla_\theta H(\theta_{k+1})|}{h^2} < +\infty$.

To prove this theorem, we need the following lemmas:

Lemma 13. *[Danskin's Theorem [6]] Suppose* $F : \mathbb{R}^m \times \mathcal{B} \to \mathbb{R}$, *where* $\mathcal{B}$ *is a Banach space, for any* $\xi \in \mathcal{B}$, $F(\cdot, \xi)$ *is smooth; and there is unique* $\xi_x \in \mathcal{B}$ *such that* $F(x, \xi_x) = \sup_{\xi\in\mathcal{B}} F(x, \xi)$ *for any* $x \in \mathbb{R}^m$. *Denote* $\Gamma(x) = \sup_{\xi\in\mathcal{B}} F(x, \xi)$. *Then* Γ *is differentialbe on* $\mathbb{R}^m$ *and its derivative can be computed as:*

$$\nabla\Gamma(x) = \partial_x F(x, \xi_x).$$

For this simplicity of presentation, introduce a shorthand notation. Consider $\vec{v} \in L^2(\mathbb{R}^d; \mathbb{R}^d, \rho)$, we denote $\text{Proj}_\rho[\vec{v}] = \nabla\psi$ as the $L^2(\rho)$-orthogonal projection of $\vec{v}$ onto the subspace of gradient fields, i.e. $\psi = \underset{\psi}{\text{argmin}} \left\{\int |\vec{v}(x) - \nabla\psi(x)|^2\rho(x)\ dx\right\}$, or equivalently, ψ solves $-\nabla\cdot(\rho(x)\nabla\psi(x)) = -\nabla\cdot(\rho(x)\vec{v}(x))$.

Lemma 14. *Suppose* $\vec{u}, \vec{v}$ *are two vector fields on* $M = \mathbb{R}^d$, $Proj_\rho[\vec{u}] = \nabla\varphi$ *and* $Proj_\rho[\vec{v}] = \nabla\psi$. *Then:*

$$\int \vec{u}(x)\cdot\nabla\psi(x)\rho(x)\ dx = \int \nabla\varphi(x)\cdot\nabla\psi(x)\rho(x)\ dx; \tag{50}$$

$$\int |\nabla\psi(x)|^2\rho(x)\ dx \leq \int |\vec{v}(x)|^2\rho(x)\ dx. \tag{51}$$

Proof. For (50):

$$\int \vec{u}(x)\cdot\nabla\psi(x)\rho(x)\,dx = \int -\nabla\cdot(\rho(x)\vec{u}(x))\psi(x)\,dx = \int -\nabla\cdot(\rho(x)\nabla\varphi(x))\psi(x)\,dx = \int \nabla\varphi(x)\cdot\nabla\psi(x)\rho(x)\,dx.$$

For (51):

$$\begin{aligned}\int |\vec{v}(x)|^2\rho(x)\ dx &= \int (|\nabla\psi(x)|^2 + 2(\vec{v}(x) - \nabla\psi(x))\cdot\nabla\psi(x) + |\vec{v}(x) - \nabla\psi(x)|^2)\rho(x)\ dx \\ &= \int |\nabla\psi(x)|^2 + |\vec{v}(x) - \nabla\psi(x)|^2)\rho(x)\ dx \geq \int |\nabla\psi(x)|^2\rho(x)\ dx.\end{aligned}$$

The second equality is due to (50). □

The following lemma gives *a prior* estimation of $|\theta_{k+1} - \theta_k|$:

Lemma 15. *Under assumption*(48), *the optimal solution of* (45) θ_{k+1} *satisfies,*

$$|\theta_{k+1} - \theta_k| \sim o(1) \quad \textit{i.e.} \quad \lim_{h\to 0^+} |\theta_{k+1} - \theta_k| = 0. \tag{52}$$

Proof. Denote the function to be minimized in (45) as $J(\theta) = \widehat{W}(\theta, \theta_k) + 2hH(\theta)$. If choosing $\theta = \theta_k$ in (45), we have $J(\theta_k) = 2hH(\theta_k)$. Thus $J(\theta_{k+1}) \leq J(\theta_k) = 2hH(\theta_k)$. Since $H(\theta_k) \geq 0$, this leads to $\widehat{W}_2^2(\theta_{k+1}, \theta_k) \leq 2hH(\theta_k)$. When h is small enough, $|\theta_{k+1} - \theta_k| \leq k(2hH(\theta_k))$, here k is the inverse function of l defined on $[0, l(r_0)]$. We know $k(0) = 0$ and k is also continuous and increasing function. This leads to $\lim_{h\to 0^+} |\theta_{k+1} - \theta_k| \leq \lim_{h\to 0^+} k(2hH(\theta_k)) = 0$. □

Before proving Theorem 12, we introduce a few additional notations. We define ϵ ball in parameter space as $B_\epsilon(\theta_k) = \{\theta \mid |\theta - \theta_k| \le \epsilon\}$, let $T_\theta^{(i)}$ be the i-th component ($1 \le i \le d$) of map T_θ, and denote

$$L(\theta_k, \epsilon) = \sum_{i=1}^{d} \mathbb{E}_{x\sim p} \sup_{\theta \in B_\epsilon(\theta_k)} \left\{ |\partial_\theta T_\theta^{(i)}(x)|^2 \right\}, \quad H(\theta_k, \epsilon) = \sum_{i=1}^{d} \mathbb{E}_{x\sim p} \sup_{\theta \in B_\epsilon(\theta_k)} \left\{ \|\partial^2_{\theta\theta} T_\theta^{(i)}(x)\|_2^2 \right\}. \tag{53}$$

Proof of Theorem 12. Let us denote

$$F(\theta, \phi) = \int (2\nabla\phi(x) \cdot (T_\theta - T_{\theta_k}) \circ T_{\theta_k}^{-1}(x) - |\nabla\phi(x)|^2)\ \rho_{\theta_k}(x)\ dx + 2hH(\theta). \tag{54}$$

As discussed before, $\hat{\psi}_\theta = \operatorname*{argmax}_\phi \{F(\theta, \phi)\}$ solves

$$-\nabla \cdot (\rho_{\theta_k}(x)\nabla\hat{\psi}_\theta(x)) = -\nabla \cdot (\rho_{\theta_k}(x)(T_\theta - T_{\theta_k}) \circ T_{\theta_k}^{-1}(x)).$$

If we write

$$\nabla\hat{\psi}_\theta = \mathrm{Proj}_{\rho_{\theta_k}}[(T_\theta - T_{\theta_k}) \circ T_{\theta_k}^{-1}], \quad \Gamma(\theta) = \sup_\phi F(\theta, \phi)$$

and apply Lemma 13, we obtain:

$$\nabla_\theta \Gamma(\theta) = 2\left(\int\ \partial_\theta T_\theta(T_{\theta_k}^{-1}(x))\ \nabla\hat{\psi}_\theta(x)\ \rho_{\theta_k}(x)\ dx + h\ \nabla_\theta H(\theta) \right).$$

Due to the differentiability of $\Gamma(\theta)$, at the optimizer θ_{k+1}, the gradient must vanish, i.e.

$$\int \partial_\theta T_{\theta_{k+1}}(T_{\theta_k}^{-1}(x))\ \nabla\hat{\psi}_{\theta_{k+1}}(x)\ \rho_{\theta_k}(x)\ dx + h\nabla_\theta H(\theta_{k+1}) = 0. \tag{55}$$

We use Taylor expansion at θ_{k+1} to get $T_{\theta_{k+1}} - T_{\theta_k} = \partial_\theta T_{\theta_k}(\theta_{k+1} - \theta_k) + R(\theta_{k+1}, \theta_k)$, in which $R(\theta, \theta')(\cdot) \in L^2(\mathbb{R}^d; \mathbb{R}^m, \rho_{\theta_k})$, the i-th entry of $R(\theta, \theta')$ is $R_i(\theta, \theta')(x) = \frac{1}{2}(\theta - \theta')^T \partial^2_{\theta\theta} T^{(i)}_{\tilde{\theta}_i(x)}(x)(\theta - \theta')$, $1 \le i \le m$, where each $\tilde{\theta}_i(x) = \lambda_i(x)\theta + (1 - \lambda_i(x))\theta'$ for some $\lambda_i(x) \in [0, 1]$. Then we can write:

$$\nabla\hat{\psi}_{\theta_{k+1}} = \mathrm{Proj}_{\rho_{\theta_k}}[(T_{\theta_{k+1}} - T_{\theta_k}) \circ T_{\theta_k}^{-1}] = \mathrm{Proj}_{\rho_{\theta_k}}[\partial_\theta T_{\theta_k} \circ T_{\theta_k}^{-1}(\theta_{k+1} - \theta_k)] + \mathrm{Proj}_{\rho_{\theta_k}}[R(\theta_{k+1}, \theta_k) \circ T_{\theta_k}^{-1}]. \tag{56}$$

On the other hand,

$$\partial_\theta T_{\theta_{k+1}} = \partial_\theta T_{\theta_k} + r(\theta_{k+1}, \theta_k). \tag{57}$$

Here $r(\theta, \theta') \in L^2(\mathbb{R}^d; \mathcal{L}(\mathbb{R}^m; \mathbb{R}^d), \rho_{\theta_k})$, the $(i, j) - th$ entry of $r(\theta, \theta')(x)$ is $(\theta_{k+1} - \theta_k)^T \partial_\theta(\partial_{\theta_j} T^{(i)}_{\tilde{\theta}_{ij}(x)}(x))$, $1 \le i \le d$, $1 \le j \le m$, where each $\tilde{\theta}_{ij}(x) = \mu_{ij}(x)\theta_{k+1} + (1 - \mu_{ij}(x))\theta_k$, for some $\mu_i j(x) \in (0, 1)$. Applying (57), (56) to (55), we obtain

$$\begin{aligned}
&\int \partial_\theta T_{\theta_k}(T_{\theta_k}^{-1}(x))\mathrm{Proj}_{\rho_{\theta_k}}[\partial_\theta T_{\theta_k} \circ T_{\theta_k}^{-1}(x)(\theta_{k+1} - \theta_k)]\ \rho_{\theta_k}(x)\ dx \\
&+ \int \partial_\theta T_{\theta_k}(T_{\theta_k}^{-1}(x))\mathrm{Proj}_{\rho_{\theta_k}}[R(\theta_{k+1}, \theta_k) \circ T_{\theta_k}^{-1}](x)\ \rho_{\theta_k}(x)\ dx \\
&+ \int r(\theta_{k+1}, \theta_k)(T_{\theta_k}^{-1}(x))\mathrm{Proj}_{\rho_{\theta_k}}[(T_{\theta_{k+1}} - T_{\theta_k}) \circ T_{\theta_k}^{-1}](x)\ \rho_{\theta_k}(x)\ dx \quad = -h\nabla_\theta H(\theta_{k+1}).
\end{aligned} \tag{58}$$

Recall definition of $\mathbf{\Psi}$ in Theorem 4, use (50) in lemma 14, we know that the first term on the left hand side of (58) equals

$$\int \nabla\mathbf{\Psi}(x)\nabla\mathbf{\Psi}(x)^T(\theta_{k+1} - \theta_k)\ \rho_{\theta_k}(x)\ dx = G(\theta_k)(\theta_{k+1} - \theta_k).$$

By applying Cauchy inequality and (51) in lemma 14, we bound the i-th entry of the second term in (58) by:

$$\left(\int |\partial_\theta T^{(i)}_{\theta_k}(x)|^2 \, dp(x) \cdot \int \sum_{i=1}^d |(\theta_{k+1}-\theta_k)\partial^2_{\theta\theta} T^{(i)}_{\tilde{\theta}_i(x)}(x)(\theta_{k+1}-\theta_k)|^2 \, dp(x)\right)^{\frac{1}{2}}$$
$$\leq \left(\mathbb{E}_p|\partial_\theta T^{(i)}_{\theta_k}(x)|^2 \cdot \mathbb{E}_p\left[\sum_{i=1}^d \|\partial^2_{\theta\theta} T^{(i)}_{\tilde{\theta}_i(x)}(x)\|_2\right]\right)^{\frac{1}{2}} |\theta_{k+1}-\theta_k|^2 \overset{\text{denote as}}{=} A^{(i)}|\theta_{k+1}-\theta_k|^2.$$

To bound the third term in (58), we consider $T_{\theta_{k+1}}(x) - T_{\theta_k}(x)$, the i-th entry can be written as

$$T^{(i)}_{\theta_{k+1}}(x) - T^{(i)}_{\theta_k}(x) = (\theta_{k+1}-\theta_k)^T \partial_\theta T_{\bar{\theta}_i(x)}(x),$$

here $\bar{\theta}_i(x) = \zeta_i(x)\theta_{k+1} + (1-\zeta_i(x))\theta_k$ for some $\zeta_i(x) \in (0,1)$. The i-th entry of the third term of (58) can be bounded by:

$$\left(\int \sum_{i=1}^d |(\theta_{k+1}-\theta_k)^T \partial_{\theta\theta} T^{(i)}_{\tilde{\theta}_{ij}(x)}(x)|^2 \, dp(x) \cdot \int |T^{(i)}_{\theta_{k+1}}(x) - T^{(i)}_{\theta_k}(x)|^2 \, dp(x)\right)^{\frac{1}{2}}$$
$$\leq \left(\mathbb{E}_p\left[\sum_{i=1}^d \|\partial^2_{\theta\theta} T_{\tilde{\theta}_{ij}(x)}(x)\|_2^2\right] \cdot \mathbb{E}_p|\partial_\theta T^{(i)}_{\tilde{\theta}_i(x)}(x)|^2\right)^{\frac{1}{2}} |\theta_{k+1}-\theta_k|^2 \overset{\text{denote as}}{=} B^{(i)}|\theta_{k+1}-\theta_k|^2.$$

We denote $A \in \mathbb{R}^m$ with entries $A^{(i)}$, $1 \leq i \leq m$ and similarly $B \in \mathbb{R}^m$ with entries $B^{(i)}$, $1 \leq i \leq m$. (58) leads to the following inequality,

$$|\theta_{k+1} - \theta_k + hG(\theta_k)^{-1}\nabla_\theta H(\theta_{k+1})| \leq \|G(\theta_k)^{-1}\|_2(|A|+|B|)\ |\theta_{k+1}-\theta_k|^2.$$

As we have shown in Lemma 15 that $|\theta_{k+1}-\theta_k| \sim o(1)$ for any $\epsilon > 0$ when step size h is small enough, we always have $\theta_{k+1} \in B_\epsilon(\theta_k)$. Recall the notations in (53), we have $|A|, |B| \leq \sqrt{L(\theta_k,\epsilon)H(\theta_k,\epsilon)}$. Thus we have

$$|\theta_{k+1} - \theta_k + hG(\theta_k)^{-1}\nabla_\theta H(\theta_{k+1})| \leq 2\sqrt{L(\theta_k,\epsilon)H(\theta_k,\epsilon)}\|G(\theta_k)^{-1}\|_2|\theta_{k+1}-\theta_k|^2.$$

Denote $\theta_{k+1} - \theta_k = \eta$, $G(\theta_k)^{-1}\nabla_\theta H(\theta_{k+1}) = \xi$ and $C = 2\sqrt{L(\theta_k,\epsilon)H(\theta_k,\epsilon)}\|G(\theta_k)^{-1}\|_2$, the previous inequality is

$$|\eta - h\,\xi| \leq C|\eta|^2. \tag{59}$$

Since $|\eta - h\xi| \geq |\eta| - h|\xi|$, we have

$$C|\eta|^2 \geq |\eta| - h|\xi|. \tag{60}$$

Solving (60) gives

$$|\eta| \leq \frac{2|\xi|h}{1+\sqrt{1-4C|\xi|h}} \quad \text{or} \quad |\eta| > \frac{1+\sqrt{1-4Ch|\xi|}}{2C}.$$

The second inequality leads to $|\theta_{k+1}-\theta_k| > \frac{1}{2C}$ for any $h > 0$, which avoids $|\theta_{k+1}-\theta_k| \sim o(1)$. Thus, when h is sufficiently small, we have

$$|\eta| \leq \frac{2|\xi|h}{1+\sqrt{1-4C|\xi|h}}. \tag{61}$$

Combining (61) and (59), we have:

$$|\theta_{k+1} - \theta_k + hG(\theta_k)^{-1}\nabla_\theta H(\theta_{k+1})| \leq \frac{C|\xi|^2}{(1+\sqrt{1-4C|\xi|h})}\ h^2 \leq C|\xi|^2h^2. \tag{62}$$

This proves the result. □

Remark 8. *One may be aware of the relation between the positive definite condition* (48) *and the positive definiteness of the metric tensor $G(\theta_k)$. A positive definite $G(\theta)$ guarantees the inequality $\widehat{W}_2^2(\theta,\theta') \geq C|\theta-\theta'|^2$ for $\theta' \in B_{r_0}(\theta)$ (r_0 depends on θ is small enough). However, we are not able to bound $\widehat{W}_2^2(\theta,\theta')$ from below when $|\theta-\theta'| > r_0$. On the other hand,* (48) *is a locally weaker condition than positive definiteness of $G(\theta)$.*

4.2.2 Implementation

From the previous sections, we know that one can solve ODE (27) at t_k by finding the saddle point of (45). Here we provide some detailed discussion on how we deal with (27).

- As in Remark 7, we may solve (47) instead of $\max_\phi \mathcal{E}(\phi)$ in every inner loop of the saddle point problem (45). Although they are mathematically equivalent, (47) has a more concise form. Our experience indicates that (47) makes our code run more efficiently than directly solving $\max_\phi \mathcal{E}(\phi)$. Thus we present the following formulation that is equivalent to (45):

$$\theta_{k+1} = \operatorname*{argmin}_\theta J(\theta), \tag{63}$$

  where $J(\theta) = \min_\phi F(\theta, \phi)$ with F defined in (54).

- In our numerical computation, we approximate ψ by $\psi_\lambda : M \to \mathbb{R}$, which is a ReLU neural network parametrized by λ [12] . We know that in this case, ψ_λ is a piece-wise affine function and its gradient $\nabla\psi_\lambda(\cdot)$ forms a piece-wise constant vector field. Figure 3, 4 illustrates such an example.

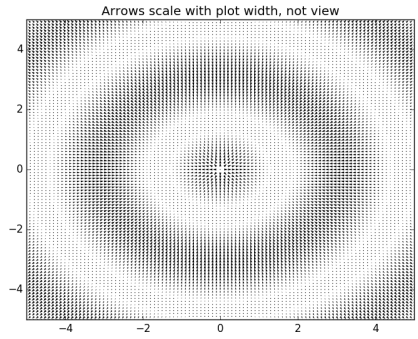

Figure 3: gradient field of $\psi(x) = \sin(|x|)$

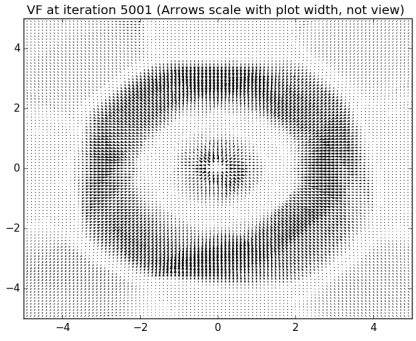

Figure 4: approximation by the gradient of a ReLU function ψ_λ

- The entire procedure of solving (63) can be formulated as nested loops:
  - (inner loop) Every inner loop aims at solving (47) on ReLU functions ψ_λ, i.e. solving:

$$\min_\lambda \left\{ \mathbb{E}_{\boldsymbol{X}\sim p} |\nabla\psi_\lambda(T_{\theta_k}(\boldsymbol{X})) - (T_\theta(\boldsymbol{X}) - T_{\theta_k}(\boldsymbol{X}))|^2 \right\}. \tag{64}$$

    One can use Stochastic Gradient Descent (SGD) methods like RMSProp [47] or Adam [21] with learning rate α_{in} to deal with this inner loop optimization. In our implementation, we will stop after M_{in} iterations. Let us denote the optimal λ in each inner loop as $\hat{\lambda}$;
  - (outer loop) We apply similar SGD method to $J(\theta)$: using Lemma 13, we are able to compute $\nabla_\theta J(\theta)$ as:

$$\nabla_\theta J(\theta) = \partial_\theta \left(\int 2\nabla\hat{\psi}(x) \cdot (T_\theta \circ T_{\theta_k}^{-1}(x)) \rho_{\theta_k}(x)\, dx + 2hH(\theta) \right).$$

    If we treat optimal $\hat{\psi}$ as $\psi_{\hat{\lambda}}$, what we need to do in each outer loop is to consider:

$$\tilde{J}(\theta) = \mathbb{E}_{\boldsymbol{X}\sim p}\, 2[\nabla\psi_{\hat{\lambda}}(T_{\theta_k}(\boldsymbol{X})) \cdot T_\theta(\boldsymbol{X})] + 2h[V(T_\theta(\boldsymbol{X})) + \mathcal{L}_\theta(\boldsymbol{X})] \tag{65}$$

    and update θ for one step by our chosen SGD method with learning rate α_{out} applied to optimize $\tilde{J}(\theta)$. In our actual computation, we will stop the outer loop after M_{out} iterations.

- We now present the entire algorithm for computing (27) based on the scheme (45). This algorithm contains the following parameters: $T, N; M_{\text{out}}, K_{\text{out}}, \alpha_{\text{out}}; M_{\text{in}}, K_{\text{in}}, \alpha_{\text{in}}$. Recall we set reference distribution p as standard Gaussian on $M = \mathbb{R}^d$.

Algorithm 1 Computing (27) by scheme (45) on the time interval $[0, T]$

Initialize θ
for $i = 1, ...N$ **do**
  Save current parameter value to θ_0: $\theta_0 = \theta$
  for $j = 1, ...M_{\text{outer}}$ **do**
    for $p = 1, ..., M_{\text{in}}$ **do**
      Sample $\{\mathbf{X}_1, ..., \mathbf{X}_{K_{\text{in}}}\}$ from p
      Apply one SGD (RMSProp, Adam etc.) step with learning rate α_{in} to loss function (of variable λ)

$$\frac{1}{K_{\text{in}}}\left(\sum_{k=1}^{K_{\text{in}}} |\nabla\psi_\lambda(T_{\theta_0}(\mathbf{X}_k)) - (T_\theta(\mathbf{X}_k) - T_{\theta_0}(\mathbf{Y}_k))|^2\right)$$

    end for
    Sample $\{\mathbf{X}_1, ..., \mathbf{X}_{K_{\text{out}}}\}$ from p
    Apply one SGD (RMSProp, Adam etc.) step with learning rate α_{out} to loss function

$$\frac{1}{K_{\text{out}}}\sum_{k=1}^{K_{\text{out}}} 2[\nabla\psi_\lambda(T_{\theta_0}(\boldsymbol{X}_k)) \cdot T_\theta(\boldsymbol{X}_k)] + 2h[V(T_\theta(\boldsymbol{X}_k)) + \mathcal{L}_\theta(\boldsymbol{X}_k)]$$

  end for
  Set $\theta_i = \theta$
end for
The sequence of probability densities $\{T_{\theta_0\#}p, T_{\theta_1\#}p, ..., T_{\theta_N\#}p\}$ will be the numerical solution of $\{\rho_{t_0}, \rho_{t_1}, ..., \rho_{t_N}\}$, where $t_i = i\frac{T}{N}$ $(i = 0, 1, ..., N-1, N)$. Here ρ_t solves original Fokker-Planck equation (5).

Remark 9. *In our implementation, $T_\theta(\boldsymbol{X}) - T_{\theta_k}(\boldsymbol{X})$ is usually of order $O(\alpha_{out})$, which is a small quantity. We can rescale it so that each inner loop can be solved in a more stable way with larger stepsize (learning rate). That is to say, we choose some small $\epsilon \sim O(\alpha_{out})$ and consider*

$$\min_\lambda \left\{\mathbb{E}_{\boldsymbol{X}\sim p}\left|\nabla\psi_\lambda(T_{\theta_k}(\boldsymbol{X})) - \left(\frac{T_\theta(\boldsymbol{X}) - T_{\theta_k}(\boldsymbol{X})}{\epsilon}\right)\right|^2\right\}, \tag{66}$$

instead of (64) *in each inner loop and set:*

$$\tilde{J}(\theta) = \mathbb{E}_{\boldsymbol{X}\sim p}\ 2[\nabla\psi_{\hat{\lambda}}(T_{\theta_k}(\boldsymbol{X})) \cdot T_\theta(\boldsymbol{X})] + \frac{2h}{\epsilon}[V(T_\theta(\boldsymbol{X})) + \mathcal{L}_\theta(\boldsymbol{X})] \tag{67}$$

in each outer loop. In actual experiments, we set $\epsilon = \alpha_{out}$.

Remark 10. *It worth mentioning that the sample size K_{in}, K_{out} in each SGD step (especially K_{in}) should be chosen reasonably large so that the inner optimization problem can be solved with enough accuracy. In our practice, we usually choose $K_{in} = K_{out} = \max\{1000, 300d\}$. Here d is the dimension of sample space. This is very different from the small batch technique applied to training neural network in deep learning [34].*

5 Asymptotic properties and error estimations

In this section, we establish numerical analysis for parametric Fokker-Planck equation (27).

5.1 An important quantity

Before our analysis, we introduce an important quantity that plays an essential role in our numerical analysis. Let us recall the optimal value of the least square problem (28) in Theorem 10 of section 3.2, or equivalently

(29) of section 3.2, (34) of section 3.3. If we denote the upper bound of all possible values to be δ_0, i.e.

$$\delta_0 = \sup_{\theta\in\Theta} \min_{\xi\in T_\theta\Theta} \left\{ \int |(\nabla \mathbf{\Psi}(T_\theta(x))^T \xi - \nabla \left(V + \beta \log \rho_\theta\right) \circ T_\theta(x)|^2 \ dp(x) \right\}, \tag{68}$$

this quantity provides crucial error bound between our parametric equation and original equation in the forthcoming analysis. Ideally, we hope δ_0 to be sufficiently small. And this can be guaranteed if the neural network we select has universal approximation power. A closer examination may relax such a requirement. In fact, we only need require the neural network to be able to approximate a family of vector fields, more specifically, we need $\partial_\theta T_\theta$ to approximate $\{\nabla(V + \beta \log \rho_\theta)\}_{\theta\in\Theta}$. In our numerical experiments, we found that using normalizing flow as T_θ works fine in various test examples. We believe that such an approximation property is shared by a large number of commonly used deep neural networks. This assertion can be further illustrated from another perspective. Let us consider T_θ with linear structure: i.e., set $T_\theta(x) = \sum_{i=1}^m \theta_i \vec{\Phi}_i(x)$, here $\{\vec{\Phi}_i\}_{i=1}^m$ are basis functions like gradient of radial basis functions(RBF). Then by (51) of Lemma 14, it is not hard to show:

$$\delta_0 \leq \sup_{\theta\in\Theta} \min_{\xi\in\mathbb{R}^m} \left\{ \int |\sum_{k=1}^m \xi_k \vec{\Phi}_i(x) - \nabla(V + \beta \log \rho_\theta) \circ T_\theta(x)|^2 \ dp(x) \right\}.$$

This inequality indicates that δ_0 is no worse than the approximation error of using linear combination of classical RBF functions [8], which can be viewed as a one-layer network with large width. It is widely believed that nonlinear deep neural networks have better flexibility and approximation power than linear approximations, which may explain why normalizing flow can achieve accurate computations (small δ_0) in high dimensional space in our examples.

It also worth mentioning that δ_0 is used for *a priori* estimate in this section, because we don't know the exact trajectory of $\{\theta_t\}$ when solving ODE (27), and we take supremum over Θ to obtain δ_0. Once solved for $\{\theta_t\}$, denote $\mathcal{C}$ as the set covering its trajectory, i.e.

$$\mathcal{C} = \{\theta \mid \exists\ t \geq 0,\ \text{s.t. } \theta = \theta_t\} \tag{69}$$

We define another quantity δ_1:

$$\delta_1 = \sup_{\theta\in\mathcal{C}} \min_{\xi\in T_\theta\Theta} \left\{ \int |(\nabla \mathbf{\Psi}(T_\theta(x))^T \xi - \nabla \left(V + \beta \log \rho_\theta\right) \circ T_\theta(x)|^2 \ dp(x) \right\}. \tag{70}$$

Clearly, we have $\delta_1 \leq \delta_0$. We can obtain corresponding *posterior* estimates for the asymptotic convergence and error analysis by replacing δ_0 with δ_1.

5.2 Asymptotic Convergence Analysis

In this section, we consider the solution $\{\theta_t\}_{t\geq 0}$ of our parametric Fokker-Planck equation (27). We define:

$$\mathcal{V} = \left\{ V \ \middle| \begin{array}{c} V \in \mathcal{C}^2(\mathbb{R}^d),\ V \text{ can be decomposed as: } V = U + \phi, \text{ with } U, \phi \in \mathcal{C}^2(\mathbb{R}^d); \\ \nabla^2 U \succeq KI \text{ with } K > 0 \text{ and } \phi \in L^\infty(\mathbb{R}^d) \end{array} \right\}$$

As we know, for Fokker-Planck equation (5), when the potential $V \in \mathcal{V}$, $\{\rho_t\}$ will converge to the Gibbs distribution $\rho_* = \frac{1}{Z_\beta} e^{-V(x)/\beta}$ as $t \to \infty$ under the measure of KL divergence [15]. For (27), we wish to study its asymptotic convergence property. We come up with the following result:

Theorem 16 (*a priori* estimation on asymptotic convergence)**.** *Consider Fokker-Planck equation* (5) *with the potential $V \in \mathcal{V}$. Suppose $\{\theta_t\}$ solves the parametric Fokker-Planck equation* (27)*, denote δ_0 as in* (68)*. Let $\rho_*(x) = \frac{1}{Z_\beta} e^{-V(x)/\beta}$ be the Gibbs distribution of original equation* (5)*. Then we have the inequality:*

$$D_{KL}(\rho_{\theta_t} \| \rho_*) \leq \frac{\delta_0}{\tilde{\lambda}_\beta \beta^2} (1 - e^{-\beta \tilde{\lambda}_\beta t}) + D_{KL}(\rho_{\theta_0} \| \rho_*) e^{-\beta \tilde{\lambda}_\beta t}. \tag{71}$$

Here $\tilde{\lambda}_\beta > 0$ is the constant associated to the Logarithmic Sobolev inequality discussed in Lemma 17 with potential function $\frac{1}{\beta} V$.

To prove Theorem 16, we need the following two lemmas:

Lemma 17. *[Holley-Stroock Perturbation] Suppose the potential $V \in \mathcal{V}$ is decomposed as $V = U + \phi$ where $\nabla^2 U \succeq KI$ and $\phi \in L^\infty$. Let $\tilde{\lambda} = Ke^{-osc(\phi)}$, where $osc(\phi) = \sup \phi - \inf \phi$. Then the following Logarithmic Sobolev inequality holds for any probability density ρ:*

$$D_{KL}(\rho\|\rho_*) \leq \frac{1}{\tilde{\lambda}}\mathcal{I}(\rho|\rho_*). \tag{72}$$

Here $\rho_* = \frac{1}{Z}e^{-V}$ and $\mathcal{I}(\rho|\rho_*)$ is the Fisher information functional defined as:

$$\mathcal{I}(\rho|\rho_*) = \int \left|\nabla \log\left(\frac{\rho(x)}{\rho_*(x)}\right)\right|^2 \rho(x)\ dx.$$

Lemma 17 is first proved in [15].

Lemma 18. *For any $\theta \in \Theta$, we have:*

$$\beta^2\ \mathcal{I}(\rho_\theta|\rho_*) \leq \delta_0 + \nabla_\theta H(\theta) \cdot G(\theta)^{-1}\nabla_\theta H(\theta), \tag{73}$$

where δ_0 is defined in (68)*,*

Proof of Lemma 18. Let us denote $\xi = G(\theta)^{-1}\nabla_\theta H(\theta)$ for convenience. Suppose $\{\theta_t\}$ solves (27) with $\theta_0 = \theta$. By Theorem 7, $\frac{d}{dt}\rho_{\theta_t}\Big|_{t=0} = -(T_\#|_\theta)_*\xi$ is orthogonal projection of $-\text{grad}_W\mathcal{H}(\rho_\theta)$ onto $T_{\rho_\theta}\mathcal{P}$ with respect to metric g^W. Thus the orthogonal relation gives:

$$\begin{aligned} g^W(-\text{grad}_W\mathcal{H}(\rho_\theta), -\text{grad}_W\mathcal{H}(\rho_\theta)) = {} & g^W(\text{grad}_W\mathcal{H}(\rho_\theta) - (T_\#|_\theta)_*\xi, \text{grad}_W\mathcal{H}(\rho_\theta) - (T_\#|_\theta)_*\xi) \\ & + g^W((T_\#|_\theta)_*\xi, (T_\#|_\theta)_*\xi). \end{aligned} \tag{74}$$

One can verify that the left hand side of (74) is:

$$g^W(-\text{grad}_W\mathcal{H}(\rho_\theta), -\text{grad}_W\mathcal{H}(\rho_\theta)) = \int |\nabla(V(x) + \beta\log\rho_\theta(x))|^2\rho(x)\ dx = \beta^2\ \mathcal{I}(\rho_\theta|\rho_*). \tag{75}$$

Recall the equivalence between (28) and (29) and the definition of δ_0 in (68), we know that the first term on the right hand side of (74) has an upper bound

$$g^W(\text{grad}_W\mathcal{H}(\rho_\theta) - (T_\#|_\theta)_*\xi, \text{grad}_W\mathcal{H}(\rho_\theta) - (T_\#|_\theta)_*\xi) \leq \delta_0. \tag{76}$$

The second term on the right hand side of (74) is:

$$\begin{aligned} g^W((T_\#|_\theta)_*\xi, (T_\#|_\theta)_*\xi) = (T_\#|_\theta)^* g^W(\xi,\xi) &= G(\theta)(G(\theta)^{-1}\nabla_\theta H(\theta),\ G(\theta)^{-1}\nabla_\theta H(\theta)) \\ &= \nabla_\theta H(\theta) \cdot G(\theta)^{-1}\nabla_\theta H(\theta) \end{aligned} \tag{77}$$

Combining (74), (75),(76) and (77) yields to (73). □

Proof of Theorem 16. Let us recall the relationship between KL divergence and relative entropy,

$$D_{\text{KL}}(\rho\|\rho_*) = \frac{1}{\beta}\mathcal{H}(\rho) + \log(Z_\beta).$$

Actually, we can treat $KL(\rho_\theta\|\rho_*)$ as a Lyapunov function for our ODE (27), because by taking time derivative of $\text{KL}(\rho_{\theta_t}\|\rho_*)$, we obtain

$$\frac{d}{dt}D_{\text{KL}}(\rho_{\theta_t}\|\rho_*) = \frac{1}{\beta}\frac{d}{dt}\mathcal{H}(\rho_{\theta_t}) = \frac{1}{\beta}\dot{\theta}_t \cdot \nabla H(\theta_t) = -\frac{1}{\beta}\nabla H(\theta_t) \cdot G^{-1}(\theta_t)\nabla H(\theta_t).$$

Using the inequality in Lemma 18, we are able to show:

$$\frac{d}{dt}D_{\text{KL}}(\rho_{\theta_t}\|\rho_*) \leq \frac{\delta_0}{\beta} - \beta\ \mathcal{I}(\rho_{\theta_t}|\rho_*).$$

By Lemma 17, we have:

$$\frac{d}{dt}D_{\mathrm{KL}}(\rho_{\theta_t}\|\rho_*) \le \frac{\delta_0}{\beta} - \beta\ \tilde{\lambda}_\beta\ D_{\mathrm{KL}}(\rho_{\theta_t}\|\rho_*).$$

Therefore we obtain, by Grownwall's inequality, the following estimate,

$$D_{\mathrm{KL}}(\rho_{\theta_t}\|\rho_*) \le \frac{\delta_0}{\tilde{\lambda}_\beta\beta^2}(1-e^{-\beta\tilde{\lambda}_\beta t}) + D_{\mathrm{KL}}(\rho_{\theta_0}\|\rho_*)e^{-\beta\tilde{\lambda}_\beta t}.$$

□

Remark 11. *Following the previous proof, we can show a similar convergence estimation for the solution* $\{\rho_t\}_{t\ge 0}$ *of* (5)*,*

$$D_{KL}(\rho_t\|\rho_*) \le D_{KL}(\rho_0\|\rho_*)\ e^{-\beta\tilde{\lambda}_\beta t} \quad \forall\ t>0. \tag{78}$$

A nominal modification of our proof for Theorem 16 leads to a *posterior* version of our asymptotic convergence analysis, which is stated in the following theorem.

Theorem 19 (*Posterior* estimation on asymptotic convergence)**.**

$$D_{KL}(\rho_{\theta_t}\|\rho_*) \le \frac{\delta_1}{\tilde{\lambda}_\beta\beta^2}(1-e^{-\beta\tilde{\lambda}_\beta t}) + D_{KL}(\rho_{\theta_0}\|\rho_*)e^{-\beta\tilde{\lambda}_\beta t},$$

where δ_1 *is defined in* (70)*.*

5.3 Wasserstein error estimations

In this subsection, we establish our error bounds for both continuous and discrete version of parametric Fokker-Planck equation (27) as approximations to the original equation (5).

5.3.1 Wasserstein error for the parametric Fokker-Planck equation

The following theorem provides an upper bound between the solutions of (5) and (27).

Theorem 20. *Assume that* $\{\theta_t\}_{t\ge 0}$ *solves* (27) *and* $\{\rho_t\}_{t\ge 0}$ *solves* (5)*. If the Hessian of the potential function* V *in* (5) *is bounded below by a constant* λ*, i.e.* $\nabla^2 V \succeq \lambda\ I$*, we have:*

$$W_2(\rho_{\theta_t},\rho_t) \le \frac{\sqrt{\delta_0}}{\lambda}(1-e^{-\lambda t}) + e^{-\lambda t}W_2(\rho_{\theta_0},\rho_0). \tag{79}$$

To prove this inequality, we need the following lemmas. The first one is about geodesic equations [32, 52].

Lemma 21 (Constant speed of geodesic)**.** *The geodesic connecting* $\rho_0,\rho_1\in\mathcal{P}(M)$ *is described by,*

$$\begin{cases} \frac{\partial\rho_t}{\partial t} + \nabla\cdot(\rho\nabla\psi_t) = 0 \\ \frac{\partial\psi_t}{\partial t} + \frac{1}{2}|\nabla\psi_t|^2 = 0 \end{cases} \qquad \rho_t|_{t=0} = \rho_0,\ \rho_t|_{t=1} = \rho_1. \tag{80}$$

Using the notation $\dot{\rho}_t = \partial_t\rho_t = -\nabla\cdot(\rho_t\nabla\psi_t) \in T_{\rho_t}\mathcal{P}(M)$*,* $g^W(\dot{\rho}_t,\dot{\rho}_t)$ *is constant for* $0\le t\le 1$ *and* $g^W(\dot{\rho}_t,\dot{\rho}_t) = W_2^2(\rho_0,\rho_1)$ *for* $0\le t\le 1$*.*

Proof. Recall the definition (8) of Wasserstein metric g^W, $g^W(\dot{\rho}_t,\dot{\rho}_t) = \int|\nabla\psi_t|^2\rho_t\ dx$. Since $\{\rho_t\}$ is the geodesic on $(\mathcal{P}(M),g^W)$, the speed $g^W(\sigma_t,\sigma_t)$ remains constant. To directly verify this, we compute the time derivative:

$$\frac{d}{dt}g^W(\dot{\rho}_t,\dot{\rho}_t) = \frac{d}{dt}\left(\int|\nabla\psi_t|^2\rho_t\ dx\right) = \int\frac{\partial}{\partial t}|\nabla\psi_t|^2\rho_t\ dx + \int|\nabla\psi_t|^2\partial_t\rho_t\ dx.$$

Using the first equation in (80), we obtain

$$\int|\nabla\psi_t|^2\partial_t\rho_t\ dx = \int|\nabla\psi_t|^2\cdot(-\nabla\cdot(\rho_t\nabla\psi_t))\ dx = \int\nabla(|\nabla\psi_t|^2)\cdot\nabla\psi_t\rho_t\ dx,$$

Taking the spatial gradient of the second equation in (80), we have

$$\partial_t(\nabla\psi_t) = -\nabla(\frac{1}{2}|\nabla\psi_t|^2).$$

Then

$$\int \frac{\partial}{\partial t}|\nabla\psi_t|^2\rho_t\ dx = \int 2\partial_t(\nabla\psi_t)\cdot\nabla\psi_t\rho_t\ dx = \int -\nabla(|\nabla\psi_t|^2)\cdot\nabla\psi_t\rho_t\ dx.$$

Adding them together, we verify $\frac{d}{dt}g^W(\dot\rho_t,\dot\rho_t)=0$, hence $\int_0^1 g^W(\dot\rho_t,\dot\rho_t)\,dt = W_2^2(\rho_0,\rho_1)$. We know $g^W(\dot\rho_t,\dot\rho_t) = W_2^2(\rho_0,\rho_1)$ for any $0\le t\le 1$. □

Lemma 22 (Displacement convexity of relative entropy)**.** *Suppose* $\{\rho_t\}$ *solves* (80)*, the relative entropy* $\mathcal{H}$ *in* (11) *has potential* V *satisfying* $\nabla^2 V \succeq \lambda I$*, then:*

$$\frac{d}{dt}g^W(grad_W\mathcal{H}(\rho_t),\dot\rho_t) \ge \lambda W_2^2(\rho_0,\rho_1).$$

Or equivalently, $\frac{d^2}{dt^2}\mathcal{H}(\rho_t)\ge\lambda W_2^2(\rho_0,\rho_1)$.

Proof. Let us write:

$$g^W(\mathrm{grad}_W\mathcal{H}(\rho_t),\dot\rho_t) = \int\nabla(V+\beta\log\rho_t)\cdot\nabla\psi_t\ \rho_t\ dx.$$

Then:

$$\frac{d}{dt}g^W(\mathrm{grad}_W\mathcal{H}(\rho_t),\dot\rho_t) = \frac{d}{dt}\left(\int\nabla(V+\beta\log\rho_t)\cdot\nabla\psi_t\ \rho_t\ dx\right) = \int(\nabla\psi_t^T\nabla^2V\nabla\psi_t + \mathrm{Tr}(\nabla^2\psi_t\nabla^2\psi_t))\ \rho_t\ dx.$$

The second equality can be carried out by direct calculations. One can check [51] or [52] for its complete derivation. Using $\nabla^2V\succeq\lambda I$, we get

$$\frac{d}{dt}g^W(\mathrm{grad}_W\mathcal{H}(\rho_t),\dot\rho_t) \ge \int\lambda|\nabla\psi_t|^2\rho_t\ dx = \lambda\ g^W(\dot\rho_t,\dot\rho_t) = \lambda W_2^2(\rho_0,\rho_1).$$

The last equality is due to Lemma 21. By the definition of Wasserstein gradient (10), $\frac{d}{dt}\mathcal{H}(\rho_t) = g^W(\mathrm{grad}_W\mathcal{H}(\rho_t),\dot\rho_t)$, we also proved $\frac{d^2}{dt^2}\mathcal{H}(\rho_t)\ge\lambda W_2^2(\rho_0,\rho_1)$.

□

Proof of Theorem 20. Figure 5 provides a sketch of our proof: For a given time t, the geodesic $\{\bar\rho_\tau\}_{0\le\tau\le1}$ on Wasserstein manifold $\mathcal{P}(M)$ that connects ρ_{θ_t} and ρ_t satisfies the geodesic equations (80). If differentiating $W_2^2(\rho_{\theta_t},\rho_t)$ with respect to time t according to Theorem 23.9 of [52], we are able to deduce

$$\frac{d}{dt}W_2^2(\rho_{\theta_t},\rho_t) = 2g^W(\dot\rho_{\theta_t},-\dot{\bar\rho}_0) + 2g^W(\dot\rho_t,\dot{\bar\rho}_1), \tag{81}$$

in which $\dot{\bar\rho}_0 = \partial_\tau\bar\rho_\tau|_{\tau=0} = -\nabla\cdot(\bar\rho_0\nabla\psi_0)$, $\dot{\bar\rho}_1 = \partial_\tau\bar\rho_\tau|_{\tau=1} = -\nabla\cdot(\bar\rho_1\nabla\psi_1)$. Notice that

$$\dot\rho_{\theta_t} = (T_\#|_{\theta_t})_*\dot\theta_t \quad \dot\rho_t = -\mathrm{grad}_W\mathcal{H}(\rho_t) = \nabla\cdot(\rho_t\nabla(V+\beta\log\rho_t)).$$

Using the definition (8) of Wasserstein metric, we can compute (recall that $\rho_{\theta_t}=\bar\rho_0$, $\rho_t=\bar\rho_1$):

$$g^W(\dot\rho_{\theta_t},\dot{\bar\rho}_0) = \int\nabla(V+\beta\log\bar\rho_0)\cdot\psi_0\ \bar\rho_0\ dx \quad g^W(\dot\rho_t,\dot{\bar\rho}_1) = \int\nabla(V+\beta\log\bar\rho_1)\cdot\psi_1\ \bar\rho_1\ dx.$$

Now we can write (81) as,

$$\begin{aligned}\frac{1}{2}\frac{d}{dt}W_2^2(\rho_{\theta_t},\rho_t) =& g^W((T_\#|_{\theta_t})_*\dot\theta_t - (-\mathrm{grad}_W\mathcal{H}(\rho_{\theta_t})),-\dot{\bar\rho}_0) + g^W(-\mathrm{grad}_W\mathcal{H}(\rho_{\theta_t}),-\dot{\bar\rho}_0) + g^W(-\mathrm{grad}_W\mathcal{H}(\rho_t),\dot{\bar\rho}_1)\\ \overset{\text{set: }\xi=-\dot\theta_t}{=}& g^W(\mathrm{grad}_W\mathcal{H}(\rho_{\theta_t}) - (T_\#|_{\theta_t})_*\xi,-\dot{\bar\rho}_0) - (g^W(\mathrm{grad}_W\mathcal{H}(\bar\rho_1),\dot{\bar\rho}_1) - g^W(\mathrm{grad}_W\mathcal{H}(\bar\rho_0),\dot{\bar\rho}_0)).\end{aligned} \tag{82}$$

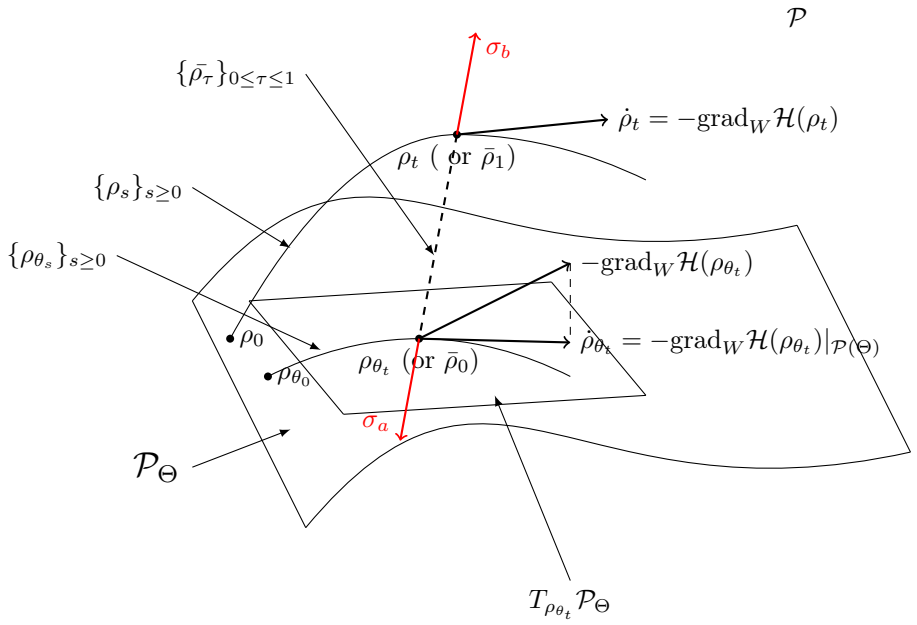

Figure 5: An illustrative diagram for the proof of Theorem 20

For the first term in (82), we use Cauchy inequality, (68), and Lemma 21, which implies $g(\sigma_a, \sigma_a) = W_2^2(\rho_{\theta_t}, \rho_t)$, to obtain

$$\begin{aligned} g^W(\mathrm{grad}_W \mathcal{H}(\rho_{\theta_t}) - (T_{\#}|_{\theta_t})_* \xi, -\dot{\bar{\rho}}_0) \le & \sqrt{g^W(\mathrm{grad}_W \mathcal{H}(\rho_{\theta_t}) - (T_{\#}|_{\theta_t})_* \xi, \mathrm{grad}_W \mathcal{H}(\rho_{\theta_t}) - (T_{\#}|_{\theta_t})_* \xi)} \sqrt{g^W(\dot{\bar{\rho}}_0, \dot{\bar{\rho}}_0)} \\ \le & \sqrt{\delta_0} W(\rho_{\theta_t}, \rho_t). \end{aligned} \tag{83}$$

For the second term in (82) , we write it as:

$$g^W(\mathrm{grad}_W \mathcal{H}(\bar{\rho}_1), \dot{\bar{\rho}}_1) - g^W(\mathrm{grad}_W \mathcal{H}(\bar{\rho}_0), \dot{\bar{\rho}}_0) = \int_0^1 \frac{d}{d\tau} g^W(\mathrm{grad}_W \mathcal{H}(\bar{\rho}_\tau), \dot{\bar{\rho}}_\tau)\, d\tau. \tag{84}$$

By Lemma 22, we have:

$$g^W(\mathrm{grad}_W \mathcal{H}(\bar{\rho}_1), \dot{\bar{\rho}}_1) - g^W(\mathrm{grad}_W \mathcal{H}(\bar{\rho}_0), \dot{\bar{\rho}}_0) \ge \lambda\, W_2^2(\rho_{\theta_t}, \rho_t). \tag{85}$$

Combining inequalities (83), (85) and (82), we get

$$\frac{1}{2}\frac{d}{dt} W_2^2(\rho_{\theta_t}, \rho_t) \le -\lambda W_2^2(\rho_{\theta_t}, \rho_t) + \sqrt{\delta_0}\, W_2(\rho_{\theta_t}, \rho_t).$$

This is:

$$\frac{d}{dt} W_2(\rho_{\theta_t}, \rho_t) \le -\lambda W_2(\rho_{\theta_t}, \rho_t) + \sqrt{\delta_0}.$$

Then the Grownwall's inequality gives

$$W_2(\rho_{\theta_t}, \rho_t) \le \frac{\sqrt{\delta_0}}{\lambda}(1 - e^{-\lambda t}) + e^{-\lambda t} W_2(\rho_{\theta_0}, \rho_0).$$

□

When the potential V is strictly convex, i.e. $\lambda > 0$. (79) in Theorem 20 provides a nice estimation of the error term $W_2(\rho_{\theta_t}, \rho_t)$ at any time t that is always upper bounded by $\max\{\frac{\sqrt{\delta_0}}{\lambda}, W_2(\rho_{\theta_0}, \rho_0)\}$.

In case that the potential V is not strictly convex, i.e. λ could be negative, the right hand side in (79) may increase to infinity when time $t \to \infty$. However, (71) and (78) reveals that both ρ_{θ_t} and ρ_t stay in a small neighbourhood of the Gibbs ρ_* when t is large. When taking this into account, we are able to show that the error term $W_2(\rho_{\theta_t}, \rho_t)$ doesn't get arbitrarily large. In the following theorem, we provide a uniform bound for the error depending on t.

Theorem 23. *Suppose $\{\rho_t\}_{t\geq 0}$ solves (5) and $\{\rho_{\theta_t}\}_{t\geq 0}$ solves (27), the Hessian of the potential $V \in \mathcal{V}$ is bounded from below by λ, i.e. $\nabla^2 V \succeq \lambda I$, then*

$$W_2(\rho_{\theta_t}, \rho_t) \leq \min\left\{ \frac{\sqrt{\delta_0}}{\lambda} + \left(E_0 - \frac{\sqrt{\delta_0}}{\lambda}\right) e^{-\lambda t},\ \sqrt{\frac{2\delta_0}{\tilde{\lambda}_\beta^2 \beta^2}} + \left(\sqrt{2K_1 - \frac{2\delta_0}{\tilde{\lambda}_\beta^2\beta^2}} + \sqrt{\frac{2K_2}{\tilde{\lambda}_\beta}}\right) e^{-\frac{\tilde{\lambda}_\beta}{2}\beta t} \right\}, \quad (86)$$

where we denote $E_0 = W_2(\rho_{\theta_0}, \rho_0)$, $K_1 = D_{KL}(\rho_{\theta_0}\|\rho_*)$, $K_2 = D_{KL}(\rho_0\|\rho_*)$.

Lemma 24 (Talagrand inequality [37, 52])**.** *If the Gibbs distribution ρ_* satisfies the Logarithmic Sobolev inequality (72) with constant $\tilde{\lambda} > 0$, ρ_* also satisfies the Talagrand inequality:*

$$\sqrt{2\frac{D_{KL}(\rho\|\rho_*)}{\tilde{\lambda}}} \geq W_2(\rho, \rho_*). \quad \text{for any } \rho \in \mathcal{P}. \quad (87)$$

Proof of Theorem 23. The first term is already provided in Theorem 20, the second term is just a quick result of Theorem 16 and Talagrand inequality: for t fixed, (71) together with Talagrand inequality (87) gives:

$$W_2(\rho_{\theta_t}, \rho_*) \leq \sqrt{2\frac{D_{\mathrm{KL}}(\rho_{\theta_t}\|\rho_*)}{\tilde{\lambda}_\beta}} \leq \sqrt{\frac{2\delta_0}{\tilde{\lambda}_\beta^2\beta^2}(1 - e^{-\tilde{\lambda}_\beta\beta t}) + 2K_1 e^{-\tilde{\lambda}_\beta\beta t}} \leq \sqrt{\frac{2\delta_0}{\tilde{\lambda}_\beta^2\beta^2}} + \sqrt{2K_1 - \frac{2\delta_0}{\tilde{\lambda}_\beta^2\beta^2}} e^{-\frac{\tilde{\lambda}_\beta}{2}\beta t}.$$

Similarly, (78) and (87) gives

$$W_2(\rho_t, \rho_*) \leq \sqrt{2\frac{D_{\mathrm{KL}}(\rho_t\|\rho_*)}{\tilde{\lambda}_\beta}} \leq \sqrt{\frac{2K_2}{\tilde{\lambda}_\beta}} e^{-\frac{\tilde{\lambda}_\beta}{2}\beta t}.$$

Applying triangle inequality of Wasserstein distance $W_2(\rho_{\theta_t}, \rho_t) \leq W_2(\rho_{\theta_t}, \rho_*) + W_2(\rho_t, \rho_*)$, we get (86). □

Based on Theorem 23, we can obtain a uniform *a priori* error estimate.

Theorem 25 (Main Theorem on *a priori* error analysis of parametric Fokker-Planck equation)**.** *The approximation error $W_2(\rho_{\theta_t}, \rho_t)$ at any time $t > 0$ can be uniformly bounded by constants $E_0 = W_2(\rho_{\theta_0}, \rho_0)$ and δ_0 defined in (68),*

1. *When $\lambda \geq 0$, the error $W_2(\rho_{\theta_t}, \rho_t)$ can be at least uniformly bounded by $O(E_0 + \sqrt{\delta_0})$.*
2. *When $\lambda < 0$, the error $W_2(\rho_{\theta_t}, \rho_t)$ can be at least uniformly bounded by $O((E_0 + \sqrt{\delta_0})^{\frac{\tilde{\lambda}_\beta\beta}{2|\lambda| + \tilde{\lambda}_\beta\beta}})$.*

Proof of Theorem 25 . Let us denote the right hand side of (86) as

$$E(t) = \min\left\{ -\frac{1}{|\lambda|}\sqrt{\delta_0} + \epsilon_0\ e^{|\lambda|t}, A\sqrt{\delta_0} + Be^{-\mu_\beta t} \right\}, \quad (88)$$

where

$$\epsilon_0 = E_0 + \frac{\sqrt{\delta_0}}{|\lambda|}, \quad A = \frac{\sqrt{2}}{\tilde{\lambda}_\beta\beta}, \quad B = \sqrt{2K_1 - \frac{2\delta_0}{\tilde{\lambda}_\beta^2\beta^2}} + \sqrt{\frac{2K_2}{\tilde{\lambda}_\beta}}, \quad \text{and} \quad \mu_\beta = \frac{\tilde{\lambda}_\beta\beta}{2}$$

are all positive numbers. When $\lambda > 0$, we have $E(t) \leq -\frac{1}{|\lambda|}\sqrt{\delta_0} + \epsilon_0\ e^{|\lambda|t} \lesssim O(\epsilon) = O(E_0 + \sqrt{\delta_0})$. When $\lambda < 0$, the first term in (88) is increasing as a function of time t while the second term is decreasing, as indicated in Figure 6. Let us denote $t_0 = \mathrm{argmax}_{t\geq 0} E(t)$, then t_0 satisfies

$$-\frac{1}{|\lambda|}\sqrt{\delta_0} + \epsilon_0\ e^{|\lambda|t_0} = A\sqrt{\delta_0} + Be^{-\mu_\beta t_0}. \quad (89)$$

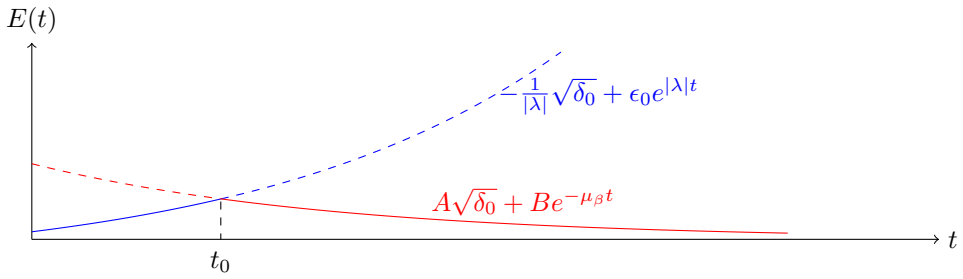

Figure 6: An illustrative diagram for the proof of Theorem 25

Since $A > 0$, (89) leads to $\epsilon_0 e^{|\lambda| t_0} > B e^{-\mu_\beta t_0}$, thus

$$t_0 > \frac{\log\left(\frac{B}{\epsilon_0}\right)}{|\lambda| + \mu_\beta}. \tag{90}$$

Using (90), we show

$$\max_{t \geq 0} E(t) = E(t_0) = A\sqrt{\delta_0} + B\ e^{-\mu_\beta t_0} < A\sqrt{\delta_0} + B^{\frac{|\lambda|}{|\lambda|+\mu_\beta}}\ \epsilon_0^{\frac{\mu_\beta}{|\lambda|+\mu_\beta}}. \tag{91}$$

As a result, $W_2(\rho_{\theta_t}, \rho_t)$ can be uniformly bounded by the right hand side of (91). Since A, B are $O(1)$ coefficients and $\epsilon_0 > \sqrt{\delta_0}$, this uniform bound is dominated by $O(\epsilon_0^{\frac{\mu_\beta}{|\lambda|+\mu_\beta}}) = O((E_0 + \sqrt{\delta_0})^{\frac{\tilde{\lambda}_\beta \beta}{2|\lambda| + \tilde{\lambda}_\beta \beta}})$. □

Remark 12. *In the case that $V \in \mathcal{V}$ is not convex, we can decompose V by $V = U + \phi$ with $\nabla^2 U \succeq KI$ ($K > 0$) and $\nabla^2 \phi \succeq K_\phi I$. We can still assume $\nabla^2 V \succeq \lambda I$, but λ may be negative. It is not hard to verify that $K_\phi < 0$ and $|K_\phi| - K \geq |\lambda|$. On the other hand, one can compute $\tilde{\lambda}_\beta = \frac{K}{\beta} e^{-\frac{osc(\phi)}{\beta}}$. Combining them together, we provide a lower bound for α:*

$$\alpha \geq \gamma(\beta, U, \phi) = \frac{1}{1 + 2\left(\frac{|K_\phi|}{K} - 1\right) e^{\frac{osc(\phi)}{\beta}}}$$

One can verify that increasing the diffusion coefficient β or convexity K, or decreasing the oscillation $osc(\phi)$ and convexity K_ϕ can improve the lower bound $\gamma(\beta, U, \phi)$ for the order α.

In a similar way, we can establish the corresponding *posterior* error estimate for $W_2(\rho_{\theta_t}, \rho_t)$:

Theorem 26 (*Posterior* error analysis of parametric Fokker-Planck equation)**.** *$W_2(\rho_{\theta_t}, \rho_t)$ at any time $t > 0$ can be uniformly bounded by constants $E_0 = W_2(\rho_{\theta_0}, \rho_0)$ and δ_1 defined in (70):*

1. *When $\lambda \geq 0$, $W_2(\rho_{\theta_t}, \rho_t)$ can be at least uniformly bounded by $O(E_0 + \sqrt{\delta_1})$;*
2. *When $\lambda < 0$, $W_2(\rho_{\theta_t}, \rho_t)$ can be at least uniformly bounded by $O((E_0 + \sqrt{\delta_1})^{\frac{\tilde{\lambda}_\beta \beta}{2|\lambda| + \tilde{\lambda}_\beta \beta}})$.*

5.3.2 Wasserstein error for the time discrete schemes

To solve (27) numerically, we need time discrete schemes, such as the one proposed in (45). In this subsection, we present the error estimate in Wasserstein distance for our scheme. We begin our analysis by focusing on the forward Euler scheme, meaning that we apply forward Euler scheme to solve (27) and compute θ_k at each time step. We denote $\rho_{\theta_k} = T_{\theta_k \#} p$. We estimate the W_2-error between ρ_{θ_k} and the real solution ρ_{t_k}. Then we analyze the W_2 distance between the solutions obtained by forward Euler scheme and our scheme (45) respectively, which in turn give us the W_2 error estimate for our scheme.

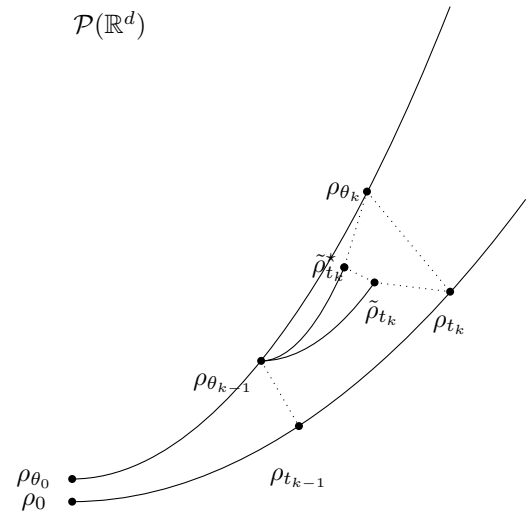

Figure 7: Trajectory of $\{\rho_{\theta_k}\}_{k=0,\dots,N}$ is our numerical solution; trajectory of $\{\rho_t\}_{t\geq 0}$ is the real solution of Fokker-Planck Equation; $\{\tilde{\rho}_t\}_{t\geq t_{k-1}}$ solves (94); $\{\tilde{\rho}^\star_t\}_{t\geq t_{k-1}}$ solves (95).

Theorem 27 (*a priori* error analysis of forward Euler scheme)**.** *Let θ_k $(k=0,1,\cdots,N)$ be the solution of forward Euler scheme applied to* (27) *at time $t_k = kh$ on $[0,T]$ with time step size $h=\frac{T}{N}$, $\rho_{\theta_k} = T_{\theta_k\#}p$, and $\{\rho_t\}_{t\geq 0}$ solves the Fokker-Planck Equation* (5) *exactly. Assume that the Hessian of the potential function $V\in\mathcal{C}^2(\mathbb{R}^d)$ can be bounded from above and below, i.e. $\lambda I \preceq \nabla^2 V \preceq \Lambda I$. Then*

$$W_2(\rho_{\theta_k},\rho_{t_k}) \leq (\sqrt{\delta_0}h + C_N h^2)\frac{1-e^{-\lambda t_k}}{1-e^{-\lambda h}} + e^{-\lambda t_k} W_2(\rho_{\theta_0},\rho_0) \quad \textit{for any} \quad t_k = kh, \quad 0\leq k\leq N, \tag{92}$$

where C_N is a constant whose explicit formula is provided in (107).

In order to estimate $W_2(\rho_{\theta_k},\rho_{t_k})$, we use the triangle inequality of W_2 distance [52] to separate it into three parts:

$$W_2(\rho_{\theta_k},\rho_{t_k}) \leq W_2(\rho_{\theta_k},\tilde{\rho}^\star_{t_k}) + W_2(\tilde{\rho}^\star_{t_k},\tilde{\rho}_{t_k}) + W_2(\tilde{\rho}_{t_k},\rho_{t_k}). \tag{93}$$

Here $\{\tilde{\rho}_t\}_{t_{k-1}\leq t\leq t_k}$ satisfies:

$$\frac{\partial\tilde{\rho}_t}{\partial t} = \nabla\cdot(\tilde{\rho}_t\nabla V) + \beta\Delta\tilde{\rho}_t\ , \quad \tilde{\rho}_{t_{k-1}} = \rho_{\theta_{k-1}}, \tag{94}$$

and $\{\tilde{\rho}^\star_t\}_{t\geq t_{k-1}}$ satisfies:

$$\frac{\partial\tilde{\rho}^\star_t}{\partial t} = \nabla\cdot(\tilde{\rho}^\star_t\nabla(V+\beta\log\rho_{\theta_{k-1}}))\ , \quad \tilde{\rho}^\star_{t_{k-1}} = \rho_{\theta_{k-1}}. \tag{95}$$

Figure 7 shows the relations of different items used in our proof. We present three lemmas that estimate three terms in (93) respectively.

Lemma 28. *$W_2(\rho_{\theta_k},\tilde{\rho}^\star_{t_k})$ in (93) can be upper bounded by $\sqrt{\delta_0}h + O(h^2)$.*

An explicit formula for the coefficient of h^2 is included in the following proof.

Proof. We establish the desired estimation by introducing several different pushforward maps as shown in Figure 8 and then applying triangle inequality. (a) We know $\rho_{\theta_{k-1}} = T_{\theta_{k-1}\#}p$ and $\rho_{\theta_k} = T_{\theta_k\#}p$, let us denote $T_{t_{k-1}\to t_k} = T_{\theta_k}\circ T^{-1}_{\theta_{k-1}}$. Then $\rho_{\theta_k} = T_{t_{k-1}\to t_k\#}\rho_{\theta_{k-1}}$. (b) Let $\xi_{k-1} = \dot{\theta}_{k-1} = -G(\theta_{k-1})^{-1}\nabla_\theta H(\theta_{k-1})$ and by convention, we denote $\mathbf{\Psi}$ as solution of (15). We consider the map $\tilde{T}_{t_{k-1}\to t_k}(\cdot) = \mathrm{Id} + h\nabla\mathbf{\Psi}(\cdot)^T\xi_{k-1}$. (c) We denote $\zeta_{k-1}(\cdot) = V(\cdot) + \beta\log\rho_{\theta_{k-1}}(\cdot)$. The particle version (recall (6)) of (95) is:

$$\dot{z}_t = -\nabla\zeta_{k-1}(z_t) \quad 0\leq t\leq h \quad \text{with initial condition } z_0 = x. \tag{96}$$

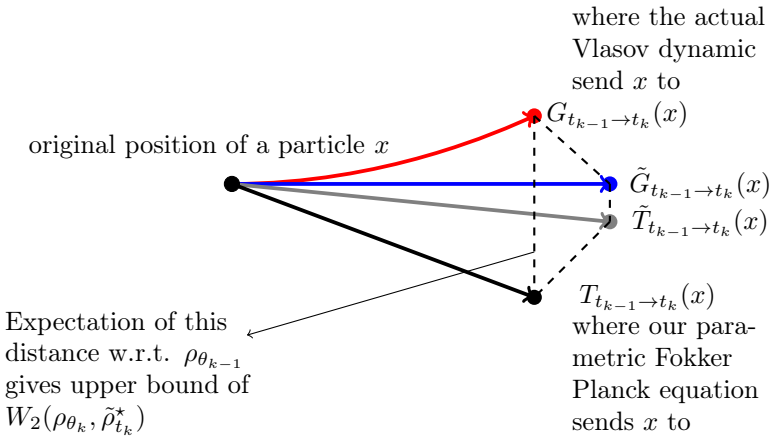

Figure 8: Illustration of proof strategy for Lemma 28

we denote the solution map of (96) by $G_{t_{k-1}\to t_k}(x) = z_{t_k}$. Then $\tilde{\rho}^\star_{t_k} = G_{t_{k-1}\to t_k \#}\rho_{\theta_{k-1}}$. (d) The map $G_{t_{k-1}\to t_k}$ is obtained by solving an ODE, in order to compare the difference with $T_{t_{k-1}\to t_k}$, we consider the ODE with fixed initial vector field:

$$\dot{\tilde{z}}_t = -\nabla\zeta_{k-1}(x) \quad 0 \le t \le h \quad \tilde{z}_0 = x. \tag{97}$$

This ODE will induce the solution map $\tilde{G}_{t_{k-1}\to t_k}(\cdot) = \mathrm{Id} - h\nabla\zeta_{k-1}(\cdot)$. With the maps defined in (a),(b),(c),(d), and using the triangle inequality of W_2 distance, we have,

$$\begin{aligned} W_2(\rho_{\theta_k}, \tilde{\rho}^\star_{t_k}) &= W_2(T_{t_{k-1}\to t_k \#}\rho_{\theta_{k-1}}, G_{t_{k-1}\to t_k \#}\rho_{\theta_{k-1}}) \\ &\le \underbrace{W_2(T_{t_{k-1}\to t_k \#}\rho_{\theta_{k-1}}, \tilde{T}_{t_{k-1}\to t_k \#}\rho_{\theta_{k-1}})}_{\text{(A)}} + \underbrace{W_2(\tilde{T}_{t_{k-1}\to t_k \#}\rho_{\theta_{k-1}}, \tilde{G}_{t_{k-1}\to t_k \#}\rho_{\theta_{k-1}})}_{\text{(B)}} \\ &\quad + \underbrace{W_2(\tilde{G}_{t_{k-1}\to t_k \#}\rho_{\theta_{k-1}}, G_{t_{k-1}\to t_k \#}\rho_{\theta_{k-1}})}_{\text{(C)}}. \end{aligned}$$

In the rest of the proof, We give upper bounds for distances (A),(B) and (C) respectively.

(A) Set $\theta(\tau) = \theta_{k-1} + \frac{\tau}{h}(\theta_k - \theta_{k-1}) = \theta_{k-1} + \tau\xi_{k-1}$. For any x, consider $x_\tau = T_{\theta(\tau)}(T^{-1}_{\theta_{k-1}}(x))$ with $0 \le \tau \le h$, then $\{x_\tau\}_{0\le\tau\le h}$ satisfies

$$\dot{x}_\tau = \partial_\theta T_{\theta(\tau)}(T^{-1}_{\theta(\tau)}(x_\tau))\xi_{k-1} \quad 0 \le \tau \le h. \tag{98}$$

If $x_0 \sim \rho_{\theta_{k-1}}$ in (98), it is clear that $x_h \sim T_{t_{k-1}\to t_k \#}\rho_{\theta_{k-1}}$. Furthermore, we denote the distribution of x_τ as ρ_τ and $\{\psi_\tau\}$ satisfying

$$-\nabla\cdot(\rho_\tau(x)\partial_\theta T_{\theta(\tau)}(T^{-1}_{\theta(\tau)}(x))) = -\nabla\cdot(\rho_\tau(x)\nabla\psi_\tau(x)) \quad 0 \le \tau \le h. \tag{99}$$

If we consider

$$\dot{y}_\tau = \nabla\psi_\tau(y_\tau) \quad 0 \le \tau \le h \quad \text{with } y_0 \sim \rho_{\theta_{k-1}},$$

and denote ϱ_τ as the distribution of y_τ, by continuity equation and (99), we know $\rho_\tau = \varrho_\tau$ for $0 \le \tau \le h$, thus $y_h \sim T_{t_{k-1}\to t_k \#}\rho_{\theta_{k-1}}$. On the other hand, when $\tau = 0$, (99) shows $\nabla\psi_0(x) = \nabla\mathbf{\Psi}(x)^T\xi_{k-1}$. Combining them together, we bound term (A) as,

$$\begin{aligned} W_2^2(T_{t_{k-1}\to t_k \#}\rho_{\theta_{k-1}}, \tilde{T}_{t_{k-1}\to t_k \#}\rho_{\theta_{k-1}}) &\le \mathbb{E}_{y_0\sim\rho_{\theta_{k-1}}}|y_h - (y_0 + h\nabla\psi_0(y_0))|^2 \\ &\le \mathbb{E}_{y_0\sim\rho_{\theta_{k-1}}}\left|\int_0^h \nabla\psi_\tau(y_\tau) - \nabla\psi_0(y_0)\, d\tau\right|^2 \end{aligned}$$

If we define the constant (only depends on θ_{k-1} and h),

$$M(\theta_{k-1},h)=\left(\mathop{\mathbb{E}}_{y_0\sim\rho_{\theta_{k-1}}}\left[\sup_{0\le\tau\le h}\left|\frac{\nabla\psi_\tau(y_\tau)-\nabla\psi_0(y_0)}{\tau}\right|^2\right]\right)^{1/2}. \tag{100}$$

we obtain,

$$W_2(T_{t_{k-1}\to t_k}\#\rho_{\theta_{k-1}},G_{t_{k-1}\to t_k}\#\rho_{\theta_{k-1}})\le\frac{1}{2}M(\theta_{k-1},h)h^2.$$

(B) We have

$$\begin{aligned}W_2^2(\tilde{T}_{t_{k-1}\to t_k}\#\rho_{\theta_{k-1}},\tilde{G}_{t_{k-1}\to t_k}\#\rho_{\theta_{k-1}})&\le\int|\tilde{T}_{t_{k-1}\to t_k}(x)-\tilde{G}_{t_{k-1}\to t_k}(x)|^2\rho_{\theta_{k-1}}(x)\,dx\\&=h^2\left(\int|\nabla\mathbf{\Psi}(x)^T\xi_{k-1}-(-\nabla\zeta_{k-1}(x))|^2\rho_{\theta_{k-1}}(x)\,dx\right)\\&=h^2\left(\int|\nabla\mathbf{\Psi}(T_{\theta_{k-1}}(x))^T\xi_{k-1}-(-\nabla(V+\beta\log\rho_{\theta_{k-1}})\circ T_{\theta_{k-1}}(x))|^2\,dp(x)\right)\le\delta_0\,h^2.\end{aligned}$$

The last inequality is due to Theorem 10 and definition (68).

(C) Recall that $\{z_t\}and\{\tilde{z}_t\}$ solve (96) and (97) with initial condition $z_0=\tilde{z}_0=x$ respectively, we can estimate term (C) as

$$W_2^2(\tilde{G}_{t_{k-1}\to t_k}\#\rho_{\theta_{k-1}},G_{t_{k-1}\to t_k}\#\rho_{\theta_{k-1}})\le\mathbb{E}_{x\sim\rho_{\theta_{k-1}}}|z_h-\tilde{z}_h|^2=\mathbb{E}_{x\sim\rho_{\theta_{k-1}}}\left|\int_0^h\nabla\zeta_{k-1}(x)-\nabla\zeta_{k-1}(z_\tau)\,d\tau\right|$$

Let us denote the constant (only depends θ_{k-1} and h)

$$N(\theta_{k-1},h)=\left(\mathop{\mathbb{E}}_{x\sim\rho_{\theta_{k-1}}}\left[\sup_{0\le\tau\le h}\left|\frac{\nabla\zeta_{k-1}(x)-\nabla\zeta_{k-1}(z_\tau)}{\tau}\right|^2\right]\right)^{1/2}. \tag{101}$$

Similar to (A), we have:

$$W_2(\tilde{G}_{t_{k-1}\to t_k}\#\rho_{\theta_{k-1}},G_{t_{k-1}\to t_k}\#\rho_{\theta_{k-1}})\le\frac{1}{2}N(\theta_{k-1},h)h^2$$

Combining the estimates for terms (A),(B) and (C), we obtain,

$$W_2(\rho_{\theta_k},\tilde{\rho}^\star_{t_k})\le\sqrt{\delta_0}\,h+\frac{M(\theta_{k-1},h)+N(\theta_{k-1},h)}{2}\,h^2.$$

□

Lemma 29. *The second term in (93) can be upper bounded by $O(h^2)$.*

Proof. Recall that $\tilde{\rho}_t$ is defined by (94) and $\tilde{\rho}^*_t$ is defined by (95). We can rewrite (95) as:

$$\frac{\partial\tilde{\rho}^\star_t}{\partial t}=\nabla\cdot(\tilde{\rho}^\star_t(\nabla V+\beta\nabla\log\rho_{\theta_{k-1}}-\nabla\log\tilde{\rho}^\star_t))+\beta\Delta\tilde{\rho}^\star_t\quad t_{k-1}\le t\le t_k$$

We consider the following Stochastic Differential Equations (SDEs) sharing the same trajectory of Brownian motion $\{\boldsymbol{B}_\tau\}_{0\le\tau\le h}$ and initial condition:

$$dx_\tau=-\nabla V(x_\tau)d\tau+\sqrt{2\beta}\,d\boldsymbol{B}_\tau \tag{102}$$

$$dx^\star_\tau=-\nabla V(x^\star_\tau)d\tau+(\beta\nabla\log\tilde{\rho}^\star_{t_{k-1}+\tau}(x^\star_\tau)-\beta\nabla\log\rho_{\theta_{k-1}}(x^\star_\tau))d\tau+\sqrt{2\beta}\,d\boldsymbol{B}_\tau \tag{103}$$

with initial condition: $x_0=x^\star_0\sim\rho_{\theta_{k-1}}$ and $0\le\tau\le h$.

Subtracting (102) from (103), we get:

$$x^\star_\tau - x_\tau = \int_0^\tau \nabla V(x_s) - \nabla V(x^\star_s) + \vec{r}(x^\star_s, s)\ ds,$$

in which we denote $\vec{r}(x,\tau) = \beta\nabla \log \tilde{\rho}^\star_{t_{k-1}+\tau}(x) - \beta\nabla \log \rho_{\theta_{k-1}}(x)$ for convenience. Hence,

$$\begin{aligned}
\mathbb{E}|x^\star_\tau - x_\tau|^2 &= \mathbb{E}\left|\int_0^\tau \nabla V(x_s) - \nabla V(x^\star_s) + \vec{r}(x^\star_s, s)\ ds\right|^2 \leq 2\ \mathbb{E}\left|\int_0^\tau \nabla V(x_s) - \nabla V(x^\star_s)\ ds\right|^2 + 2\ \mathbb{E}\left|\int_0^\tau \vec{r}(x^\star_s, s)\ ds\right|^2 \\
&\leq 2\ \mathbb{E}\left[\tau\ \int_0^\tau |\nabla V(x_s) - \nabla V(x^\star_s)|^2\ ds\right] + 2\ \mathbb{E}\left[\tau\ \int_0^\tau |\vec{r}(x^\star_s, s)|^2\ ds\right] \\
&= 2\tau\left(\int_0^\tau \mathbb{E}|\nabla V(x_s) - \nabla V(x^\star_s)|^2 + \mathbb{E}|\vec{r}(x^\star_s, s)|^2\ ds\right)
\end{aligned}$$

Since Hessian of V is bounded above by Λ, $|\nabla V(x) - \nabla V(y)| \leq \Lambda|x-y|$ for any $x, y \in \mathbb{R}^d$, we have the inequality:

$$\mathbb{E}|x^\star_\tau - x_\tau|^2 \leq 2\tau\Lambda^2\ \int_0^\tau \mathbb{E}|x^\star_s - x_s|^2\ ds + 2\tau\ \int_0^\tau \mathbb{E}|\vec{r}(x^\star_s, s)|^2\ ds \tag{104}$$

If we define $U_\tau = \int_0^\tau \mathbb{E}|x^\star_s - x_s|^2\ ds$ and $R_\tau = \int_0^\tau \mathbb{E}|\vec{r}(x^\star_s, s)|^2\ ds$, (104) becomes:

$$U'_\tau \leq 2\Lambda^2\tau U_\tau + 2\tau R_\tau$$

By integrating this inequality, we have $U_\tau \leq \int_0^\tau 2e^{\Lambda(\tau^2-s^2)}sR_s\ ds$ and $U'_\tau \leq 4\Lambda^2\tau\int_0^\tau e^{\Lambda(\tau^2-s^2)}sR_s ds + 2\tau R_\tau$. Therefore

$$W_2(\tilde{\rho}^\star_{t_k}, \tilde{\rho}_{t_k}) \leq \sqrt{\mathbb{E}|x^*_h - x_h|^2} = U'_h \leq \sqrt{4\Lambda^2 h\int_0^h e^{\Lambda(h^2-s^2)}sR_s\ ds + 2hR_h}$$

Let us define a constant

$$L_{k-1}(\theta_{k-1}, h) = \sup_{0\leq\tau\leq h}\left\{\mathbb{E}\left|\frac{\nabla \log \rho_{t_{k-1}+\tau}(x^\star_\tau) - \nabla \log \rho_{t_{k-1}}(x^\star_\tau)}{\tau}\right|\right\},$$

then for any $0 \leq \tau \leq h$, we can estimate $R_\tau \leq \int_0^h |\beta L_{k-1}(\theta_{k-1}, h)s|^2\ ds \leq \frac{1}{3}\beta^2 L_{k-1}(\theta_{k-1}, h)^2 h^3$, which leads to:

$$W_2(\tilde{\rho}^\star_{t_k}, \tilde{\rho}_{t_k}) \leq \sqrt{4\Lambda^2 h\int_0^h e^{\Lambda(h^2-s^2)}sR_s\ ds + 2hR_h} \leq \sqrt{\frac{4}{3}\Lambda^2 e^{\Lambda h^2}\beta^2 L^2 h^6 + \frac{2}{3}\beta^2 L^2 h^4} \tag{105}$$

Here we denote L as $L_{k-1}(\theta_{k-1}, h)$ for convenience. Obviously, when h is small, the term containing h^4 in (105) dominates the upper bound term. Thus we obtain

$$W_2(\tilde{\rho}^\star_{t_k}, \tilde{\rho}_{t_k}) \leq \beta L_{k-1}(\theta_{k-1}, h)h^2,$$

when h is small enough.

□

Remark 13. *Analyzing the discrepancy of stochastic particles under different movements provides a natural upper bound for W_2 distance. Both Lemma 28 and Lemma 29 are derived by making use of the particle version of their corresponding density evolution. Such proving strategy was motivated from section 3.3.*

Lemma 30. *The third term in (93) satisfies,*

$$W_2(\rho_{t_k}, \tilde{\rho}_{t_k}) \leq e^{-\lambda h}W_2(\rho_{t_{k-1}}, \rho_{\theta_{k-1}})$$

This lemma is a direct corollary of the following theorem:

Theorem 31. *Suppose the potential $V \in C^2(\mathbb{R}^d)$ satisfying $\nabla^2 V \succeq \lambda I$ for a finite real number λ, i.e. the matrix $\nabla^2 V(x) - \lambda I$ is semi-positive definite for any $x \in \mathbb{R}^d$. Given $\rho_1, \rho_2 \in \mathcal{P}$, and denote $\rho_t^{(1)}$ and $\rho_t^{(2)}$ the solutions of Fokker-Planck equation with different initial distributions ρ_1 and ρ_2 respectively, i.e.*

$$\frac{\partial \rho_t^{(1)}}{\partial t} = \nabla \cdot (\rho_t^{(1)} \nabla V) + \beta \Delta \rho_t^{(1)} \quad \rho_0^{(1)} = \rho_1,$$
$$\frac{\partial \rho_t^{(2)}}{\partial t} = \nabla \cdot (\rho_t^{(2)} \nabla V) + \beta \Delta \rho_t^{(2)} \quad \rho_0^{(2)} = \rho_2.$$

Then

$$W_2(\rho_t^{(1)}, \rho_t^{(2)}) \leq e^{-\lambda t} W_2(\rho_1, \rho_2) \tag{106}$$

This is a known stability result on Wasserstein gradient flows. One can find its proof in [3] or [52]. With the results in Lemmas 28,29,30, we are ready to prove Theorem 27.

Proof. (Proof of Theorem 27) For convenience, we write

$$\mathrm{Err}_k = W_2(\rho_{\theta_k}, \rho_{t_k}) \quad k = 0, 1, ..., N.$$

Combining Lemma 28, Lemma 29 and Lemma 30, the triangle inequality (93) becomes

$$\mathrm{Err}_k \leq \sqrt{\delta_0}\ h + \left(\frac{M(\theta_{k-1}, h) + N(\theta_{k-1}, h)}{2} + \beta L_{k-1}(\theta_{k-1}, h) \right) h^2 + e^{-\lambda h}\ \mathrm{Err}_{k-1}.$$

Let us denote:

$$C_N = \max_{0 \leq k \leq N-1} \left\{ \frac{M(\theta_{k-1}, h) + N(\theta_{k-1}, h)}{2} + \beta L_{k-1}(\theta_{k-1}, h) \right\}. \tag{107}$$

We have:

$$\mathrm{Err}_k \leq \sqrt{\delta_0} h + C_N h^2 + e^{-\lambda h} \mathrm{Err}_{k-1} \tag{108}$$

Multiplying $e^{\lambda k h}$ to both sides of (108), we get:

$$e^{\lambda k h} \mathrm{Err}_k \leq (\sqrt{\delta_0}\ h + C_N\ h^2) e^{\lambda k h} + e^{\lambda (k-1) h} \mathrm{Err}_{k-1}. \tag{109}$$

For any n, $1 \leq n \leq N$, summing (109) from 1 to n, we reach

$$e^{\lambda n h} \mathrm{Err}_n \leq (\sqrt{\delta_0} h + C_N h^2) \left(\sum_{k=1}^{n} e^{\lambda k h} \right) + \mathrm{Err}_0 = (\sqrt{\delta_0} h + C_N h^2) \frac{e^{\lambda (n+1) h} - e^{\lambda h}}{e^{\lambda h} - 1} + \mathrm{Err}_0.$$

Recall that $t_n = nh$ for $1 \leq n \leq N$, it leads to:

$$\mathrm{Err}_n \leq (\sqrt{\delta_0} h + C_N h^2) \frac{1 - e^{-\lambda t_n}}{1 - e^{-\lambda h}} + e^{-\lambda t_n} \mathrm{Err}_0 \quad n = 1, ..., N.$$

□

Theorem 27 indicates that the error $W_2(\rho_{\theta_k}, \rho_{t_k})$ is upper bounded by $O(\sqrt{\delta_0}) + O(C_N h) + O(W_2(\rho_{\theta_0}, \rho_0))$. Here $O(\sqrt{\delta_0})$ is the essential error term that originates from the approximation mechanism of our parametric Fokker-Planck equation. The $O(C_N h)$ error term is induced by the finite difference scheme. And the $O(W_2(\rho_{\theta_0}, \rho_0))$ term is the initial error.

It worth mentioning that the error bound for forward Euler scheme in (92) matches the error bound for the continuous scheme (79) as we reduce the effects introduced by finite difference. To be more precise, under the assumption $\lim_{h \to 0} C_N h = 0$, we have:

$$\begin{aligned} &\lim_{h \to 0} (\sqrt{\delta_0} h + C_N h^2) \frac{1 - e^{-\lambda t}}{1 - e^{-\lambda h}} + e^{-\lambda t} W_2(\rho_{\theta_0}, \rho_0) \\ = &\lim_{h \to 0} (\sqrt{\delta_0} + C_N h)(1 - e^{-\lambda t}) \frac{h}{1 - e^{-\lambda h}} + e^{-\lambda t} W_2(\rho_{\theta_0}, \rho_0) = \frac{\sqrt{\delta_0}}{\lambda}(1 - e^{-\lambda t}) + e^{-\lambda t} W_2(\rho_{\theta_0}, \rho_0) \end{aligned}$$

this indicates that error bounds (92) and (79) are compatible as $h \to 0$.

Similar to the discussion in previous sections, we can naturally extend Theorem 27 to a *posterior* estimate.

Theorem 32 (*posterior* error analysis of forward Euler scheme)**.**

$$W_2(\rho_{\theta_k}, \rho_{t_k}) \le (\sqrt{\delta_1}h + C_N h^2)\frac{1-e^{-\lambda t_k}}{1-e^{-\lambda h}} + e^{-\lambda t_k} W_2(\rho_{\theta_0}, \rho_0) \quad \textit{for any} \quad t_k = kh, \quad 0 \le k \le N.$$

The explicit definition of the constant C_N is in (107)*.*

Up to this point, we mainly analyze the error term for the forward Euler scheme. In our numerical implementation, we adopt the scheme (45), which turns out to be a semi-implicit scheme with $O(h^2)$ local error. In the following discussion, we compare the difference between the numerical solutions of our semi-implicit scheme and forward Euler scheme.

Recall that the parametric Fokker-Planck equation (27) is an ODE: $\dot{\theta} = G(\theta)^{-1}\nabla_\theta H(\theta)$. We consider two numerical schemes:

$$\theta_{n+1} = \theta_n - hG(\theta_n)^{-1}\nabla_\theta H(\theta_n) \quad \theta_0 = \theta,\ n = 1, 2, ..., N \quad \text{forward Euler scheme,} \tag{110}$$

$$\hat{\theta}_{n+1} = \hat{\theta}_n - hG(\hat{\theta}_n)^{-1}\nabla_\theta H(\hat{\theta}_{n+1}) \quad \hat{\theta}_0 = \theta,\ n = 1, 2, ..., N \quad \text{semi-Implicit-Euler scheme.} \tag{111}$$

We denote $F(\theta') = G(\theta')^{-1}\nabla_\theta F(\theta'')$, and set:

$$L_1 = \max_{1\le n\le N}\left\{\|F(\theta_n) - F(\hat{\theta}_n)\|/\|\theta_n - \hat{\theta}_n\|\right\}, \quad L_2 = \max_{1\le k\le N-1}\{\|\nabla_\theta H(\hat{\theta}_n) - \nabla_\theta H(\hat{\theta}_{n+1})\|/\|\hat{\theta}_n - \hat{\theta}_{n+1}\|\},$$
$$M_1 = \max_{1\le n\le N}\{\|G(\hat{\theta}_n)^{-1}\|\}, \quad M_2 = \max_{1\le n\le N}\{\|\nabla_\theta H(\hat{\theta}_n)\|\},$$

where $\|\cdot\|$ is a vector norm (or its corresponding matrix norm).

Theorem 33 (Relation between forward Euler and proposed semi-implicit schemes)**.** *The numerical solutions θ_n and $\hat{\theta}_n$ of the forward Euler and semi-implicit schemes with time stepsize h and $Nh = T$ satisfy*

$$\|\theta_n - \hat{\theta}_n\| \le ((1 + L_1 h)^n - 1)\frac{M_1^2 M_2 L_2}{L_1}h \quad n = 1, 2, ..., N$$

This result implies that $\|\theta_n - \hat{\theta}_n\|$ can be upper bounded by $(e^{L_1 T} - 1)\frac{M_1^2 M_2 L_2}{L_1}h$. When assuming the upper bounds $L_1, L_2, M_1, M_2 \sim O(1)$ as $h \to 0$ (or equivalently $N \to \infty$), the differences between our proposed semi-implicit scheme and forward Euler scheme can be bounded by $O(h)$. As a consequence, we are able to establish $O(h)$ error bound for our proposed scheme (45).

Proof of Theorem 33. If we subtract (111) from (110),

$$(\theta_{n+1} - \hat{\theta}_{n+1}) = (\theta_n - \hat{\theta}_n) - h(G(\theta_n)^{-1}\nabla_\theta H(\theta_n) - G(\hat{\theta}_n)^{-1}\nabla_\theta H(\hat{\theta}_{n+1}))$$

and denote $e_n = \theta_n - \hat{\theta}_n$, we may rewrite this equation as

$$e_{n+1} = e_n - h(F(\theta_n) - F(\hat{\theta}_n) + G(\hat{\theta}_n)^{-1}(\nabla_\theta H(\hat{\theta}_n) - \nabla_\theta H(\hat{\theta}_{n+1}))).$$

Recall the definitions of L_1, L_2, M_1, we have

$$\|e_{n+1}\| \le \|e_n\| + hL_1\|e_n\| + hM_1 L_2\|\hat{\theta}_{n+1} - \hat{\theta}_n\|.$$

By the semi-simplicit scheme, we have

$$\hat{\theta}_{n+1} - \hat{\theta}_n = -hG(\hat{\theta}_n)^{-1}\nabla_\theta H(\hat{\theta}_{n+1})$$

Thus $|\hat{\theta}_{n+1} - \hat{\theta}_n\| \le hM_1 M_2$. This gives us a recurrent inequality,

$$\|e_{n+1}\| \le \|e_n\| + hL_1\|e_n\| + M_1^2 M_2 L_2 h^2,$$

which implies

$$\left(\|e_{n+1}\| + \frac{M_1^2 M_2 L_2}{L_1}h\right) \le (1 + hL_1)\left(\|e_n\| + \frac{M_1^2 M_2 L_2}{L_1}h\right) \quad n = 0, 1, ..., N-1.$$

This leads to:

$$\|e_n\| \leq ((1+hL_1)^n - 1)\frac{M_1^2 M_2 L_2}{L_1} h.$$

When we solve the ODE on $[0,T]$ with $h = T/N$, we have $(1+hL_1)^n \leq (1+hL_1)^N = \left(1+\frac{L_1 T}{N}\right)^N \leq e^{L_1 T}$. This means all terms $\{\|e_n\|\}_{1\leq n\leq N}$ can be upper bounded by $(e^{L_1 T}-1)\frac{M_1^2 M_2 L_2}{L_1} h$. □

Remark 14. *In order to make our argument clear and concise, we omitted the errors introduced by the approximation of ReLU function ψ_λ. Careful analysis on how well $\nabla\psi_\lambda$ can approximate a general gradient field is among our future research directions.*

Remark 15. *The convergence property of the Stochastic Gradient Descent method (mainly Adam method) used in our Algorithm 1 is not discussed in details. One can check its convergence analysis in the paper [21].*

6 Numerical examples

In this section, we consider solving Fokker-Planck equation (5) on $\mathbb{R}^d$ with $\beta = 1$ and initial condition $\rho_0(x) = \mathcal{N}(0, I_d)$[2] by using Algorithm 1. We demonstrate several numerical examples with different potential functions V. In the following experiments, unless specifically stated, we choose the length of normalizing flow T_θ as 60. We set $\psi_\lambda : \mathbb{R}^d \to \mathbb{R}$ as ReLU network with length 6 and hidden dimension 20. We use Adam (Adaptive Moment Estimation) Stochastic Gradient Descent method [21] with default parameters $\beta_1 = 0.9, \beta_2 = 0.999; \epsilon = 10^{-8}$. For the parameters of Algorithm 1, we choose $\alpha_{\text{out}} = 0.005$, $\alpha_{\text{in}} = 0.0005$. We follow Remark 10 to choose $K_{\text{in}}, K_{\text{out}} = \max\{1000, 300d\}$. Based on our experience, we set $M_{\text{out}} = O(\frac{h}{\alpha_{\text{out}}})$. The suitable value of M_{in} can be chosen after several quick tests to make sure that every inner optimization problem (64) can be solved.

6.1 Quadratic Potential

Our first set of examples uses quadratic potential V. In this case, we can compute the explicit solution of (5). These examples are used for the verification purpose, because we can check the results with exact solutions.

6.1.1 2D cases

We take $d = 2$, and set $V(x) = \frac{1}{2}(x-\mu)^T\Sigma^{-1}(x-\mu)$, with $\mu = [3,3]^T$ and $\Sigma = \text{diag}([0.25, 0.25])$. The solution of (5) is:

$$\rho_t = \mathcal{N}(\mu(t), \Sigma(t)) \quad \mu(t) = (1-e^{-4t})\mu,\ \Sigma(t) = \begin{bmatrix} \frac{1}{4}+\frac{3}{4}e^{-8t} & \\ & \frac{1}{4}+\frac{3}{4}e^{-8t} \end{bmatrix} \quad t \geq 0.$$

We solve the equation in time interval $[0, 0.7]$ with time stepsize 0.005. We set $M_{\text{out}} = 20$ and $M_{\text{in}} = 100$.

To compare against the exact solution, we set $M = 6000$ and sample $\{\boldsymbol{X}_1, ..., \boldsymbol{X}_M\} \sim T_{\theta_k \#} p$ at time t_k and use:

$$\hat{\mu}^k = \frac{1}{M}\sum_{j=1}^M \boldsymbol{X}_j, \quad \hat{\Sigma}^k = \frac{1}{M-1}\sum_{j=1}^M (\boldsymbol{X}_j - \hat{\mu}_k)(\boldsymbol{X}_j - \hat{\mu}_k)^T$$

to compute for its empirical mean and covariance of $\hat{\rho}_k$. We plot the curves $\{\hat{\mu}^{(k)}\}$, $\{(\hat{\Sigma}_{11}^{(k)}, \hat{\Sigma}_{22}^{(k)})\}$, $\{(\hat{\mu}_1^{(k)}$ in , $\hat{\Sigma}_{11}^{(k)})\}$ in Figure 12, these plots properly captures the exponential convergence exhibited by the explicit solution $\{\mu(t)\}$, $\{(\Sigma_{11}(t), \Sigma_{22}(t))\}$, $\{(\mu_1(t), \Sigma_{11}(t))\}$.

[2]We can set initial value θ_0 so that $T_{\theta_0} = Id$ and thus $\rho_0 = T_{\theta_0 \#} p$ is standard Gaussian distribution.

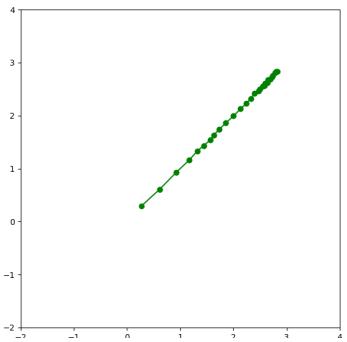

Figure 9: $\{\hat{\mu}^{(k)}\}$

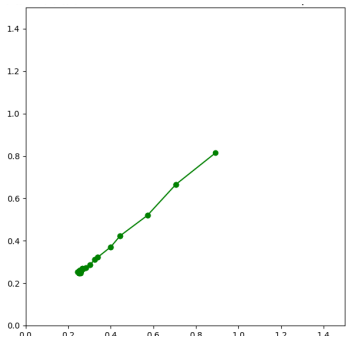

Figure 10: $\{(\hat{\Sigma}_{11}^{(k)}, \hat{\Sigma}_{22}^{(k)})\}$

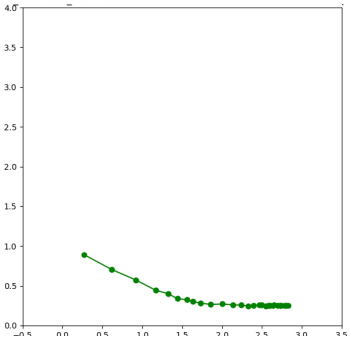

Figure 11: $\{(\hat{\mu}_{(k)}, \hat{\Sigma}_{11}^{(k)})\}$

Figure 12: Plot of empirical statistics

We also exam the network $\psi_{\hat{\lambda}}$ trained at the end of each outer iteration. Generally speaking, the gradient field $\nabla\psi_{\hat{\lambda}}$ reflects the movements of the particles under the Vlasov-typed dynamic (6) at every time step. Here are the graph of $\psi_{\hat{\lambda}}$ at $k = 10, k = 140$ (Figure 13, Figure 14). As we can see from these graphs, the gradient field is in the same direction, but judging from the variation of two $\psi_{\hat{\lambda}}$s, when $k = 10$, $|\nabla\psi_{\hat{\lambda}}|$ is much greater than its value at $k = 140$. This is because when $t = 140$, the distribution is already close to the Gibbs distribution, the particles no longer need to move for a long distance to reach their final destination.

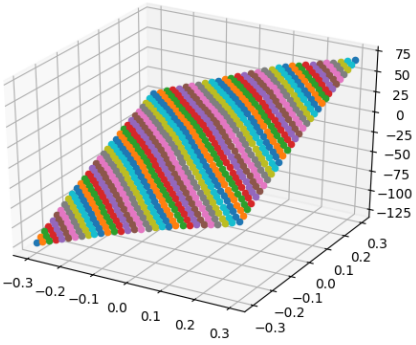

Figure 13: Graph of $\psi_{\hat{\lambda}}$ after $M_{\text{out}} = 20$ outer iterations at $k = 10$th time step

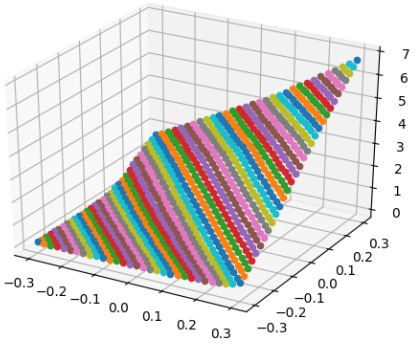

Figure 14: Graph of $\psi_{\hat{\lambda}}$ after $M_{\text{out}} = 20$ outer iterations at $k = 140$th time step

In the next example, we apply our algorithm to the Fokker-Planck equation with non-isotropic potential

$$V(x) = \frac{1}{2}(x-\mu)^T\Sigma^{-1}(x-\mu) \quad \mu = \begin{bmatrix} 3 \\ 3 \end{bmatrix} \text{ and } \Sigma = \begin{bmatrix} 1 & \\ & \frac{1}{4} \end{bmatrix}.$$

One can verify that the solution to (5) is

$$\rho_t = \mathcal{N}(\mu_t, \Sigma_t) \quad \mu_t = \begin{bmatrix} 3(1-e^{-t}) \\ 3(1-e^{-4t}) \end{bmatrix}, \ \Sigma_t = \begin{bmatrix} 1 & \\ & \frac{1}{4}(1+3e^{-8t}) \end{bmatrix}.$$

We use the same parameters as before. We solve (5) on time interval $[0, 1.4]$ with time step size 0.005.

Similarly, we also plot the empirical mean trajectory, one can compare it with the true solution $\mu(t) = (3(1-e^{-t}), 3(1-e^{-4t}))$. Both the curvature and the exponential convergence to μ are captured by our numerical result. To demonstrate the effectiveness of our formulation, we also compare our result with the

mean trajectory obtained by computing the flat gradient flow $\dot{\theta} = -\nabla_\theta H(\theta)$, which is plotted in Figure 16. It reveals very different behavior of the flat gradient (∇_θ) flow and Wasserstein gradient ($G(\theta)^{-1}\nabla_\theta$) flow. Clearly, our approximation based on Wasserstein gradient flow captures the exact mean function much more accurately.

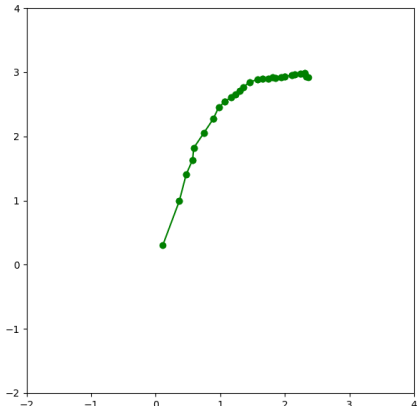

Figure 15: mean trajectory of $\{\rho_{\theta_t}\}$ w.r.t. $\dot{\theta} = -G(\theta)^{-1}\nabla_\theta H(\theta)$

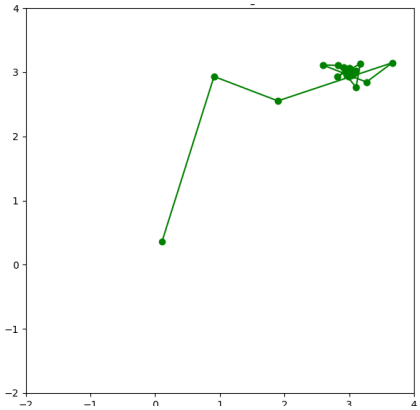

Figure 16: mean trajectory of $\{\rho_{\theta_t}\}$ w.r.t. $\dot{\theta} = -\nabla_\theta H(\theta)$

We compare the graph of trained $\psi_{\hat{\lambda}}$ at different time steps $k = 10, 140$ (Figure 17, 18). The directions of $\nabla\psi_{\hat{\lambda}}$ at $k = 10$ and $k = 140$ is different from the previous example. This is caused by the non-isotropic quadratic (Gaussian) potential V used in this example.

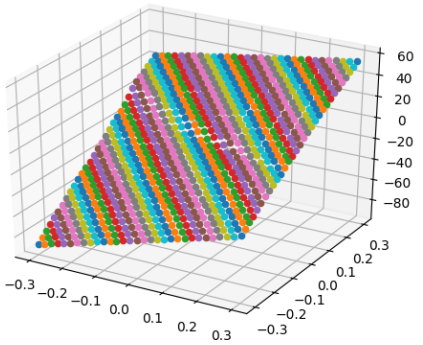

Figure 17: Graph of $\psi_{\hat{\lambda}}$ after $M_{\text{out}} = 20$ outer iterations at $k = 10$th time step

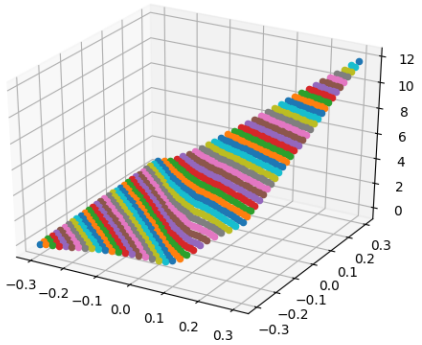

Figure 18: Graph of $\psi_{\hat{\lambda}}$ after $M_{\text{out}} = 20$ outer iterations at $k = 140$th time step

6.1.2 Higher dimension

We implement our algorithm in higher dimensional space. In the next example, we take $d = 10$, and consider the quadratic potential

$$V(x) = \frac{1}{2}(x-\mu)^T\Sigma^{-1}(x-\mu) \quad \Sigma = \text{diag}(\Sigma_A, I_2, \Sigma_B, I_2, \Sigma_C) \quad \mu = (1,1,0,0,1,2,0,0,2,3)^T.$$

Here we set the diagonal blocks as:

$$\Sigma_A = \begin{bmatrix} \frac{5}{8} & -\frac{3}{8} \\ -\frac{3}{8} & \frac{5}{8} \end{bmatrix} \quad \Sigma_B = \begin{bmatrix} 1 & \\ & \frac{1}{4} \end{bmatrix} \quad \Sigma_C = \begin{bmatrix} \frac{1}{4} & \\ & \frac{1}{4} \end{bmatrix}.$$

We solve the equation in time interval $[0, 0.7]$ with time stepsize 0.005. We set $M_{\text{out}} = 20$ and $M_{\text{in}} = 100$. To demonstrate the results, 6000 samples from the reference distribution p are drawn and pushforwarded by using our computed map T_{θ_k}. We plot a few snapshots of the pushforwarded points (from $t = 0.05$ to $t = 0.70$) in Figure 19. One can check that the distribution of our numerical computed samples gradually converges to the Gibbs distribution $\mathcal{N}(\mu, \Sigma)$.

We solve (5) on time interval $[0, 2]$ with time step size $h = 0.005$. We set $K_{\text{in}} = K_{\text{out}} = 3000$ and choose $M_{\text{out}} = 30$, $M_{\text{in}} = 100$. To demonstrate the results, 6000 samples from the reference distribution p are drawn and pushforwarded by using our computed map T_{θ_k}. We exhibit several snapshots of the projection of the samples on $0-1$, $4-5$ and $8-9$ plane in Figure 19 at different time nodes. One can verify that the distribution of our numerical computed samples gradually converges to the Gibbs distribution $\mathcal{N}(\mu, \Sigma)$.

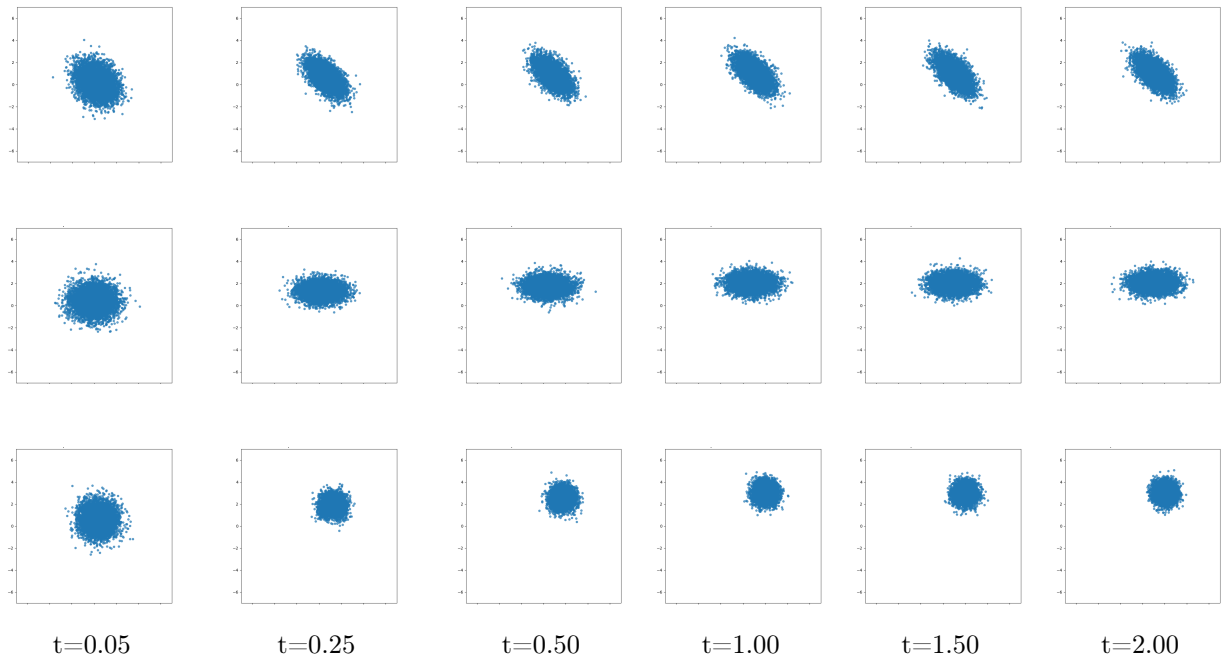

Figure 19: Sample points of computed ρ_{θ_t} projected on (top to bottom) 0-1, 4-5, 8-9 plane at different times

The explicit solution to the Fokker-Planck equation is always Gaussian distribution $\mathcal{N}(\mu(t), \Sigma(t))$ with mean $\mu(t)$ and covariance matrix $\Sigma(t)$:

$$\mu(t) = (1-e^{-t}, 1-e^{-t}, 0, 0, 1-e^{-t}, 2(1-e^{-4t}), 0, 0, 2(1-e^{-4t}), 3(1-e^{-4t}))^T$$

$$\Sigma(t) = \text{diag}(\Sigma_A(t), I, \Sigma_B(t), I, \Sigma_C(t))$$

$$\text{with } \Sigma_A(t) = \begin{bmatrix} \frac{5}{8} + f(t) & -\frac{3}{8} + f(t) \\ -\frac{3}{8} + f(t) & \frac{5}{8} + f(t) \end{bmatrix}, \ \Sigma_B(t) = \begin{bmatrix} 1 & \\ & \frac{1+3e^{-8t}}{4} \end{bmatrix}, \ \Sigma_C(t) = \begin{bmatrix} \frac{1+3e^{-8t}}{4} & \\ & \frac{1+3e^{-8t}}{4} \end{bmatrix}$$

$$\text{here } f(t) = -\frac{2}{7}e^{-t} + \frac{1}{3}e^{-2t} + \frac{55}{168}e^{-8t}$$

To compare against the exact solution, we set sample size $M = 6000$ and compute the empirical mean $\hat{\mu}^k$ and covariance $\hat{\Sigma}^k$ of our numerical solution $\hat{\rho}_k$ at time t_k. We evaluate the error between $\hat{\mu}^{(k)}$ and $\mu(t_k)$; $\hat{\Sigma}^{(k)}$ and $\Sigma(t_k)$. We plot the error curves of $\|\hat{\mu}^{(k)} - \mu(t_k)\|_2$ (Figure 20) and $\|\hat{\Sigma}^{(k)} - \Sigma(t_k)\|_F$ (Figure 21). Here $\|\cdot\|_F$ is the matrix Frobenius norm. Figure 22 captures the exponential decay of H along its Wasserstein gradient flow, this verifies the entropy dissipation property of Fokker-Planck equation with convex potential function V.

In this case, we take a closer look at the loss in the inner loops. Figure 23 shows the first 10 (out of 20) loss plots when applying SGD method to solve (66) with $k = 200$ ($t = 200 \cdot h = 1.0$). The remaining loss plots from the 11th outer iteration to 20th iteration are similar to the plots in the second row. The

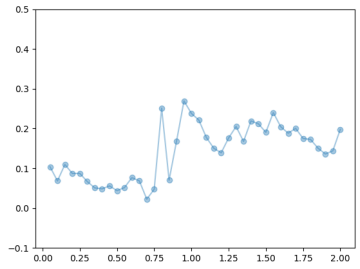

Figure 20: mean error (l_2)

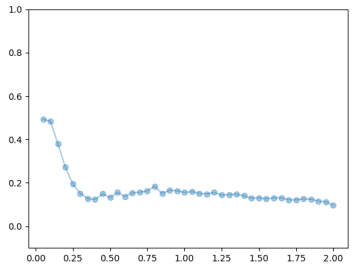

Figure 21: covariance error ($\|\cdot\|_F$)

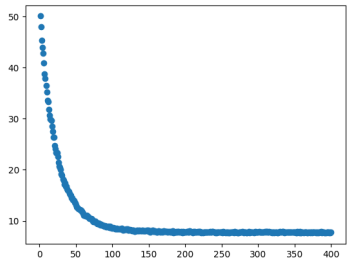

Figure 22: Plot of $\{H(\theta)\}$

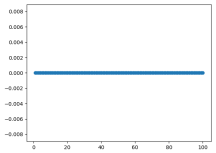

1st inner iteration

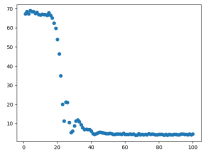

2nd inner iteration

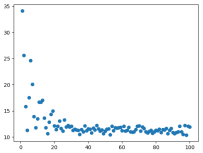

3rd inner iteration

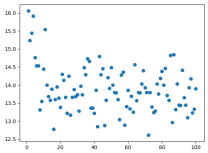

4th inner iteration

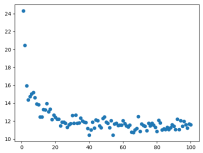

5th inner iteration

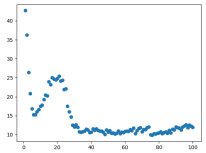

6th inner iteration

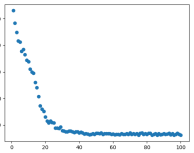

7th inner iteration

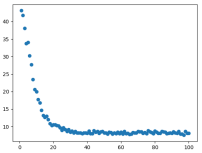

8th inner iteration

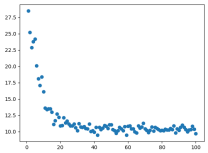

9th inner iteration

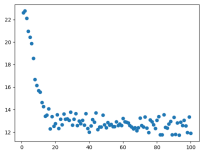

10th inner iteration

Figure 23: Plots of inner loop losses

situations are similar for other time step k. We believe that $M_{\text{in}} = 100$ works well in this problem, the SGD method we used can thoroughly solve the variational problem (66) for each outer loop.

6.2 Experiments with more general potentials

In this section, we exhibit two examples with more general potentials in higher dimensional space.

6.2.1 Styblinski-Tang potential

In this example, we set dimension $d = 30$, and consider the Styblinski–Tang function [50]

$$V(x) = \frac{3}{50}\left(\sum_{i=1}^{d} x_i^4 - 16x_i^2 + 5x_i\right).$$

We solve (5) with potential V on time interval $[0, 3]$ with time step size $h = 0.005$. We set $K_{\text{in}} = K_{\text{out}} = 9000$ and $M_{\text{in}} = 100$, $M_{\text{out}} = 30$.

To exhibit sample results, due to the symmetric structure of the potential function, we project the sample points in $\mathbb{R}^{30}$ to some random plane, such as $5 - 15$ plane used in this paper. The sample plots and their estimated densities are presented in Figure 24.

In this special example, the potential function is the direct addition of same functions, we can exploit this property and show that any marginal distribution

$$\varrho_j(x_j, t) = \int \ldots \int \rho(x, t)\ dx_1 \ldots dx_{j-1} dx_{j+1} \ldots dx_d$$

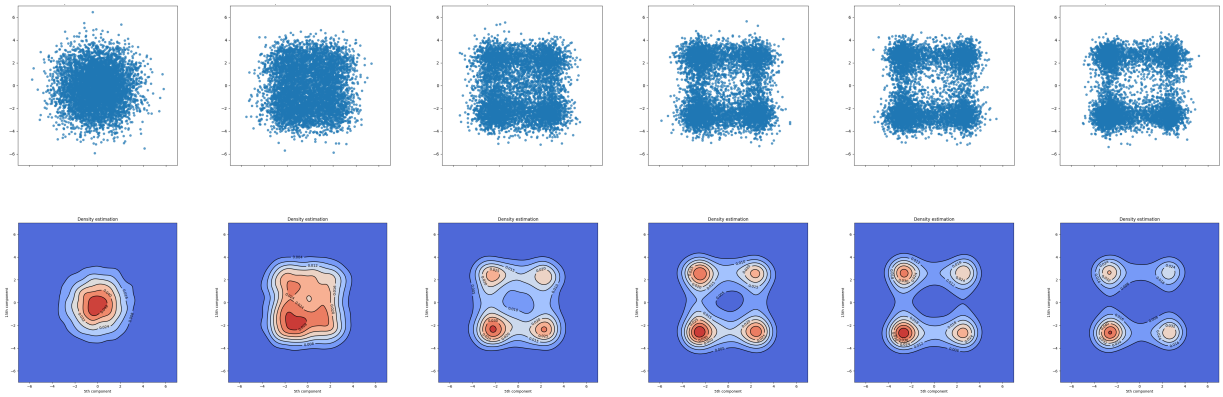

t=0.30 t=0.60 t=0.90 t=1.20 t=1.50 t=1.80

Figure 24: Sample points and estimated densities of ρ_{θ_t} on $5-15$ plane at different time nodes

of the solution ρ_t solves the following 1D Fokker-Planck equation:

$$\frac{\partial \varrho(x,t)}{\partial t} = \frac{\partial}{\partial x}(\varrho(x,t)\ V'(x)) + \beta \Delta \varrho(x,t) \quad \varrho(\cdot,0) = \mathcal{N}(0,1) \quad \text{with } V(x) = \frac{3}{50}(x^4 - 16x^2 + 5x). \tag{112}$$

We then solve the SDE associated to (112):

$$dX_t = V'(X_t)\ dt + \sqrt{2\beta} dB_t \quad X_0 \sim \mathcal{N}(0,1). \tag{113}$$

Since (113) is an SDE in one dimensional space, we may solve it with guaranteed accuracy by Euler-Maruyama scheme [22] and use it as a benchmark for our numerical solution. The following Figure 25 exhibits the both the estimated densities for our numerical solutions (marginal distribution on the 15th component) and the solution of (113) given by Euler-Maruyama scheme with step size 0.005. The sample sizes for both solutions equal to 6000.

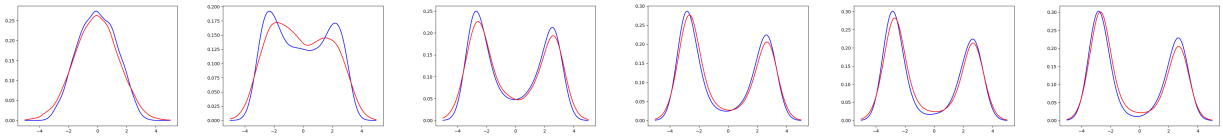

t=0.30 t=0.60 t=0.90 t=1.20 t=1.50 t=1.80

Figure 25: Estimated densities of our numerical solution(red) (projected onto the 15th component) and the solution given by Euler Maruyama scheme(blue)

We also illustrate the graphs of ψ_λ on $5-15$ plane trained at different time steps in Figure 26.

6.2.2 Rosenbrock potential

In this example, we set dimension $d = 10$. We consider the Rosenbrock typed function [46]:

$$V(x) = \frac{3}{50}\left(\sum_{i=1}^{d-1} 10(x_{k+1} - x_k^2)^2 + (x_k - 1)^2\right),$$

which involve interactions among its coordinates. We solve the corresponding (5) on time interval $[0,1]$ with step size $h = 0.005$. In this example, we set the length of normalizing flow T_θ as 100. We set $K_{\text{in}} = K_{\text{out}} = 3000$ and $M_{\text{in}} = 100$, $M_{\text{out}} = 60$.

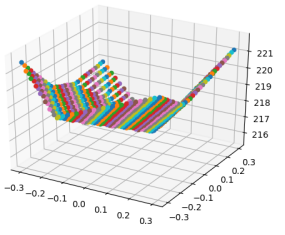

Graph of ψ_λ at time step $k = 30$

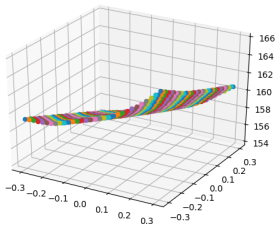

Graph of ψ_λ at time step $k = 60$

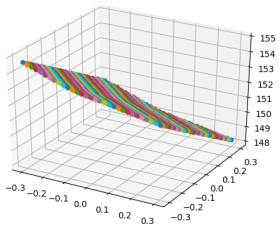

Graph of ψ_λ at time step $k = 150$

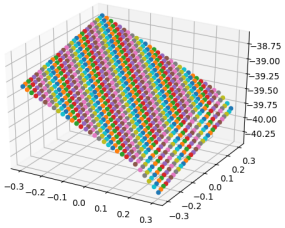

Graph of ψ_λ at time step $k = 240$

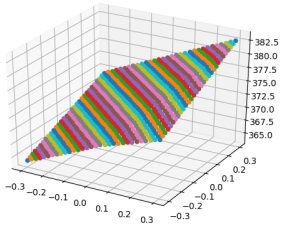

Graph of ψ_λ at time step $k = 300$

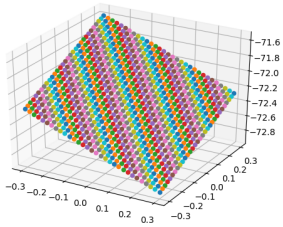

Graph of ψ_λ at time step $k = 360$

Figure 26: Graph of ψ_λ on $5 - 15$ plane trained at different time steps

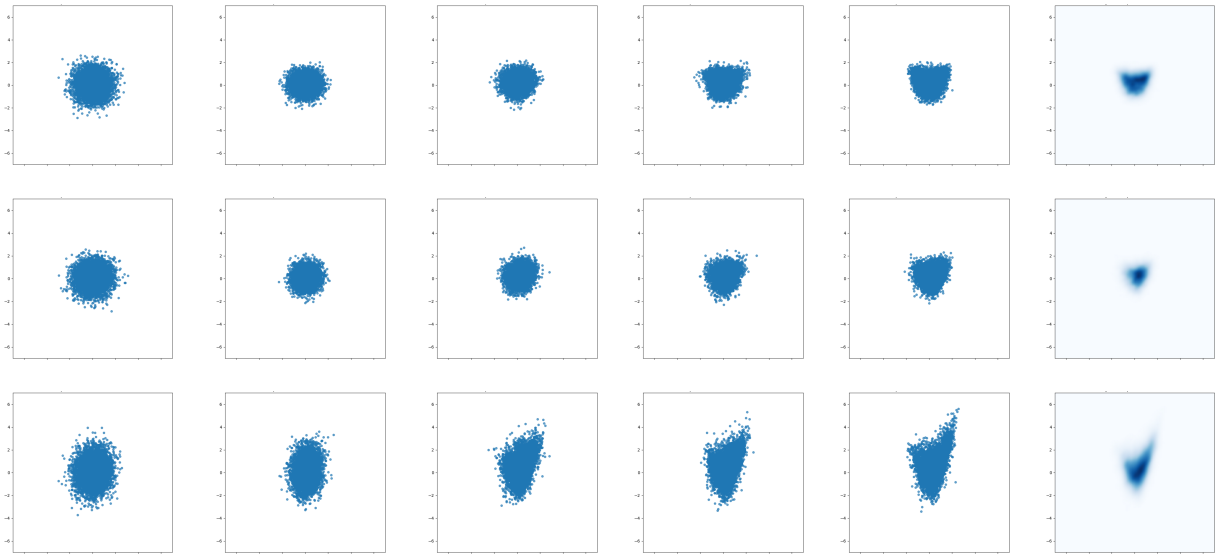

t=0.05 t=0.20 t=0.35 t=0.50 t=1.00 density $t = 1.0$

Figure 27: Sample points and estimated densities on (top to bottom) 1-2, 7-8, 9-10 planes at different times

Here are the sample results, we exhibit the projection of sample points on the $1 - 2$, $7 - 8$ and $9 - 10$ plane in Figure 27. The rightmost figures are plots of estimated densities at $t = 1.0$.

We exhibit the graphs of ψ_λ on $0 - 1$ plane trained at different time steps in Figure 28:

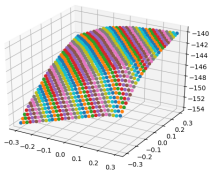

Graph of $\psi_{\hat{\lambda}}$ $(k = 10)$

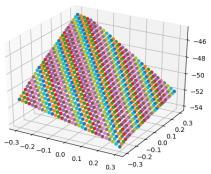

Graph of $\psi_{\hat{\lambda}}$ $(k = 20)$

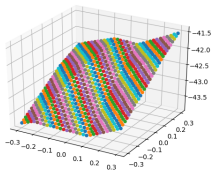

Graph of $\psi_{\hat{\lambda}}$ $(k = 30)$

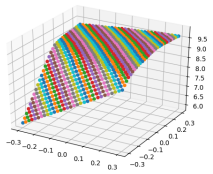

Graph of $\psi_{\hat{\lambda}}$ $(k = 40)$

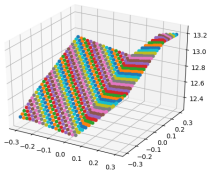

Graph of $\psi_{\hat{\lambda}}$ $(k = 80)$

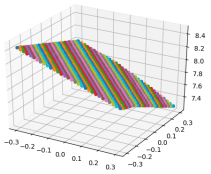

Graph of $\psi_{\hat{\lambda}}$ $(k = 120)$

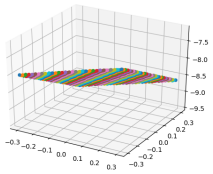

Graph of $\psi_{\hat{\lambda}}$ $(k = 160)$

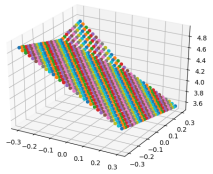

Graph of $\psi_{\hat{\lambda}}$ $(k = 200)$

Figure 28: Graph of ψ_{λ} on $0 - 1$ plane trained at different time steps

6.3 Solving the equation with different diffusion coefficients

The different behaviors of Fokker-Planck equation caused by different diffusion coefficients β can be captured by our algorithm. As the following figure shows, we apply our method to solve Fokker-Planck equation with Styblinski-Tang potential function with $\beta = 0.1, 1.0, 10.0$ and exhibit samples points and estimated density surfaces at the time $t = 3.0$.

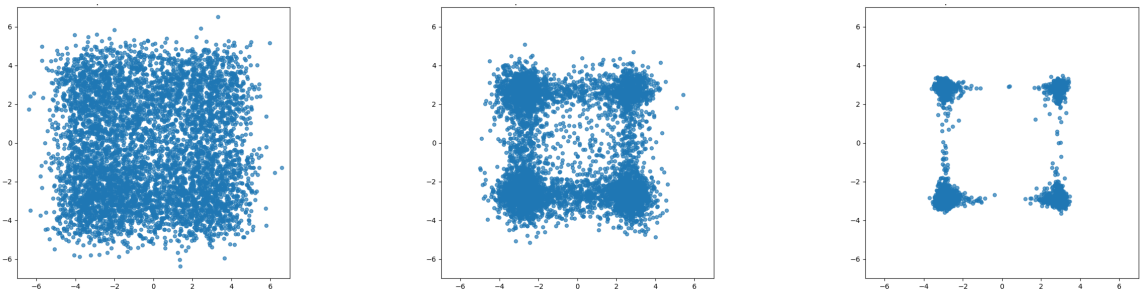

Figure 29: Samples drawn at $t = 3.0$, from left to right: $beta = 10$, $\beta = 1.0$, $\beta = 0.1$

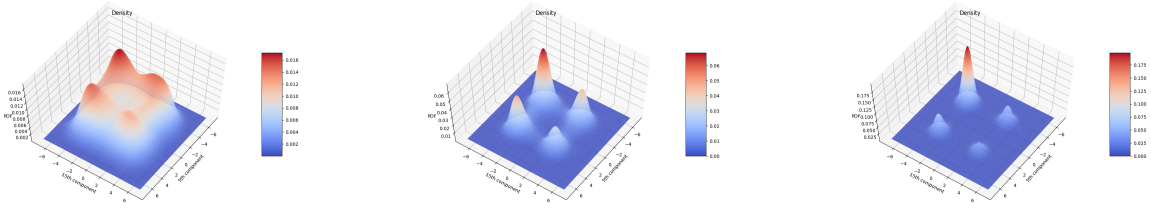

Figure 30: Estimated density surface at $t = 3.0$, from left to right: $beta = 10$, $\beta = 1.0$, $\beta = 0.1$

7 Discussion

In this paper, we design and analyze an algorithm for computing high dimensional Fokker-Planck equations. Our approach is based on transport information geometry with probability formulations arisen in deep learning generative models. We first introduce the parametric Fokker-Planck equations, a set of ODE, to approximate the original Fokker-Planck equation. The ODE can be viewed as the "spatial" discretization of the PDE using neural networks. We propose a variational version of the semi-implicit Euler scheme and design a discrete time updating algorithm to compute the solution of the parametric Fokker-Planck equations. Our method is a sampling based approach that is capable to handle high dimensional cases. It can also be viewed as an alternative of the JKO scheme used in conjunction with neural networks. More importantly, we prove the asymptotic convergence and error estimates, both under the Wasserstein metric, for our proposed scheme.

We hope that our study may shed light on principally designing deep neural networks and other machine learning approaches to compute solutions of high dimensional PDEs, and systematically analyzing their error bounds for understandable and trustworthy computations. Our parametric Fokker-Planck equations are derived by approximating the density function in free energy using neural networks, and then following the rules in calculus of variation to get its Euler-Langrange equation. The energy law and principles in variational framework build a solid foundation for our "spatial" discretization that is able to inherit many desirable physical properties shared by the PDEs, such as relative entropy dissipation in a neural network setting. Our numerical scheme provides a systemic mechanism to design sampling efficient algorithms, which are critical for high dimensional problems. One distinction of our method is that, contrary to the data dependent machine learning studies in the literature, our approach does not require any knowledge of the "data" from the PDEs. In fact, we generate the "data" to compute the numerical solutions, just like the traditional numerical schemes do for PDEs. More importantly, we carried out the numerical analysis, using tools such as KL divergence and Wasserstein metric from the transport information geometry, to study the the asymptotic convergence and error estimates in probability space. We emphasize that the Wasserstein metric provides a suitable geometric structure to analyze the convergence behavior in generative models, which are widely used in machine learning field. For this reason, we believe that our investigations can be adopted to understand many machine learning algorithms, and to design efficient sampling strategies based on pushforward maps that can generate flows of samples in generative models.

We also believe that the approaches in algorithm design and error analysis developed in this study can be extended to other equations, such as porous media equation, Schrödinger equation, and Schrödinger bridge system, and many more. Those topics are worth to be further investigated in the future.

References

[1] S Amari. Natural Gradient Works Efficiently in Learning. *Neural Computation*, 10(2):251–276, 1998.

[2] S Amari. *Information Geometry and Its Applications*. Number volume 194 in Applied Mathematical Sciences. Springer, Japan, 2016.

[3] Luigi Ambrosio, Nicola Gigli, and Giuseppe Savaré. *Gradient flows: in metric spaces and in the space of probability measures*. Springer Science & Business Media, 2008.

[4] Martin Arjovsky, Soumith Chintala, and Léon Bottou. Wasserstein generative adversarial networks. In *International Conference on Machine Learning*, pages 214–223, 2017.

[5] Nihat Ay, Jürgen Jost, Hông Vân Lê, and Lorenz Johannes Schwachhöfer. *Information Geometry*. Ergebnisse Der Mathematik Und Ihrer Grenzgebiete A @series of Modern Surveys in Mathematics$\mathbb{3}$. Folge, Volume 64. Springer, Cham, 2017.

[6] Tamer Başar and Pierre Bernhard. *H-infinity optimal control and related minimax design problems: a dynamic game approach*. Springer Science & Business Media, 2008.

[7] Andrew Brock, Jeff Donahue, and Karen Simonyan. Large scale gan training for high fidelity natural image synthesis. *arXiv preprint arXiv:1809.11096*, 2018.

[8] Daniel A Cervantes Cabrera, Pedro Gonzalez-Casanova, Christian Gout, L Héctor Juárez, and L Rafael Reséndiz. Vector field approximation using radial basis functions. *Journal of Computational and Applied Mathematics*, 240:163–173, 2013.

[9] Jose A Carrillo, Katy Craig, Li Wang, and Chaozhen Wei. Primal dual methods for wasserstein gradient flows. *arXiv preprint arXiv:1901.08081*, 2019.

[10] JS Chang and G Cooper. A practical difference scheme for fokker-planck equations. *Journal of Computational Physics*, 6(1):1–16, 1970.

[11] Joseph L Doob. The brownian movement and stochastic equations. *Annals of Mathematics*, pages 351–369, 1942.

[12] Xavier Glorot, Antoine Bordes, and Yoshua Bengio. Deep sparse rectifier neural networks. In *Proceedings of the fourteenth international conference on artificial intelligence and statistics*, pages 315–323, 2011.

[13] Ian Goodfellow, Jean Pouget-Abadie, Mehdi Mirza, Bing Xu, David Warde-Farley, Sherjil Ozair, Aaron Courville, and Yoshua Bengio. Generative adversarial nets. In *Advances in neural information processing systems*, pages 2672–2680, 2014.

[14] Ulf Grenander and Michael I Miller. Representations of knowledge in complex systems. *Journal of the Royal Statistical Society: Series B (Methodological)*, 56(4):549–581, 1994.

[15] Richard Holley and Daniel Stroock. Logarithmic sobolev inequalities and stochastic ising models. *Journal of statistical physics*, 46(5):1159–1194, 1987.

[16] Arthur Jacot, Franck Gabriel, and Clément Hongler. Neural tangent kernel: Convergence and generalization in neural networks. In *Advances in neural information processing systems*, pages 8571–8580, 2018.

[17] R. Jordan, D. Kinderlehrer, and F. Otto. The Variational Formulation of the Fokker–Planck Equation. *SIAM Journal on Mathematical Analysis*, 29(1):1–17, 1998.

[18] Richard Jordan, David Kinderlehrer, and Felix Otto. The variational formulation of the fokker–planck equation. *SIAM journal on mathematical analysis*, 29(1):1–17, 1998.

[19] Yuehaw Khoo, Jianfeng Lu, and Lexing Ying. Solving parametric pde problems with artificial neural networks. *arXiv preprint arXiv:1707.03351*, 2017.

[20] Yuehaw Khoo, Jianfeng Lu, and Lexing Ying. Solving for high-dimensional committor functions using artificial neural networks. *Research in the Mathematical Sciences*, 6(1):1, 2019.

[21] Diederik P Kingma and Jimmy Ba. Adam: A method for stochastic optimization. *arXiv preprint arXiv:1412.6980*, 2014.

[22] Peter E Kloeden and Eckhard Platen. *Numerical solution of stochastic differential equations*, volume 23. Springer Science & Business Media, 2013.

[23] Pankaj Kumar and S Narayanan. Solution of fokker-planck equation by finite element and finite difference methods for nonlinear systems. *Sadhana*, 31(4):445–461, 2006.

[24] John D. Lafferty. The Density Manifold and Configuration Space Quantization. *Transactions of the American Mathematical Society*, 305(2):699–741, 1988.

[25] Wuchen Li. Geometry of probability simplex via optimal transport. *arXiv:1803.06360 [math]*, 2018.

[26] Wuchen Li, Alex Tong Lin, and Guido Montúfar. Affine natural proximal learning. *unknown*, 2019.

[27] Wuchen Li, Shu Liu, Hongyuan Zha, and Haomin Zhou. Parametric fokker-planck equation. In Frank Nielsen and Frédéric Barbaresco, editors, *Geometric Science of Information*, pages 715–724, Cham, 2019. Springer International Publishing.

[28] Wuchen Li and Guido Montufar. Natural gradient via optimal transport. *arXiv:1803.07033 [cs, math]*, 2018.

[29] Wuchen Li and Guido Montufar. Ricci curvature for parametric statistics via optimal transport. *arXiv preprint arXiv:1807.07095*, 2018.

[30] Alex Tong Lin, Wuchen Li, Stanley Osher, and Guido Montufar. Wasserstein proximal of GANs, 2019.

[31] Qiang Liu and Dilin Wang. Stein Variational Gradient Descent: A General Purpose Bayesian Inference Algorithm. *arXiv:1608.04471 [cs, stat]*, 2016.

[32] John Lott. Some geometric calculations on wasserstein space. *Communications in Mathematical Physics*, 277(2):423–437, 2008.

[33] James Martens and Roger Grosse. Optimizing neural networks with kronecker-factored approximate curvature. In *International conference on machine learning*, pages 2408–2417, 2015.

[34] Dominic Masters and Carlo Luschi. Revisiting small batch training for deep neural networks. *arXiv preprint arXiv:1804.07612*, 2018.

[35] Edward Nelson. *Quantum Fluctuations*. Princeton Series in Physics. Princeton University Press, Princeton, N.J, 1985.

[36] Felix Otto. The Geometry of Dissipative Evolution Equations: The Porous Medium Equation. *Communications in Partial Differential Equations*, 26(1-2):101–174, 2001.

[37] Felix Otto and Cédric Villani. Generalization of an inequality by talagrand and links with the logarithmic sobolev inequality. *Journal of Functional Analysis*, 173(2):361–400, 2000.

[38] Michele Pavon, Esteban G. Tabak, and Giulio Trigila. The data-driven Schroedinger bridge. *arXiv:1806.01364 [math]*, 2018.

[39] Philipp Petersen and Felix Voigtlaender. Optimal approximation of piecewise smooth functions using deep relu neural networks. *Neural Networks*, 108:296–330, 2018.

[40] Lukas Pichler, Arif Masud, and Lawrence A Bergman. Numerical solution of the fokker–planck equation by finite difference and finite element methods—a comparative study. In *Computational Methods in Stochastic Dynamics*, pages 69–85. Springer, 2013.

[41] Di Qi and Andrew J. Majda. Low-dimensional reduced-order models for statistical response and uncertainty quantification: Barotropic turbulence with topography. *Physica D: Nonlinear Phenomena*, 343:7–27, 2017.

[42] Maziar Raissi, Paris Perdikaris, and George E Karniadakis. Physics-informed neural networks: A deep learning framework for solving forward and inverse problems involving nonlinear partial differential equations. *Journal of Computational Physics*, 378:686–707, 2019.

[43] Danilo Jimenez Rezende and Shakir Mohamed. Variational inference with normalizing flows. *arXiv preprint arXiv:1505.05770*, 2015.

[44] Hannes Risken. *The Fokker-Planck Equation*, volume 18 of *Springer Series in Synergetics*. Springer Berlin Heidelberg, Berlin, Heidelberg, 1989.

[45] Gareth O Roberts, Richard L Tweedie, et al. Exponential convergence of langevin distributions and their discrete approximations. *Bernoulli*, 2(4):341–363, 1996.

[46] HoHo Rosenbrock. An automatic method for finding the greatest or least value of a function. *The Computer Journal*, 3(3):175–184, 1960.

[47] Sebastian Ruder. An overview of gradient descent optimization algorithms. *arXiv preprint arXiv:1609.04747*, 2016.

[48] Tamar Schlick. *Molecular modeling and simulation: an interdisciplinary guide: an interdisciplinary guide*, volume 21. Springer Science & Business Media, 2010.

[49] Justin Sirignano and Konstantinos Spiliopoulos. Mean field analysis of neural networks. *arXiv preprint arXiv:1805.01053*, 2018.

[50] S. Surjanovic and D. Bingham. Virtual library of simulation experiments: Test functions and datasets. Retrieved February 8, 2020, from `http://www.sfu.ca/~ssurjano`, 2020.

[51] Cédric Villani. *Topics in optimal transportation*. American Mathematical Soc., 2003.

[52] Cédric Villani. *Optimal transport: old and new*, volume 338. Springer Science & Business Media, 2008.

[53] E Weinan, Jiequn Han, and Arnulf Jentzen. Deep learning-based numerical methods for high-dimensional parabolic partial differential equations and backward stochastic differential equations. *Communications in Mathematics and Statistics*, 5(4):349–380, 2017.

[54] Max Welling and Yee W Teh. Bayesian learning via stochastic gradient langevin dynamics. In *Proceedings of the 28th international conference on machine learning (ICML-11)*, pages 681–688, 2011.

[55] Yaohua Zang, Gang Bao, Xiaojing Ye, and Haomin Zhou. Weak adversarial networks for high-dimensional partial differential equations. *arXiv preprint arXiv:1907.08272*, 2019.